



HAL
open science

Reduction of Complexity in Combustion Thermochemistry

Americo E Cunha Jr

► **To cite this version:**

Americo E Cunha Jr. Reduction of Complexity in Combustion Thermochemistry. Reactive fluid environment. Pontifícia Universidade Católica do Rio de Janeiro, 2010. English. NNT: . tel-01541173

HAL Id: tel-01541173

<https://hal.science/tel-01541173>

Submitted on 27 Jun 2017

HAL is a multi-disciplinary open access archive for the deposit and dissemination of scientific research documents, whether they are published or not. The documents may come from teaching and research institutions in France or abroad, or from public or private research centers.

L'archive ouverte pluridisciplinaire **HAL**, est destinée au dépôt et à la diffusion de documents scientifiques de niveau recherche, publiés ou non, émanant des établissements d'enseignement et de recherche français ou étrangers, des laboratoires publics ou privés.

Copyright

Americo Barbosa da Cunha Junior

**Reduction of Complexity in
Combustion Thermochemistry**

DISSERTAÇÃO DE MESTRADO

DEPARTAMENTO DE ENGENHARIA MECÂNICA

Postgraduate Program in Mechanical Engineering

Rio de Janeiro
August 2010



Americo Barbosa da Cunha Junior

**Reduction of Complexity in Combustion
Thermochemistry**

Dissertação de Mestrado

Dissertation presented to the Postgraduate Program in Mechanical Engineering of the Departamento de Engenharia Mecânica do Centro Técnico Científico da PUC–Rio, as partial fulfillment of the requirements for the degree of Mestre em Engenharia Mecânica.

Advisor: Prof. Luís Fernando Figueira da Silva

Rio de Janeiro
August 2010



Americo Barbosa da Cunha Junior

**Reduction of Complexity in Combustion
Thermochemistry**

Dissertation presented to the Postgraduate Program in Mechanical Engineering of the Departamento de Engenharia Mecânica do Centro Técnico Científico da PUC–Rio, as partial fulfillment of the requirements for the degree of Mestre em Engenharia Mecânica. Approved by the following commission:

Prof. Luís Fernando Figueira da Silva

Advisor

Departamento de Engenharia Mecânica
Pontifícia Universidade Católica do Rio de Janeiro

Prof. Angela Ourivio Nieckele

Departamento de Engenharia Mecânica
Pontifícia Universidade Católica do Rio de Janeiro

Prof. Guenther Carlos Krieger Filho

Departamento de Engenharia Mecânica
Universidade de São Paulo

Dr. Ricardo Serfaty

Centro de Pesquisa e Desenvolvimento da Petrobras
Petróleo Brasileiro S.A.

Prof. José Eugenio Leal

Coordinator of the Centro Técnico Científico
Pontifícia Universidade Católica do Rio de Janeiro

Rio de Janeiro — August 19, 2010

All rights reserved. It is forbidden partial or complete reproduction without previous authorization of the university, the author and the advisor.

Americo Barbosa da Cunha Junior

The author graduated from Pontifícia Universidade Católica do Rio de Janeiro in Mechanical Engineering and Applied Mathematics. Currently he works as a professor of mathematics at the same university.

Bibliographic data

Cunha, Americo Barbosa

Reduction of Complexity in Combustion Thermochemistry / Americo Barbosa da Cunha Junior; advisor: Luís Fernando Figueira da Silva . — 2010.

134 f. : il. ; 30 cm

1. Dissertação (Mestrado em Engenharia Mecânica) - Pontifícia Universidade Católica do Rio de Janeiro, Rio de Janeiro, 2010.

Inclui bibliografia

1. Engenharia Mecânica – Teses. 2. modelagem da combustão. 3. cinética química detalhada. 4. modelo reduzido. 5. tabulação adaptativa. I. Figueira da Silva, Luís Fernando. II. Pontifícia Universidade Católica do Rio de Janeiro. Departamento de Engenharia Mecânica. III. Título.

CDD: 621

Acknowledgments

First of all, I wish to express my deepest gratitude to my parents, Americo Barbosa da Cunha and Heleny da Gloria Santos da Cunha, for their unconditional love, constant support to my plans, for teaching me the value of the truth and the importance of taking the consequences of my mistakes. I love you both more than anything. As important is the acknowledgment to my sister Amanda Gloria Santos da Cunha, for unconsciously being my best friend.

I want to express gratitude to my advisor Prof. Luís Fernando Figueira da Silva for his support during all stages of this work and his significant contribution to my development as a researcher. Also, I would like to thank him for the careful technical and grammatical review of this document.

I want to express my gratitude to professors Angela Ourivio Nieckele, Carlos Tomei, George Svetlichny, Luís Fernando Alzuguir Azevedo, Marcelo Miranda Viana da Silva, Márcio da Silveira Carvalho, Nicolau Corção Saldanha, Paulo Roberto de Souza Mendes, Ricardo Sá Earp and Rubens Sampaio Filho. These professors have influenced me in a positive way and contributed a lot to my formation as an engineer, mathematician and researcher. Furthermore, I wish to register a special acknowledgment to professors Carlos Frederico Borges Palmeira, Gregorio Salcedo Muñoz, Rubens Sampaio Filho and Washington Braga Filho for the friendship shown during the last years.

During the development of this work some people have helped me whenever requested. I am very grateful to them and want to register my sincere thanks to: Fernando Oliveira de Andrade and Silvia Emilia de Jesus Barbosa da Cunha for reviewing the grammar of the text; Bruno de Barros Mendes Kassar and Daniel Fleischman for many programming tips and help in tracking bugs in the code developed; Carlos Tomei for helping me with the development presented in section 5.3; and Thomas Maurice Lewiner for help me with the customization of `BIBTEX` citation style.

I wish to thank the members of my jury, Angela Ourivio Nieckele, Guenther Carlos Krieger Filho and Ricardo Serfaty, for their valuable comments and suggestions that help to improve the quality of the final version of this dissertation. In especial professor Guenther, who also provided the code which serves as example for the code developed in this work.

In addition, I am very grateful to my friends and colleagues from PUC–Rio for their enjoyable company, especially Alan da Silva Esteves, Andrea Cristina Carvalho dos Anjos, André Luiz Tenório Rezende, André Reinaldo Novgorodcev Júnior, Bruno de Barros Mendes Kassar, Bruno Messer, Daniel Fleischman, Elder Marino Mendonza Orbegoso, Fernando Oliveira de Andrade, Leonardo Weiskopf, Luis Enrique Alva Huapaya, Nattan Roberto Caetano and Roberta de Queiroz Lima.

I also wish to thank the staff of the Mechanical Engineering Department at PUC–Rio for their assistance, especially Mrs. Flavia Rocha Souza and Mrs. Rosely Ribeiro de Almeida Marins.

An especial acknowledgment goes to the staff of PUC–Rio’s Library for their efficiency and friendliness always demonstrated during my visits or web requests for some lost paper or book.

Due to my lack of attention during the replacement of a hard disk, some colleagues from the Laboratory of Computation in Transport Phenomena have lost part of their work. It is unusual to apologize in a section titled Acknowledgments, but as I harmed some people, even unintentionally, I take this section to express once again my sincere apologies to André Luiz Tenório Rezende, David Ivan Maldonado Távora, Javier Enrique Basurco Cayllahua, Luis Enrique Alva Huapaya, Luiz Eduardo Bittencourt Sampaio and Luiz Renato Minchola Morán.

Finally, I wish to thank the Brazilian Council for Scientific and Technological Development (CNPq) and Foundation for Research Support in Rio de Janeiro State (FAPERJ) for their financial support during the first and second year of the M.Sc. course, respectively.

Abstract

Cunha, Americo Barbosa; Figueira da Silva, Luís Fernando. **Reduction of Complexity in Combustion Thermochemistry**. Rio de Janeiro, 2010. 134p. Dissertação de Mestrado — Departamento de Engenharia Mecânica, Pontifícia Universidade Católica do Rio de Janeiro.

The development of computational models for the numerical simulation of chemically reacting flows operating in the turbulent regime requires the solution of partial differential equations that represent the balance of mass, linear momentum, chemical species and energy. Moreover, the chemical reactions of the model may require a detailed reaction mechanism for the description of the physicochemical phenomena involved. One of the biggest challenges is the stiffness of the numerical simulation of these models and the nonlinear nature of species rate of reaction. This dissertation presents an overview of the main techniques available in the literature for the development of reduced models of chemical kinetics, particularly for the combustion, as well as the techniques for efficient computation of the chemically reacting flows models. After a presentation of the associated mathematical formulation, the methodology dubbed *in situ* adaptive tabulation (ISAT) is implemented and its accuracy, efficiency and memory usage are evaluated in the simulation of homogeneous stirred reactor models. The combustion of carbon monoxide with oxygen and methane with air mixtures is considered, which detailed reaction mechanisms involve 4 and 53 species, 3 and 325 reactions respectively. The results of these simulations indicate that the development implementation of the ISAT technique has a absolute global error of less than 1%. Moreover, the ISAT technique provided gains, in terms of computational time, of up to 80% when compared to the direct integration of the full chemical kinetics. However, in terms of memory usage the present implementation of ISAT technique was found to be excessively demanding.

Keywords

combustion modelling. detailed thermochemistry. reduced model. adaptive tabulation.

Resumo

Cunha, Americo Barbosa; Figueira da Silva, Luís Fernando. **Redução de Complexidade da Cinética Química da Combustão**. Rio de Janeiro, 2010. 134p. Dissertação de Mestrado — Departamento de Engenharia Mecânica, Pontifícia Universidade Católica do Rio de Janeiro.

O desenvolvimento de modelos computacionais para simulação de escoamentos reativos operando em regime de turbulência requer a solução das equações diferenciais parciais que representam os balanços de massa, quantidade de movimento linear, espécies químicas e energia. Além disso, as reações químicas do modelo necessitam de um mecanismo cinético detalhado para descrição dos fenômenos físico-químicos associados. Um dos maiores desafios encontrados é a rigidez da simulação numérica desses modelos e a natureza não linear do termo de produção das espécies químicas. Esta dissertação apresenta uma revisão das principais técnicas disponíveis na literatura para o desenvolvimento de modelos reduzidos de cinética química, em particular para a combustão, bem como de técnicas para solução eficiente dos modelos de escoamentos reativos. Após uma apresentação da formulação matemática associada, a metodologia denominada tabulação adaptativa *in situ* (ISAT) é implementada e avaliada quanto a sua acurácia, eficiência e uso de memória na simulação de alguns modelos de reator homogêneo agitado. Avalia-se a combustão de misturas de monóxido de carbono/oxigênio e metano/ar cujos mecanismos cinéticos tem 4 e 53 espécies, 3 and 325 reações respectivamente. Os resultados destas simulações indicam que a presente implementação da técnica ISAT tem erro relativo global inferior a 1%. Além disso, a técnica ISAT propiciou ganhos, em termos de tempo computacional, de até 80% quando comparado a simulação direta da cinética detalhada. Entretanto, em termos de utilização da memória, a implementação desenvolvida da técnica ISAT se mostrou excessivamente exigente.

Palavras-chave

modelagem da combustão. cinética química detalhada. modelo reduzido. tabulação adaptativa.

Contents

1	Introduction	23
1.1	Historical and Economical Aspects	23
1.2	Combustion Applied to Industrial Devices	24
	<i>Industrial Process Furnaces</i>	24
	<i>Gas Turbines</i>	25
1.3	Fundamental Challenges	26
1.4	Objectives of this Dissertation	27
1.5	Outline of this Dissertation	27
2	Literature Review	28
2.1	Introduction to the Reduction Approaches	28
2.2	Reduction to Skeleton Mechanisms	28
	<i>Sensitivity Analysis</i>	29
	<i>Proper Orthogonal Decomposition</i>	30
	<i>Directed Relation Graph</i>	31
2.3	Dimension Reduction	32
	<i>Reaction Lumping</i>	32
	<i>Quasi-Steady State Approximation</i>	33
	<i>Rate-Controlled Constrained Equilibrium</i>	35
	<i>Computational Singular Perturbation</i>	36
	<i>Intrinsic Low-Dimensional Manifold</i>	37
	<i>Proper Orthogonal Decomposition</i>	39
	<i>Invariant Constrained Equilibrium Edge Pre-image Curve</i>	40
2.4	Storage/Retrieval	42
	<i>Look-Up Table</i>	42
	<i>Repro-Modelling</i>	43
	<i>Piece-Wise Reusable Implementation of Solution Mapping</i>	44
	<i>Artificial Neural Network</i>	45
	<i>In Situ Adaptive Tabulation</i>	46
2.5	The State of the Art	50
3	Modelling of Stirred Reactors	51
3.1	Fundamental Definitions	51
3.2	Gas Phase Thermochemistry	53
	<i>Equation of State for Perfect Gases</i>	53
	<i>Stoichiometry</i>	53
	<i>Reaction Mechanism</i>	54
	<i>Rate of Reaction</i>	55
	<i>Thermochemical Equilibrium</i>	56
3.3	Equations of Balance	57
3.4	Partially Stirred Reactor with IEM Model	57

3.5	Pairwise Mixing Stirred Reactor	58
3.6	The Geometry of Reactive Systems	60
	<i>Composition Space</i>	60
	<i>Mixture Temperature</i>	61
	<i>Reaction Mapping</i>	61
	<i>Reaction Vector</i>	62
	<i>Evolution Equations of PaSR/IEM</i>	63
	<i>Evolution Equations of PMSR</i>	63
4	Numerical Procedure	64
4.1	Operator Splitting Technique	64
4.2	Integration of Mixing Vector	65
	<i>IEM Mixing Model</i>	65
	<i>PMSR Mixing Model</i>	65
4.3	Integration of the Reaction Vector	66
	<i>Backward Differentiation Formula</i>	66
	<i>Truncation Error Control</i>	67
5	<i>In Situ</i> Adaptive Tabulation	69
5.1	Linearized Reaction Mapping	69
5.2	Ellipsoid of Accuracy	70
5.3	Hyper-ellipsoid Growth	72
5.4	Adaptive Tabulation Procedure	75
6	Results and Discussion	79
6.1	Code Verification	79
	<i>Numerical Integration Verification Test</i>	79
	<i>Error Control Verification Test</i>	81
6.2	Analysis of ISAT Accuracy	83
	<i>Error Metrics</i>	83
	<i>PMSR with a CO/O₂ Mixture</i>	84
	Influence of the time scale ratio	84
	Influence of the statistical process seed	90
	Influence of the ISAT error tolerance	90
	Influence of the ISAT lower bound	91
	<i>PMSR with a CH₄/Air Mixture</i>	92
6.3	Analysis of ISAT Performance	95
	<i>ISAT Performance for CO/O₂ Mixtures</i>	96
	<i>ISAT Performance for CH₄/Air Mixtures</i>	99
6.4	Analysis of ISAT Memory Usage	101
	<i>ISAT Memory Complexity</i>	101
	<i>ISAT Memory Cost for CO/O₂ Mixtures</i>	103
	<i>ISAT Memory Cost for CH₄/Air Mixtures</i>	103
7	Conclusions and Suggestions	105
7.1	Contributions of this Dissertation	105

7.2	Suggestions for Further Works	106
	Bibliography	108
A	Dimensionless Parameters	119
A.1	Dimensionless Time	119
A.2	Reduced Temperature	119
A.3	Ensemble Average of Reduced Temperature	119
A.4	Ensemble Variance of Reduced Temperature	120
B	Analysis of ISAT Efficiency	122
B.1	Necessary Condition for Efficiency	122
B.2	Empirical Metrics	122
B.3	Addition/Retrieve Relation	123
C	Conference Paper	124

List of Figures

1.1	Schematic representation of an industrial process furnace. Adapted from http://en.wikipedia.org/wiki/Furnace	24
1.2	Sketch of reverse flow combustor gas turbine. Adapted from http://en.wikipedia.org/wiki/Capstone_Turbine	25
2.1	Illustration of the classification of the different approaches. <i>S/M</i> : reduction to skeletal mechanism; <i>D/R</i> : dimension reduction; <i>S/R</i> : storage and retrieval.	29
3.1	Sketch of the composition space and its subsets.	60
3.2	Sketch of a trajectory in composition space departing from an initial composition ϕ_0 until the chemical equilibrium.	62
5.1	The region of accuracy for a constant approximation is a hyper-ellipsoid in composition space.	71
5.2	Growth process of the original hyper-ellipsoid.	73
5.3	Sketch of the binary search trees created by ISAT algorithm (leaves are black and nodes white).	76
5.4	Sketch of cutting plane in relation to EOA position.	77
5.5	Binary search tree before and after the addition of a new node.	78
5.6	A flowchart showing all step of ISAT algorithm.	78
6.1	Evolution of T and Y_{OH} for the first verification test.	81
6.2	Behavior of the ISAT global error as function of the error tolerance for the second verification test.	83
6.3	Comparison between DI and ISAT results of ensemble average of reduced temperature for cases 1 and 2.	85
6.4	Comparison between DI and ISAT results of ensemble variance of reduced temperature for cases 1 and 2.	86
6.5	Evolution of relative local error for ensemble average of the reduced temperature and of the O mass fraction for cases 1 and 2.	87
6.6	Evolution of relative local error for ensemble variance of the reduced temperature and of the O mass fraction for cases 1 and 2.	88
6.7	Comparison between DI and ISAT computations of the mean histograms (over the last 50 residence times) of the reduced temperature for cases 1 and 2.	88
6.8	Comparison between DI and ISAT computations of the mean histograms (over the last 50 residence times) of the O mass fraction for cases 1 and 2.	89
6.9	Comparison between DI and ISAT results (using different seeds) of reduced temperature ensemble average and the corresponding relative local errors for cases 1 and 2.	89
6.10	Comparison between DI and ISAT computations (using different seeds) of the mean histograms (over the last 50 residence times) of the reduced temperature for cases 1 and 2 .	90

6.11	Absolute global errors for cases 1 and 2 as function of the error tolerance, using a binary search tree with 50k entries.	91
6.12	Comparison between DI and ISAT results of the ensemble average of the reduced temperature and <i>OH</i> mass fraction for case 3.	93
6.13	Comparison between DI and ISAT results of the ensemble variance of the reduced temperature and <i>OH</i> mass fraction for case 3.	94
6.14	Evolution of relative local error of the first two statistical moments of the reduced temperature and <i>OH</i> mass fraction for case 3.	94
6.15	Comparison between DI and ISAT computations of the mean histograms (over the last 50 residence times) of the reduced temperature and <i>HCO</i> mass fraction for case 3.	95
6.16	Evolution of the ISAT algorithm outputs and of the height of ISAT binary search tree for cases 1 and 2.	96
6.17	Evolution of the rates of change of each ISAT algorithm outputs and of the height of the ISAT binary search tree for cases 1 and 2.	97
6.18	Evolution of the ISAT algorithm outputs and of the height of the ISAT binary search tree for case 3.	100
6.19	Evolution of the rates of change of each ISAT algorithm outputs and of the height of the ISAT binary search tree for case 3.	100

List of Tables

1.1	Energy supply structure by source for Brazil in 2008 and World in 2007 (EPE, 2009) [16].	23
3.1	Reaction mechanism for carbon monoxide (CO) oxidation. In this table M represent a third body with a specific efficiency for each species ($f_{O_2} = 0.4$, $f_{CO} = 0.75$ and $f_{CO_2} = 1.5$).	54
6.1	Skeletal reaction mechanism for methane/air combustion.	80
6.2	PMSR parameters used in the code verification tests.	82
6.3	Parameters used in the simulation of a CO/O_2 mixture in a PMSR.	85
6.4	Mean and maximum relative errors for cases 1 and 2, using a binary search tree with 50k entries.	86
6.5	Absolute global error as function of ε_{tol} and κ .	92
6.6	Parameters for a PMSR of CH_4/Air that behaves like a partially stirred reactor.	93
6.7	Mean and maximum relative errors for case 3, using a binary search tree with 60k entries.	95
6.8	Comparison between the computational time spent by DI and ISAT in cases 1 and 2 and the corresponding speed-up factors.	99
6.9	Comparison between the memory cost of some data types in cases 1 and 2 using two different implementations of the ISAT technique.	103
6.10	Comparison between the memory cost of some data types in case 3 using two different implementations of the ISAT technique.	104
B.1	Empirical metrics for the computational time spent at each output of ISAT algorithm and DI.	123

Nomenclature

Upper-case Roman

$\mathbf{A}(\phi, t)$	mapping gradient matrix
\mathbf{B}	scaling matrix
\mathbf{G}	rank-one modification matrix
\mathbf{I}	identity matrix
\mathbf{J}	Jacobian matrix of \mathbf{N}
\mathbf{L}'	new EOA Cholesky matrix
\mathbf{L}	EOA Cholesky matrix
\mathbf{N}	nonlinear system of algebraic equations
$\mathbf{R}(\phi, t)$	reaction mapping of ϕ
$\mathbf{R}^c(\phi, t)$	constant approximation for $\mathbf{R}(\phi, t)$
$\mathbf{R}^l(\phi, t)$	linear approximation for $\mathbf{R}(\phi, t)$
$\mathbf{S}(\phi, t)$	reaction vector
\mathbf{U}	real square orthogonal matrix
\mathbf{V}	real square orthogonal matrix
\mathcal{A}	accessed region
\mathcal{C}	composition space
\mathcal{M}_i	i -th chemical species symbol
\mathcal{R}	realizable region
\bar{W}	mean molar mass
$\tilde{\mathbf{A}}$	modification of \mathbf{A}
$A_{ij}(\phi, t)$	components of $\mathbf{A}(\phi, t)$
A_j	j -th reaction pre-exponential factor
C	mixture concentration
C_i	i -th chemical species molar concentration
E_j	j -th reaction activation energy
H_i°	i -th chemical species enthalpy of formation
K	number of time steps

K_{c_j}	j -th reaction equilibrium in concentration units
K_{p_j}	j -th reaction equilibrium in pressure units
N_A	Avogadro number
R	universal gas constant
$R_i(\phi, t)$	i -th component of $\mathbf{R}(\phi, t)$
S_i°	i -th chemical species entropy in standard state
T	temperature
T°	temperature at standard state
V	system volume
W_i	i -th chemical species molar mass
X_i	i -th chemical species molar fraction
X_{Fu}	fuel molar fraction
X_{Ox}	oxidizer molar fraction
Y_i	i -th chemical species mass fraction

Lower-case Roman

\mathbf{v}	cutting plane normal vector
\dot{m}	mass flow rate
\mathbf{u}	velocity field
\tilde{l}_i	modified length of EOA in i -th direction
a	cutting plane scalar
c_{p_i}	i -th chemical species specific heat
h	specific enthalpy
h_i	i -th chemical species specific enthalpy
h_i°	i -th chemical species specific enthalpy of formation
k_j	j -th reaction rate constant
l_i	half-length of EOA in i -th principal direction
m	system total mass
m_i	i -th chemical species mass
n	system total number of moles

n_i	i -th chemical species number of moles
n_r	number of elementary reactions
n_s	number of chemical species
n_ϕ	number of composition components
n_A	number of additions
n_{DE}	number of direct evaluations
n_{DI}	number of direct integrations
n_G	number of growths
n_{in}	number of particles to input the system
n_L	number of leaves
n_N	number of nodes
n_{pair}	number of particles for pairing
n_p	number of reactor particles
n_R	number of retrieves
n_{tab}	number of entries in the binary search tree
p	pressure
p^o	pressure at the standard state
q	order of BDF method
r_j	j -th reaction rate
t	time
t_0	initial time
t_n	n -th time instant
u_r	machine unit roundoff
w_i	i -th error weight

Upper-case Greek

$\Gamma(t)$	mixing vector
Σ	real square diagonal matrix
$\Delta\tau$	time interval
ΔH_j^o	j -th reaction net change in enthalpy

ΔS_j^o	j -th reaction net change in entropy
Δt	time step
Δt_n	n -th time step
Γ_ρ	continuity equation right hand side term
$\Gamma_{\mathbf{u}}$	momentum equation right hand side term
Γ_h	energy equation right hand side term
Γ_{Y_i}	i -th chemical species equation right hand side term
Ω_i	i -th chemical species equation chemical source term
Φ	equivalence ratio
$\tilde{\Sigma}$	modification of Σ

Lower-case Greek

α_j	coefficients of BDF method
β_j	j -th reaction temperature exponent
ϵ	vector with the local truncation errors
$\tilde{\phi}$	transformed ϕ
ϕ	composition
ϕ_0	initial composition
ϕ_q	query composition
ϕ_{mix}	solution of the mixing system
ζ	constant vector
ζ_1	constant vector
ζ_2	constant vector
$\delta\phi$	composition displacement
$\dot{\omega}_i$	i -th chemical species reaction rate
ϵ_i	i -th component of ϵ
ϵ_G	global error of ISAT
γ	rank-one modification constant
κ	lower bound
ν''_{ij}	reverse stoichiometric coefficients

ν'_{ij}	forward stoichiometric coefficients
ν_{ij}	overall stoichiometric coefficients
$\phi_i(t_n)$	i -th component of $\phi(t_n)$
$\tilde{\phi}_q$	Euclidean norm of $\tilde{\phi}_q$
ψ	generic property
ρ	mixture density
ρ_i	i -th chemical species partial density
σ_i	singular values of \mathbf{A}
τ_m	mixing time scale
τ_p	pairwise time scale
τ_r	residence time
τ_A	average time spent at each addition
τ_{DE}	average time spent at each direct evaluation
τ_{DI}	average time spent at each direct integration
τ_G	average time spent at each growth
τ_R	average time spent at each retrieve
ε	local error of linear approximation
ε_{ψ_r}	relative local error of ψ
ε_{abs}	solver absolute tolerance
ε_g	absolute global error of ISAT
ε_{rel}	solver relative tolerance
ε_{tol}	error tolerance of ISAT
$\tilde{\sigma}_i$	singular values of $\tilde{\mathbf{A}}$

Superscripts

*	dimensionless quantity
T	transposition operation
(j)	index of the j -th particle
+	forward reaction
-	reverse reaction

m m -th approximation

Subscripts

0 initial condition

DI direct integration calculation

eq equilibrium condition

in input condition

$ISAT$ ISAT calculation

st stoichiometric condition

Other Symbols

$ceil(\cdot)$ ceil function

\int integral

$\frac{\partial}{\partial t}$ partial derivative with respect to t

\prod product

\sum summation

$\frac{d}{dt}$ total derivative with respect to t

\equiv definition

$\langle \cdot \rangle_{\infty}$ function maximum

$\langle \cdot \rangle_M$ function mean

$\langle \cdot \rangle$ ensemble average

$\|\cdot\|_{wrms}$ weighted root mean square norm

$\|\cdot\|_2$ Euclidean norm

$\#(\text{data})$ memory cost of **data**

$\mathcal{O}(\cdot)$ big O notation

$\langle \cdot'^2 \rangle$ ensemble variance

Abbreviations

ANN artificial neural network

CSP computational singular perturbation

D/R	dimension reduction
DI	direct integration
DRG	directed relation graph
EOA	ellipsoid of accuracy
ICE-PIC	invariant constrained equilibrium edge pre-image curve
IEM	interaction by exchange with the mean
ILDm	intrinsic low-dimensional manifold
ISAT	<i>in situ</i> adaptive tabulation
LES	large eddy simulation
LUT	look-up table
ODE	ordinary differential equation
PaSR	partially stirred reactor
PDF	probability density function
PMSR	pairwise mixing stirred reactor
POD	proper orthogonal decomposition
PRISM	piece-wise reusable implementation of solution mapping
PSR	perfect stirred reactor
QSSA	quasi-steady state approximation
RANS	Reynolds averaged Navier-Stokes
RCCE	rate-controlled constrained equilibrium
RM	repro-modelling
S/M	skeletal mechanism
S/R	storage/retrieval
SA	sensitive analysis
SVD	singular value decomposition

Chemical Species

C_2H_2	acetylene
C_2H_4	ethylene
CH_2O	formaldehyde

CH_3	methyl radical
CH_3O	methoxy radical
CH_4	methane
CO	carbon monoxide
CO_2	carbon dioxide
H	hydrogen atom
H_2	hydrogen
H_2O	water
H_2O_2	hydrogen peroxide
HCO	formyl radical
HO_2	hydroperoxy radical
M	third body
N_2	nitrogen
NO_x	nitrogen oxide
O	oxygen atom
O_2	oxygen
OH	hydroxyl radical

“In questions of science, the authority of a thousand is not worth the humble reasoning of a single individual.”

Galileo Galilei (1564 – 1642) , *Third letter on sunspots to Mark Wesler* .

1

Introduction

This chapter presents a brief introduction of the applications of combustion phenomena to industrial processes, followed by the objectives and outline of this dissertation.

1.1

Historical and Economical Aspects

The combustion process is present in the history of mankind since the beginning of the first civilizations. The ability to control fire allowed significant changes in early humans lives. Mankind uses fire as a source of heat and light, which made possible to cook food, to stay warmed during the nights and cold weather, to keep the wild animals away, etc. Today, combustion plays a key role on the evolution and development of the modern civilization. Around 92% of all energy produced in the planet and 81% of the energy produced in Brazil uses combustion phenomena based processes (EPE, 2009) [16].

Table 1.1 shows the energy supply structure in Brazil in 2008 and in the world in 2007. From these data it is possible to see that a predominance exists of the processes that use combustion (biomass, coal, natural gas and oil and oil by-products) for energy production.

Table 1.1: Energy supply structure by source for Brazil in 2008 and World in 2007 (EPE, 2009) [16].

Source	Brazil (%)	World (%)
Biomass	28.6	9.8
Coal	5.8	26.5
Hydraulic and Eletric Energy	14.0	2.2
Natural Gas	10.3	20.9
Oil and Oil by-products	36.6	34.0
Other	3.4	0.7
Uranium	1.5	5.9

1.2

Combustion Applied to Industrial Devices

Combustion has a unique role in industrial and household applications. Some of the industrial and household devices that use combustion process on their operation are industrial process furnaces, burners, boilers, gas turbines, internal combustion engines, natural gas heaters, etc.

1.2.1

Industrial Process Furnaces

Industrial process furnaces are used, for example, as reactor and/or source of heat for the chemical reactions present in the refining and petrochemical industries. The design of these reactors should consider their function, mechanism of warming, fuel type and the oxidizer injection mechanism. Several industrial furnaces have major common characteristics, as represented in Figure 1.1 where a furnace and its process are shown.

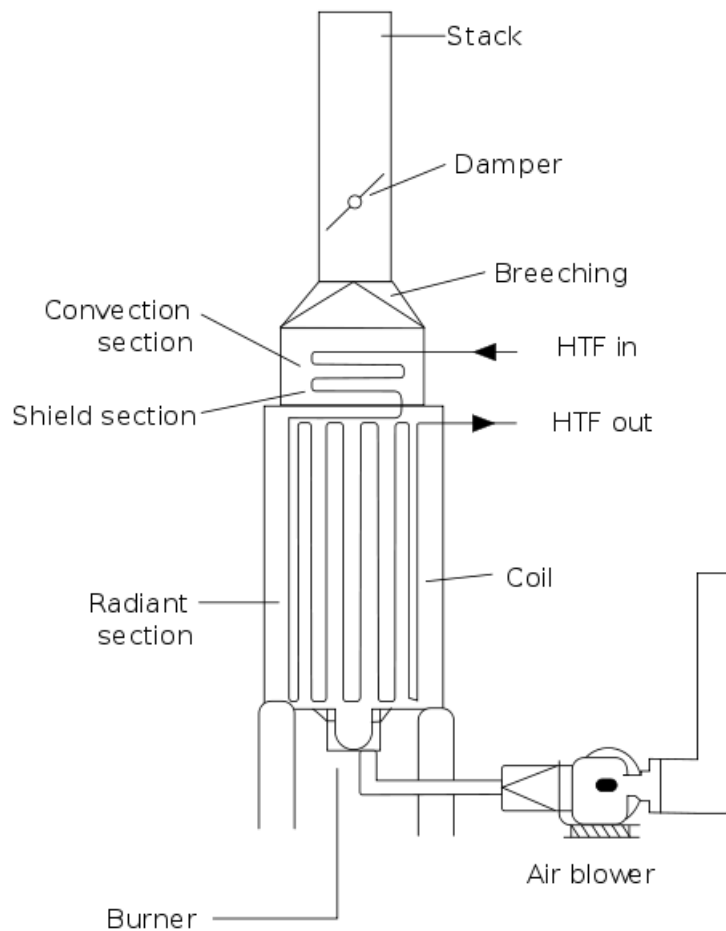


Figure 1.1: Schematic representation of an industrial process furnace. Adapted from <http://en.wikipedia.org/wiki/Furnace>

The fuel enters the burner and it is consumed along with the air supplied by the blower. At certain types of furnaces it is possible to find more than one burner, which can be arranged in cells, for instance. The burners may also be mounted on the floor, on the wall or on the ceiling of the oven (Baukal Jr. & Schwartz, 2001) [3].

In the radiant section, where combustion occurs, the flame heats the pipe, transferring heat to the fluid in its interior mainly by a radiative exchange mechanism (Baukal Jr. & Schwartz, 2001) [3]. The working fluid passing through tubes is heated until the desired temperature is reached. Downstream to the radiant section there usually exists a section where most of the heat is recovered by convection before the gases are expelled.

1.2.2 Gas Turbines

Gas turbines are rotating machines that convert energy from combustion process of an internal gas flow into electrical power, for instance. The gas turbine is designed to operate according to a Brayton cycle in which, firstly, the air is compressed isentropically, then, in a second stage, the pressurized air receives heat via the combustion process that occurs at constant pressure, next, the heated-pressurized air undergoes an isentropic expansion which takes the air to its initial pressure and, finally, the heated air is cooled to its initial temperature through a isobaric process.

The Figure 1.2 presents a sketch of a reverse flow combustor gas turbine. In the combustion chamber, fuel and air are mixed ignited. As a consequence, both the temperature and the specific volume of the gas increase, resulting in a flow velocity increment, which is directed to the expansion turbine blades.

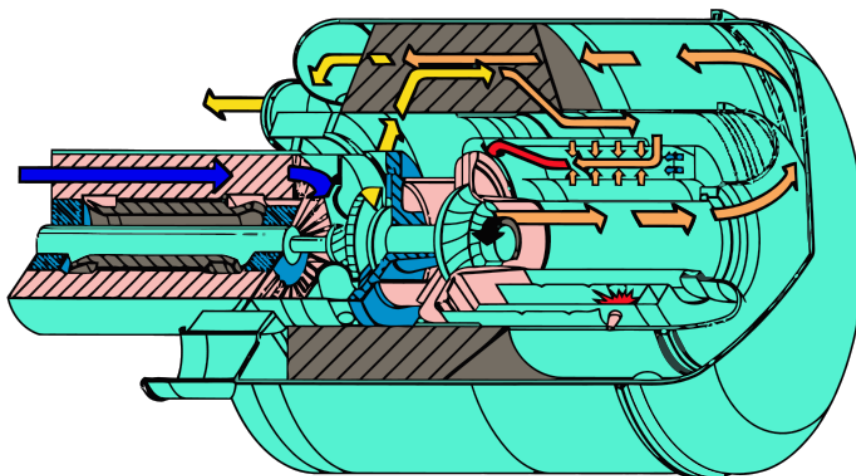


Figure 1.2: Sketch of reverse flow combustor gas turbine. Adapted from http://en.wikipedia.org/wiki/Capstone_Turbine

The energy resulting from this process may be extracted as axis work, compressed air or thrust, being used to supply systems such as aircrafts, ships, trains, electric generation plants, etc.

1.3 Fundamental Challenges

Most of the engineering problems related to combustion in industrial applications, regarding design and optimization of devices such as those described above, can be synthesized into two main aspects: energy efficiency and environmental control. Energy efficiency is the aspect related to the improvement of the thermodynamical performance of the process in which apparatus of interest operates, and may be summarized as the production of more outcome spending less energy. Environmental control is the aspect related to the decreasing of pollution generated by the process of fuel burning, in particular to the reduction of the emissions of chemicals harmful to human health or responsible for the greenhouse effect, such as nitrogen oxides (NO_x), carbon dioxide (CO_2) and soot.

Thermodynamical optimization devoted to obtaining a cleaner burning — with a lower level of pollutants emissions — is a multidisciplinary task that requires basic knowledge of thermodynamics, fluid mechanics and heat transfer. Besides the basic understanding of physical processes, to obtain solutions with the required accuracy for certain applications, sophisticated numerical techniques are increasingly used as predictive tools. The development of these techniques and their viable implementation, so that the solutions are obtained with the required precision in an acceptable time, is a challenging research area.

In the modeling of chemically reactive flows, difficulties are encountered due to the characteristics inherent to the complex nature of the combustion phenomenon. Furthermore, nearly all chemically reactive flows with practical applications operate in the turbulent regime. The modelling of combustion/turbulence interactions is an open problem, even after four decades of sustained research (Peters, 2009) [67].

In order to correctly predict the behavior of complex chemically reactive flows, the use of the large eddy simulation (LES) technique, coupled with a reaction mechanism that realistically describes the combustion process, is perhaps the most promising development. In particular, such a development requires two ingredients: a comprehensive detailed reaction mechanism and methodologies to reduce the reaction mechanism cost of use and stiffness (Lu & Law, 2009) [55].

1.4

Objectives of this Dissertation

The computational models for chemically reactive flows are very expensive in terms of time processing. These models demand the evaluation of the rate of reaction of the chemical species, which is a difficult task, in terms computer performance, due to numerical stiffness and its nonlinear nature. This dissertation aims to develop a technique to reduce the time complexity associated to the modelling of turbulent chemically reactive flows with detailed thermochemistry.

Techniques for reduction of reaction mechanisms and for efficient computation of the chemically reactive flows models with detailed thermochemistry are presented in this work throughout a literature review. The method dubbed *in situ* adaptive tabulation is implemented and tested in the simulation of stirred reactor models in order to evaluate its potential as an efficient strategy for the computation of realistic combustion thermochemistry in LES calculations.

1.5

Outline of this Dissertation

This dissertation is composed of seven chapters and three appendices. The second chapter presents a literature review of the existing techniques to reduce the size of a reaction mechanism and efficiently solve a chemically reactive flow model with detailed thermochemistry. The third chapter gives an overview of the fundamental aspects of modelling of stirred reactors. The fourth chapter presents a numerical procedure to integrate the governing equations of stirred reactors models. The fifth chapter develops the theory of the *in situ* adaptive tabulation. The sixth chapter describes the verification tests and the simulation results for a partially stirred reactor subjected to different parameters and reaction mechanisms. The seventh chapter summarizes the contributions of this dissertation, its main conclusions and suggests some paths for future works. The first appendix presents the procedure of construction of the dimensionless parameters. In the second appendix is shown the analysis of efficiency for *in situ* adaptive tabulation algorithm. Finally, the third appendix presents a conference paper which summarizes the main results of this dissertation.

2

Literature Review

In this chapter is presented a literature review concerning the existing techniques to reduce the size of a reaction mechanism and efficiently solve models for turbulent chemically reactive flows with detailed combustion thermochemistry. This review follows a historical perspective on the development of reduction techniques.

2.1

Introduction to the Reduction Approaches

According to Ren (2006) [76], among the existing methodologies to reduce the complexity of turbulent chemically reactive flows models with detailed combustion thermochemistry, three types of approaches have been shown to be particularly fruitful: (i) the reduction to skeletal mechanisms; (ii) dimension reduction; and (iii) storage and retrieval techniques. Combinations of these techniques are also reported in the literature.

In order to illustrate the possible interplay between the different techniques, Figure 2.1 presents a diagram with three sets, each one corresponding to reduction technique approach, namely: *reduction to skeletal mechanism (S/M)*; *dimension reduction (D/R)*; and *storage/retrieval (S/R)*. The regions where there is an intersection between the sets correspond to the hybrid approaches. In the sense of this diagram the ideal approach would be the one which could combine the advantages of the three techniques without the associated shortcomings. The following sections review these approaches from this point of view.

2.2

Reduction to Skeleton Mechanisms

The reduction of a detailed reaction mechanism, through a process which involves eliminating species and reactions that have a negligible influence on the combustion process results in the so-called skeletal mechanism. Due to the nature of the reduction process, such mechanisms are simpler than the original mechanism (Law, 2006) [45].

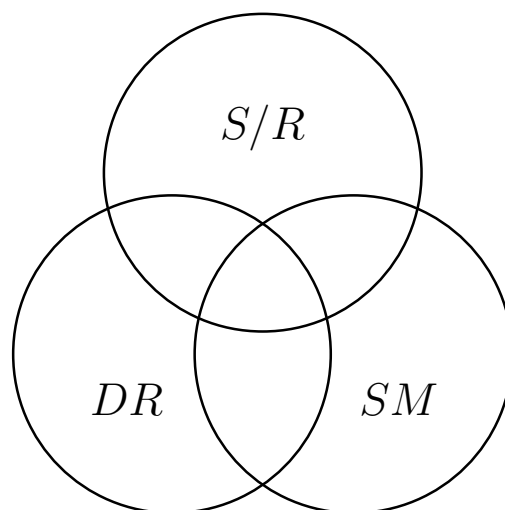


Figure 2.1: Illustration of the classification of the different approaches. S/M : reduction to skeletal mechanism; D/R : dimension reduction; S/R : storage and retrieval.

Skeletal mechanisms need to have quantified the resulting accuracy with respect to the original one. Such a measure could be given by comparing the calculated responses of system properties, such as mass fractions, temperature, etc., obtained from the skeletal mechanism to those issued from the detailed reaction mechanism.

2.2.1

Sensitivity Analysis

The procedure of *sensitivity analysis* (SA) is similar to that adopted in stability analysis, which is used in the nonlinear dynamical systems theory to interpret the bifurcation phenomena and to forecast the existence of oscillations. The basic underlying principle of sensitivity analysis is to determine the local behavior of the system subject to small disturbances in the phase space, i.e., to quantify how the system responds to variations on each of the controlling rate constants at a given set of conditions. The sensitivity coefficient, defined for a particular rate constant, is a measure of the importance for the system behavior of a particular reaction. A small — or even null — sensitivity to a perturbation is indicative that a specific reaction is redundant and could be removed from the reaction mechanism without affecting the overall accuracy (Griffiths, 1995) [25]. A complete overview on the sensitivity analysis technique is provided by Rabitz et al. (1983) [74].

This technique is a local approach — note that a global approach is also possible — with a rigorous mathematical foundation that allows eliminating all the reactions that exhibit low sensitivity to a given set of conditions. Although considerable reductions of reaction mechanisms can be achieved, it is possible that the reduced reaction mechanism generated in this way still has too many chemical species, making an associated numerical solution expensive, from the point of view of computational costs (Griffiths, 1995) [25].

Müller et al. (1992) [61] use the sensitivity analysis technique to reduce a detailed reaction mechanism for heptane with 1011 elementary reactions and 171 species to 79 elementary reactions and 40 species, which represents a reduction of approximately 77% of the number of species involved. As a consequence, the number of balance equations required to be solved in order to predict the system evolution is decreased accordingly.

2.2.2

Proper Orthogonal Decomposition

The technique of *proper orthogonal decomposition* (POD), also known as Karhunen-Loève decomposition or principal components analysis, involves a mathematical procedure which allows the transformation of a number of possibly correlated variables into a smaller number of uncorrelated variables, called principal components. This technique is an important complement to the sensitivity analysis in the context of skeleton mechanisms, since the last one is known to yield vast amounts of data, from which it may be difficult to determine the relative importance in complex systems (Jolliffe, 2002) [33].

The POD provides an absolute measure of how significant is part of the reaction mechanism. Thus, this analysis may be used to provide an objective criterion for selecting a reduced reaction mechanism. The analysis is based on the spectral decomposition (eigenvalues and eigenvectors) of the auto-correlation tensor, obtained from measurements, theoretical considerations or computer simulations. In the context of reaction mechanisms reduction, this tensor is represented, in an appropriate basis, by a data matrix in which the columns are the sensitivity coefficients. Its eigenvectors represent sets of reactions that are coupled and the relative magnitude of the vector components give relative contributions of it. The eigenvector components also contain information about the connections between the reactions. Thus, it is possible to determine which groups of reactions could be eliminated by establishing limits for the significant eigenvalue and eigenvector components (Griffiths, 1995) [25].

2.2.3

Directed Relation Graph

The technique called *directed relation graph* (DRG) proposed by Lu & Law (2005) [52] is an automatic general procedure to generate skeletal mechanisms from detailed thermochemistry. It consists on creating a relation graph where each node corresponds to a chemical species from the detailed reaction mechanism and the valued-oriented-edges express the dependence of a specific species in the rate of production of other species. Given an initial set of significant chemical species, the graph is recursively transversed until it is obtained a set with the minimum number of species that correctly describe the rate of production of the initial species. Then, the elementary reactions of the detailed reaction mechanism which do not include any of the species of the minimum set are eliminated. The skeletal mechanism is obtained by the union of the species in the minimum set and the remaining reactions.

The DRG method has two great advantages, when compared with the sensitivity analysis: (i) easy implementation; (ii) it is more efficient from the computational point of view, since the time of processing is linearly proportional to the number of species in the reaction mechanism (Lu & Law, 2005) [52].

Lu & Law (2005) [52] test the DRG technique to the reduction of a detailed reaction mechanism for ethylene oxidation with 70 species and 463 elementary reactions. DRG allows to obtain a skeletal mechanism with 33 species and 205 elementary reactions. This skeletal mechanism shows good agreement when compared to the detailed one for the calculations of a laminar flame speed and nonpremixed counterflow ignition for a wide range of pressure, temperature and equivalence ratio.

Lu & Law (2006a) [53] improved the capability of the DRG technique applying a new algorithm for the graph generation which is linear in the number of reactions. The new version of the DRG technique is applied to a n-heptane detailed reaction mechanism with 561 species and an iso-octane detailed reaction mechanism with 857 species, obtaining skeletal mechanisms with 188 and 233 species, respectively.

Pepiot-Desjardins & Pitsch (2008) [66] propose a variant of the DRG technique that uses a different strategy to quantify the interdependence of the chemical species. This new strategy allows one to generate more accurately the minimum sets of species. A test case is performed generating a skeletal mechanism for iso-octane with 195 species from a detailed one with 850 species.

2.3

Dimension Reduction

The dimension reduction approach is based on the assumption that a high-dimensional dynamical system can be parametrized in a low-dimensional subset of the original phase space. Some of the techniques that are part of this category consist on mathematical oriented approaches, mostly based on the theory of dynamical systems. Another possibility involves a large physical insight, which explores the restrictions imposed, for instance, by the second principle of thermodynamics in order to simplify the description of the system. A description of the dimension reduction techniques found in the literature that are relevant to the present study is given below.

2.3.1

Reaction Lumping

One early reduction technique involves the order reduction by lumping of variables. This approach is based on the transformation of the reaction vector to a lower dimensional vector of lumped-species (Okino & Mavrovouniotis, 1998) [64].

The reactive systems which present a number of chemical species tending to infinity and the decaying of the species following the same reaction order allow one to treat the reacting mixture as a continuous distribution. The technique of reaction lumping applied to these systems — known as *continuum lumping* — combines all the reactants into a single lump and tracks its disappearance. This method has the advantage of demanding only a small set of experimental data to fit the parameters of the reduced reaction mechanism, since specific reactions and components concentrations do not need to be known. This last characteristic is also a weakness, when the technique is applied to problems that require information about concentrations or reaction types, since such information is not easily extracted from or inserted into the continuum lumping (Okino & Mavrovouniotis, 1998) [64].

The application of the reaction lumping technique to reactive system for what a reaction mechanism is known — called *discrete lumping* — creates lumped models from the set of equations that govern the evolution of the reactive system. This technique presents, as positive points, the reduction of the chemical species number and the possibility of estimating the error introduced. As drawback, the reduced reaction mechanism generated by the discrete lumping may still contain multiple time scales and the technique limitates the information that can be extracted about a specific chemical species within a certain reaction structure (Okino & Mavrovouniotis, 1998) [64].

The technique of reaction lumping is discussed in Chen (1987) [9] where its application for hydrogen/air, methane/air and methyl radical/air combustion is illustrated. In this work a computer program is developed to construct reduced reaction mechanisms from detailed reaction mechanisms containing a large number of chemical species and elementary reactions. Reduced reaction mechanisms for methane/air and methyl radical/air combustion are obtained, making use (or not) of the steady state assumption for the hydrogen atom. A reduced reaction mechanism for lean air combustion, without C_2 chain reactions, is also obtained, leading to the conclusion that these reactions do not change neither the number nor the stoichiometry of the global reactions in the reduced reaction mechanism for methane, but changes reaction rates for the C_2 chain. Additionally, that study shows that the assumption of steady state for hydrogen atom alters the reduced reaction mechanism into a different form, i.e., the number and the stoichiometry of the global reactions are changed as well as their reaction rates.

2.3.2

Quasi-Steady State Approximation

The technique of *quasi-steady state approximation* (QSSA) is perhaps the oldest one concerning the reduction of reaction mechanisms. This technique was first developed by Bodenstein & Lind (1907) [6] and Bodenstein & Lütkemeyer (1924) [7] in the framework of the process of formation of hydrogen bromide.

The general formulation of the QSSA, independent of particular features of the system considered, given a general treatment for the error introduced by the QSSA is developed by Frank-Kamenetskii (1940) [19], see also Turányi & Tóth (1992) [93] and Turányi et al. (1993) [92].

The main idea of the QSSA technique is described as follows. Some chemical reactions present the formation of highly reactive intermediate species. After an initial buildup in concentration, these intermediate components are formed as rapidly as they are consumed, so that the rate of formation and the rate of consumption equilibrate. Due to this equilibrium, the rate of reaction of these species are negligible and, therefore, these species can be assumed as being in steady state. The steady state hypothesis allows the replacement of an ordinary differential equation (ODE) by an algebraic equation in the system of equations that describes the dynamical behavior of the chemical reaction. The use of the steady state assumption for several species provides a considerable simplification on the system dynamics (Turányi et al., 1993) [92].

When the QSSA technique is employed, the species for which steady state is assumed are called minor species, whereas the others are the major species. Keck (1990) [34] questions whether entropy production is always nonnegative — as required by the thermodynamics second principle — when QSSA is employed. In his work, the thermodynamical system composed by the major and the minor species is considered, and an expression is given for the entropy production of the system composed by two terms, one for the entropy production of the major species and another for minor species. The term associated with the major species is always nonnegative (≥ 0) and the term related to the minor species can be positive or negative. Thus, it is not possible to ensure that entropy production is always nonnegative. However, Ren & Pope (2004) [77] argument that QSSA is employed only when information about the systems major species is of interest, thus selecting only the major species as thermodynamical system is more appropriate than considering the system composed by the major and minor species. Ren & Pope (2004) [77] show that, for a system composed only by the major species, the elements conservation and the nonnegative entropy production are both satisfied.

Variants of the QSSA are developed, for example, by Lu & Law (2006b) [54]. This work involves eliminating part of — or even all — the nonlinearities of the set of algebraic equations obtained by employing the QSSA, resulting in a near-linear — or even linear — system of equations. If the resulting system is not linear, then it is linearized. Such a procedure is justified on the physical argument that the quasi-steady state species generally occur in low concentrations, such that the probability of collision between two minor species is smaller than the probability of collision of the major species. The linear system obtained is, in general, sparse and it is solved using a technique based on graph theory, which takes advantage of the sparse structure of the linear system to speed-up its solution. The technique allows the generation of a 16 species reduced reaction mechanism for a ethylene/air mixture, departing from a detailed reaction mechanism characterized by 70 species. Accurate and efficient results are demonstrated for the simulation of auto-ignition (relative error less than 0.1%) and perfectly stirred reactors (relative error less than 0.01%).

Hughes et al. (2009) [31] combine the use of the QSSA with local sensitivity methods, via reaction lumping, and consider reaction mechanisms for n-heptane and cyclohexane. A detailed reaction mechanism with 358 species and 2411 reactions is used for the n-heptane; whereas the reaction mechanism for the cyclohexane involves 499 species and 2323 reactions. The obtained

reduced reaction mechanism for n-heptane has 81 species and 452 reactions and yields an excellent reproduction of the temperatures evolution and prediction of the ignition delay time as a function of temperature, for a stoichiometric n-heptane/air mixtures at 13.5 bar. This reduced reaction mechanism leads to a computational cost which is less than 5% of that of the detailed reaction mechanism. The cyclohexane reduced reaction mechanism involves 26 species and 133 reactions, allowing a final computational cost that is 0.2% of the associated detailed reaction mechanism. The reduced reaction mechanisms also represents accurately the prediction of ignition delays. Both cases also exhibit an impressive speed-up of up to a factor of 500, when compared to the detailed reaction mechanisms, which are found to be proportional to square of the number of species.

2.3.3

Rate-Controlled Constrained Equilibrium

The *rate-controlled constrained equilibrium* (RRCE) technique proposed by Keck & Gillespie (1971) [35] assumes that the evolution of a complex system may be described, with an acceptable accuracy, by a relatively small number of reactions that mainly control the system evolution, the so-called rate-controlling reactions. These reactions establish constrains on the allowed states of the system that are slowly changing. This technique also assumes that the system relaxes to the associated constrained equilibrium state due to the existence of fast reactions. This relaxation occurs in time scales which are fast, when compared to that characteristic of the constraints evolution. Considering the above hypothesis, a thermochemical system in nonequilibrium state tends to relax to its final equilibrium state through a sequence of rate-controlled constrained-equilibrium states, each of which may be determined by maximizing the entropy of the system subject to the instantaneous values of the constraints. An extensive review of the RCCE technique is developed by Keck (1990) [34].

Some advantages that the RCCE technique offers are: (i) a small number of equations is required in order to predict the state of a complex system; (ii) the rate constants are necessary only to the calculation of the faster, rate-controlling, reactions; (iii) the balance principles are automatically satisfied, since they appear explicitly as constraints in the technique formulation; (iv) nonnegative entropy is guaranteed, as is the correct stable state of equilibrium; (v) the accuracy of the technique can be increased with the addition of new constraints, until the exact solution is obtained when the number of independent constraints equals the system's number of degrees

of freedom; (vi) the technique is extensible, i.e., different constraints may be included stemming from steady state reactions, body forces, selection rules and diffusion phenomena, for instance; and (vii) the technique is applicable to complex systems and its accuracy increases with the system size. Two obvious disadvantages are: (i) the need of a manual identification of the constraints; and (ii) the requirement for efficient algorithms for integration of the rate of reactions and to compute the conjugate Lagrange multipliers (Keck, 1990) [34].

This technique has been applied to high temperature reactions, for example, the calculation of the nitric oxide and carbon monoxide formation in internal combustion engines or industrial burners. Morr & Heywood (1974) [60] perform a 14 species and 2 constrains RCCE calculation to predict carbon monoxide concentration in a steady state cylindrical burner and compare the results with measured values. The first constrain is the total moles of gas, controlled by a set of four dissociation and recombination reactions. The second one is the carbon monoxide number of moles, controlled by five carbon monoxide oxidation reactions. The results obtained for carbon monoxide concentration using both constraints are slightly lower than the measured values, but lie within the combined uncertainty of the measurements and of the rate constants used. Keck & Gillespie (1971) [35] perform a 14 species and 2 constrains calculation to predict nitric oxide formation and removal in an internal combustion engine. The first constrain is on the fixed nitrogen controlled by a set of five chemical reactions. The second constrain considered is the total number of moles in the system. The results obtained with the 14 species and 2 constrains RCCE calculation are compared to those results obtained from a steady state solution. In the early engine cycle — when nitric oxide is being removed — the nitric oxide concentration obtained from the steady state solution is shown to be lower than nitric oxide concentration obtained from RCCE. The opposite behavior is observed for other cycles.

2.3.4 Computational Singular Perturbation

The *computational singular perturbation* (CSP) technique proposed by Lam (1985) [42] and discussed in detail in the works of Lam (1993) [43] and Lam & Goussis (1994) [44], is a general procedure for analysis and reduction of thermochemical systems. This method is a formal mathematical approach that does not only simplify reaction mechanisms but also reduces the set of governing equations of the system. The CSP technique allows one to automatically decouple the system time scales in fast and slow modes. The fast modes are those time scales which are less than a desired time resolution,

the others are called slow or active modes. It follows the elimination of the exhausted and dormant modes. The exhausted modes are the time scales that decay due to the competition between consumption and generation of species and are not significant for the behavior of the system after certain period. The dormant modes have no influence on the system dynamics, since they are much slower than the active modes. The technique iteratively identifies a basis of vectors that allows one to decouple the time scales in fast and slow modes.

The main advantages of the CSP technique are: (i) that important reactions can be identified only using data from the reduced system, in opposition to SA, which needs information from the full system; (ii) no *a priori* knowledge about the system dynamics is required; (iii) the method is applicable to problems with multiple time scales. A disadvantage associated to the CSP technique is the impossibility of determining *a priori* the size of the regions which the technique is applicable (Okino & Mavrouniotis, 1998) [64].

Goussis & Lam (1992) [23] develop a study of the homogeneous oxidation of methanol/air at constant pressure using CSP. A numerical experiment is performed using a fuel-lean (equivalence ratio = 0.6) mixture at a pressure of 1 atm and temperature of 1027 K. A reaction mechanism with 30 species and 173 reactions is used. The reduced system obtained includes 16 species and produces results nearly identical to those of the full reaction mechanism for the hydrogen atom and carbon monoxide mass fractions with error smaller than 1%.

2.3.5 Intrinsic Low-Dimensional Manifold

Maas & Pope (1992a) [58] develop a general procedure for reducing reaction mechanisms called intrinsic low-dimensional manifold (ILDM). This geometrically-based technique is issued from the dynamical systems theory. Based on a local spectral analysis (eigenvalues) of the linearized system of governing equations, the fast time scales of the chemically reacting system are identified. Then, assuming that these fast time scales, which are associated with relaxation processes in chemical reaction, proceed infinitely fast, i.e., that these processes are in local equilibrium, the space state may be globally simplified. This simplification results on a reduced number of parameters, or progress variables, which allows a considerable reduction in the number of differential equations that have to be solved.

In contrast to other techniques, such as the QSSA, no assumption is required about reactions in partial equilibrium or species in steady state. The ILDM is formed upon specification of the desired reduced system dimension

only. The simplification procedure is automatic, once it is given the state properties as functions of the reduced parameters, i.e., the coordinates that parametrize the system in the low dimensional manifold. This characteristic is valuable when high dimensional systems are of interest. After the reduction of the system dimension, the reduced system properties are stored in a multi-dimensional table to be recovered *a posteriori* via multi-linear interpolation (Griffiths, 1995) [25].

Maas & Pope (1992a) [58] apply the ILDM technique to the reduction of a reaction mechanism with 13 species and 67 reactions to describe the combustion of carbon monoxide-hydrogen/air in a spatially homogeneous, closed, adiabatic, isobaric reactor. Both one-dimensional and a two-dimensional manifolds have been generated which correctly represent the major and the minor species in the nonequilibrium evolution of the chemical system.

Maas & Pope (1992b) [57] develop a procedure to apply the ILDM technique to reactive systems where molecular transport is present. The study of a perfect stirred reactor model demonstrates that the reduced reaction mechanisms obtained by this technique provide a good description of the detailed evolution in situations where the time scale of the physical process is reasonably slower when compared to the fast, decoupled, time scales. This study also shows that when the time scales difference become too small, the ILDM technique demands a higher dimensional manifold in order to correctly predict the reactive system behavior.

The storage of the reduced information in a multi-dimensional table requires a large amount of memory. In order to overcome this difficult Niemann et al. (1997) [63] propose an ILDM approach which uses orthogonal polynomials to interpolate the stored reduced information obtained from a tabulation step which computes the system properties as function of the progress variables in a coarse grid among the system phase space. This procedure allows the decreasing of the ILDM mesh resolution, and thus the storage requirements. For instance, storage is reduced by a factor of 200 when a stoichiometric hydrogen/oxygen system is considered.

König & Maas (2005) [40] introduce a mathematical approach to the calculation of ILDMs sensitivities with respect to kinetic data. This method is applied to a $CO/H_2/O_2/N_2$ -system, which consists of 13 species that react in 67 elementary reactions. The temperature of the unburnt gases is 298 K, and the syngas mixture is stoichiometric with a proportion (in volume) for $CO:H_2:N_2$ equal to 4:3:3. The validity of the technique is demonstrated by a comparison between results obtained via ILDM calculations of a perturbed and

an unperturbed reaction mechanism. The study also shows that the behavior of reduced reaction mechanism obtained via this ILDM approach is qualitatively comparable to the behavior of the corresponding detailed reaction mechanism.

König & Maas (2009) [41] develop an technique to generate on demand ILDMs in generalized coordinates extensible to the domain of slow chemistry using a hierarchical concept that progressively increases the original manifold dimension. Also, in this version of the ILDM technique the tabulation of the system properties as function of the reduced variables is made on demand, i.e., only the actually accessed part of the phase space is tabulated allowing to reduce the amount of memory and computational time spent during the ILDM calculations. A syngas/air one-dimensional calculation for a free, adiabatic, premixed, flame in a laminar flow field is used to validate the technique. A reaction mechanism with 13 species and 67 reactions describes the chemical kinetics of this system. The new technique presents an 82% of reduction in memory storage and 22% of reduction in computational time when compared to the classical ILDM approach.

2.3.6

Proper Orthogonal Decomposition

When used as a technique of dimension reduction, POD is used to determine spatial structures that are time applicants called coherent structures. These coherent structures allow the construction of a reduced model in which the dynamical behavior is representative of the original system, since they preserve most of the original system information (Holmes et al., 1998) [30]

The POD procedure can be summarized as follows. Consider a process that varies in time and space and that, after an initial transient, approaches a steady state. Sample discrete data from this process are obtained by following the evolution in time of a set of initial conditions. Then an auto-correlation tensor is computed, where its components are covariances between these discrete data, considering the time average as the ensemble average. The eigenvectors of this auto-correlation tensor are the coherent structures described above and form the basis that maximizes the expectation of information from the original system (Holmes et al., 1998) [30].

The reduced reaction mechanism is obtained by projecting the full reaction mechanism into the subspace spanned by the eigenvectors that correspond to the largest eigenvalues. The nonlinear behavior of the original model is preserved, once the nonlinearity is invariant by projection into a linear of affine space. Also, the method demands only standard matrix operations, which is attractive from the computational point of view (Pinnau, 2008) [68].

Graham & Kevrekidis (1996) [24] propose an alternate approach for the POD technique, in which the sample discrete data is obtained from the short time integration of a large set of initial conditions. This approach is used to study the dynamics of a reaction-diffusion system, using the short time integration of 1000 initial conditions to construct the auto-correlation tensor. The reduced model obtained from the new procedure is shown to contain information about the global dynamics that is not contained in the reduced model obtained from the standard POD approach.

Singer & Green (2009) [86] combine an adaptive strategy for the POD method with an operator splitting technique to study the evolution of a reaction-diffusion system. The technique is applied to an one-dimensional laminar premixed methane/air flame using GRI mechanism version 3.0 [89], with 53 species and 325 reactions. The results of the simulation show that temperature and species mass fractions are predicted with an error smaller than 0.25% when compared with the direct integration of the full reaction mechanism. A speed-up factor of 3.5 is reported, which is related to the fewer evaluations of the source term required to compute the Jacobian matrices.

Berkooz et al. (1993) [4] and Hølems (1998) [30] provide a comprehensive review of the POD technique, including the associated mathematical properties. Rathinam & Petzold (2004) [75] discuss other theoretical considerations related to POD technique such as: (i) errors involved in solving a nonlinear ODE initial values problem with POD; (ii) the study of small perturbations in the ensemble of data from which POD reduced model is constructed; (iii) an analysis of computational complexity of solving ODE initial value problem; and (iv) the study of savings obtained by the use of POD technique.

2.3.7

Invariant Constrained Equilibrium Edge Pre-image Curve

The *invariant constrained equilibrium edge pre-image curve* (ICE-PIC) is an automatic dimension reduction technique developed by Ren et al. (2006) [80]. The fundamental idea of ICE-PIC method is the identification of a low-dimensional manifold which is invariant, continuous and piecewise smooth. The reactive system is parametrized in this low-dimensional manifold and when the full composition of the chemical species needs to be locally recovered from the reduced composition in the low-dimensional manifold, the pre-image curve technique proposed by Ren & Pope (2005) [78] is used. The term “locally recovered” means that, for the ICE-PIC technique to reconstruct the species properties from the reduced composition, it is not necessary to reconstruct the

whole manifold. The ICE-PIC technique is tested in the simulation of a steady, isobaric, adiabatic, one-dimensional premixed laminar flame of a stoichiometric hydrogen/air mixture with an unburnt temperature of 300 K and pressure of 1 atm. The mixture thermochemistry is described by reaction mechanism of Li et al. (2004) [48] (9 species and 21 reactions). The simulations show that compared to the results obtained with PREMIX code by Kee et al. (1985) [36], the ICE-PIC accurately reconstructs the species composition and system temperature (normalized errors smaller than 1.5×10^{-3}). Compared to QSSA and RRCE, ICE-PIC technique yields the smaller maximum error. Considering the ILDM method, it is possible to obtain maximum error smaller than that obtained with ICE-PIC, but ILDM is a technique in which the low-dimensional manifold does not exist for all ranges of temperatures.

Ren et al. (2007) [81] use the ICE-PIC technique to study the autoignition of a homogeneous, adiabatic, isobaric, stoichiometric methane/air mixture at 1500 K and 1 atm, described by GRI mechanism version 1.2 [89] (32 species and 175 reactions). The results of ICE-PIC are shown to be at least 2 orders of magnitude more accurate than QSSA and RCCE techniques. This work also investigates the application of a variant of the ICE-PIC method for an inhomogeneous system: a steady, one-dimensional, adiabatic, isobaric, laminar flame of stoichiometric methane/air mixture also described by GRI 1.2 [89], with an unburnt temperature of 298 K and pressure of 1 atm. The results show that the inclusion of transport coupling in ICE-PIC formulation can reduce the error associated to the reduction of dimension by a factor of a hundred.

The capability of the ICE-PIC technique to treat a combustion system that exhibits a complex dynamics is tested and demonstrated by Ren & Pope (2007a) [79]. In this work, the ICE-PIC technique is applied to the oxidation of a carbon monoxide/hydrogen mixture in a continuously stirred tank reactor at low pressure, the same system described by Brad et al. (2007) [8]. A reaction mechanism with 11 species and 33 reactions is used in the modelling of the reactive mixture. The simulation results show that a reduced description using a low-dimensional manifold of dimension five is able to quantitatively predict the complex dynamics of the continuously stirred tank reactor. This study also shows that the ICE-PIC method is not sensitive to changes in the coordinates (species) that parametrize the reduced system, which is an advantage when compared with QSSA and RCCE methods.

2.4

Storage/Retrieval

The storage/retrieval approach stores the simulation results for *a posteriori* use (retrieval). This approach presents some variants for data storage, such as multi-dimensional tables, binary search trees, etc., but the retrieval is done basically via multi-dimensional interpolation or extrapolation.

2.4.1

Look-Up Table

A *look-up table* (LUT) is a data structure often used to replace an ODE integration with an array indexing operation. The savings, in terms of processing time, can be significant, since retrieving a value from memory is often faster than solving a differential equation. This technique presents a pre-processing step, where direct integration of the governing equations is performed, and the results are tabulated. In the simplest approach, the region of interest in the domain is covered with a regular mesh and the equations are solved for each point of this mesh. Then, *a posteriori* calculations are performed via multi-linear interpolation from tabulated values.

The major advantages of the LUT technique are: (i) the possibility of controlling the interpolation error by refining the mesh; and (ii) the speed-up in the time spent to solve the governing equations. However, the technique has limitations, mainly due to the large amount of memory required to store the table.

Chen et al. (1989 [11] and 1995 [10]) present applications of the LUT technique. The first work uses the LUT technique to efficiently solve the equations corresponding to the probability density function (PDF) modelling of a turbulent nonpremixed methane flame, whereas the second deals with the simulation of a hydrogen flame and prediction of NO_x emissions.

Ribert et al. (2006) [82] propose a technique, called self-similarity flame tabulation, to tabulate turbulent combustion properties using a detailed reaction mechanism. In this technique the species reaction rates and mass fractions are tabulated as function of a limited set of coordinates, such as progress variable, mixture fraction, enthalpy, etc., obtained from the simulations of a one-dimensional laminar premixed flames. The species mass fractions and reaction rates present a self-similar behavior with the progress variable, which is explored in the tabulation technique in order to reduce the size of the tabulation table. This technique has been applied, for a fixed value of initial pressure and temperature, to several adiabatic one-dimensional laminar premixed methane/air flames, for different values of equivalence ratio.

The simulations use the Qin et al. (2000) [73] reaction mechanism, with 34 species and 463 reactions, and the PREMIX code by Kee et al. (1985) [36]. The look-up table stores reduced values of species mass fraction and reaction rates as function of the sum of the CO and CO_2 mass fractions and the corresponding scaling relations, which are functions of the mixture equivalence ratio. The simulations using the new technique are verified by comparisons with numerical results obtained using a detailed reaction mechanism, and presented good agreement with the values obtained from a detailed chemistry for several simple hydrocarbon fuels (methane, propane and ethane) and various values of equivalence ratio.

Fiorina et al. (2009) [17] proposed a tabulation strategy that also explores the self-similar properties of tabulated species mean reaction rates in order to decrease the demand for storage memory in the look-up table. A successful application of this technique is reported to a Reynolds Averaged Navier-Stokes (RANS) simulation of a nonpremixed turbulent methane/air flame, the *Sandia Flame D*, experimentally addressed by Barlow & Frank (1998) [2]. A reduction of three orders of magnitude in look-up tables storage memory is obtained with excellent agreement between computations using detailed reaction mechanism and reduced look-up table.

2.4.2

Repro-Modelling

Turányi (1994) [94] proposes the *repro-modelling* (RM) technique, which, for a detailed reaction mechanism, extracts functional relationships between the system properties (species concentration, temperature, etc.) and the species reaction rates. The extracted information is stored in a multivariate polynomial of high order and may be accumulated from a large number of simulations for a specific range of conditions. This data is then used to evaluate the governing equations, a procedure which is faster than to simulate using the detailed reaction mechanism.

Turányi (1994) [94] applies this technique to simulate the ignition of wet carbon monoxide in air. The repro-modelling obtained a speed-up of 24,000 and 11,700, respectively, using two or three variables in comparison to the solution using detailed thermochemistry, given by the SENKIN code (Lutz et al., 1987) [56].

2.4.3

Piece-Wise Reusable Implementation of Solution Mapping

The *piece-wise reusable implementation of solution mapping* (PRISM) technique proposed by Tonse et al. (1999) [91], consists in partitioning the chemical phase space into adjacent hypercubes. As the reaction trajectory evolves in composition space, polynomials are calculated for a given hypercube when the trajectory first enters it. From a set of polynomials it is possible to obtain the time evolution of any composition within the hypercube. Then, the hypercube and polynomial information are stored in a particular data structure, which is a combination of a binary tree and a double-linked list, for being reused in future. As the calculations proceed, instead of solving differential equations, only algebraic polynomials evaluations are necessary to predict the system evolution.

The PRISM technique has been applied to three different hydrogen combustion simulations (Tonse et al., 1999) [91], using a reaction mechanism with 9 species and 26 reactions. The simulated cases are: (i) a zero-dimensional, stoichiometric, premixed hydrogen/air mixture with an initial temperature of 1200 K; (ii) a one-dimensional premixed laminar flame, in a 10 mm tube closed in one end and open in the other at atmospheric pressure, filled near the open end with burned gas, while the remaining is filled with stoichiometric hydrogen/air mixture at room temperature; (iii) a nonpremixed two-dimensional turbulent jet with coaxial hydrogen (21 m/s and 300 K) and air (1 m/s and 300 K) inflows. All the simulated cases present an excellent accuracy, the relative error is smaller than 0.2%, for temperature and species mass fraction, and the computational efficiency, compared to the direct integration of the governing equations is increased by a factor of 10.

Najm et al. (2005) [62] propose a novel implementation of the CSP technique combined with the PRISM technique, involving an adaptive tabulation of the basis vectors, which allows fast identification of the reduced chemical model at any point of the phase space. In the new technique, first, the CSP is used to reduce the dimension of the chemical phase space, then, the PRISM technique is applied in order to efficiently compute the system evolution. The key point is that first applying CSP allows the PRISM tabulation procedure to construct low dimensional hypercubes, since the dimension of the new chemical phase space is smaller than the original one. This technique is applied to a four-dimensional system of stiff ODE in order to assess its efficiency, showing a high level of accuracy, relative error less than 2%, and yielding a significant reduction in computational time.

2.4.4

Artificial Neural Network

An *artificial neural network* (ANN) is a computational model inspired by the structure of the brain, in order to provide features similar to human behavior, such as learning, association, generalization and abstraction. The ANN are composed of several processing elements (artificial neurons), highly interconnected, that perform simple operations and send the results to neighboring processors. Due to its structure, the neural networks are very effective in learning patterns from data nonlinear, incomplete, noisy and even composed of contradictory examples. Examples of typical applications are: pattern recognition, time series forecasting and classification, (Gurney, 1997) [26].

Christo et al. (1996) [12] introduce an integrated approach using ANN and joint PDF transport equation for the simulation of turbulent flames. A hydrogen/carbon dioxide turbulent jet diffusion flame is modelled using three step reduced reaction mechanism. The results show good agreement of flame and flow characteristics with those obtained by LUT or direct integration procedures. For small reaction mechanisms, the ANN method does not show significant gains in computational time and memory storage, when compared to LUT and direct integration techniques.

Blasco et al. (1999) [5] introduce an ANN approach which partitionates the computational domain and trains the neural network for each sub-domain. This method allows the increasing of solution accuracy. The method is tested in a methane/air system evolving according to a reduced reaction mechanism with 7 species and 4 reactions. The ANN approach presents a speed-up factor of 2750 times, when compared to the direct integration procedure, and demands 1000 times less memory for storage than the LUT technique. The method also presents an average error of 0.64%.

Ihme et al. (2009) [32] use an optimized ANN approach in the large eddy simulation of Dally et al. (1998) [15] bluff-body swirl-stabilized methane-hydrogen/air flame. The chemically reactive flow field is modelled using a flamelet/progress variable approach. The study shows that the accuracy of the optimized ANN in LES simulations is comparable to the accuracy of the refined structured tables, but with a smaller memory storage cost. Data retrieval from an ANN is shown to be more expensive, when compared to LUT techniques. The integrated approach LES/ANN presents good results when compared to experimental data for the mean and variance of the velocity components, mixture fraction, temperature, H_2O and CO_2 mass fractions. Small discrepancies on CO_2 profiles in the fuel-rich side of the flame are observed, possible due to CO_2 sensibility to changes in the progress variable.

2.4.5 In Situ Adaptive Tabulation

The methodology dubbed *in situ adaptive tabulation* (ISAT), proposed by Pope (1997) [70], consists in progressively creating (*in situ*) a binary search tree which stores in its leaves an initial composition, its time integral value and the corresponding jacobian matrix. A search is performed along this binary search tree whenever the integration of the governing equations is required and a tabulated solution is recovered. If the information recovered from the tree is satisfactory, in the sense that an error tolerance is such that the recovered solution lies inside an ellipsoid of accuracy, a linear extrapolation using the tabulated values issued to provide an adequate approximate solution. This approximate solution has a local error which is second order accurate in time, thus ensuring that the global error is of first order.

The ISAT technique presents an advantage, when compared to LUT techniques, in terms of memory savings. Since the tabulation is performed *in situ* only the compositions that effectively occur in the flow are tabulated, thus leading to large memory savings. This is a significative advantage when dealing with complex reaction mechanisms. Furthermore, the error control allows the usage of a conservative criterion for choosing an error tolerance. However, when a large reaction mechanism is involved and the frequency of additions in the binary search tree is high, the memory usage of the ISAT technique is significant. The major advantage of the ISAT technique, compared to the other storage/retrieval approaches, is the coupling flexibility, which allows ISAT to be used in parallel with practically all of the other methodologies presented herein.

Yang & Pope (1998b) [98] apply the ISAT technique for calculations in the first few principal directions of the composition space — the mixture properties at a given thermodynamical state that present more sensibility to variation on this state — for a premixed pairwise mixing stirred reactor. Two reaction mechanisms are used, a skeletal one (16 species and 40 reactions), for methane/air mixture combustion and the GRI mechanism version 2.11 [89] (49 species and 279 reactions), for natural gas combustion with air. The results show very good accuracy for species mass fraction in both cases, with tabulation error smaller than 4.0×10^{-4} when compared to the direct integration of the governing equations. This variant of ISAT only tabulates the accessed region of the composition space, which allows the ISAT technique to perform few additions and several recoveries in the binary search tree. Thus, the method presents an impressive speed-up factor of 1,655 for methane/air system, when compared to the direct integration of the skeletal mechanism.

Saxena & Pope (1998) [83] model a piloted jet diffusion flame of methane/air using an approach based on the joint PDF. This flame corresponds to the *Flame L* that has been characterized experimentally by Masri et al. (1988) [59]. The domain of calculation consists of a coflow burner, with a central jet of methane (300 K and 41 m/s) with radius equal to 3.6 mm and an outer annulus jet of air (300 K and 15 m/s) with radius equal to 9 mm. The ISAT technique is used to efficiently solve the governing equations for the skeletal mechanism which contains 16 species and 41 reactions. The obtained results of mixture fraction, temperature and species mass fraction are compared to other numerical studies using simpler reaction mechanisms. The results show a better qualitative agreement with the experimental data than other works.

Saxena & Pope (1999) [84] investigate performance, issues such as accuracy, efficiency and storage requirements, in the use of ISAT technique to numerically solve the joint PDF of velocity-frequency-composition in a turbulent chemically reactive flow. To examine the accuracy, the ISAT error control is analyzed in the simulation of a pairwise mixing stirred reactor with a skeletal methane/air mechanism (16 species and 41 reactions). It is shown that minor species incur a larger global error than the major species. The ISAT technique shows to be efficient to solve the joint PDF, with a speed-up of up to 60 over the direct integration of the governing equations. This work also shows that, for 100 stochastic particles, the storage requirements of ISAT for the finest error tolerance (0.0008) is 50 Mbytes, a reasonable value.

Tang & Pope (2002) [90] develop a hybrid methodology for thermochemistry reduction in turbulent reactive flows, combining the dimension reduction of RCCE and tabulation of ISAT. Firstly, the RCCE technique is used to reduce the reaction mechanism size, then, the *in situ* tabulation is performed to efficiently solve the governing equations. Nonpremixed methane/air combustion in a statistically homogeneous turbulent reactor is addressed using GRI mechanism version 1.2 [89] (32 species and 175 reactions). A direct integration of the governing equations with the full reaction mechanism is also performed and considered to be the exact solution. The hybrid technique uses as constraints for RCCE, the four chemical elements conservation, enthalpy conservation and the following chemical species: H_2O , CO_2 , O_2 , CH_4 , CO , H_2 , OH , O , CH_3 , C_2H_2 , and C_2H_4 . Thus, the resulting reduced reaction mechanism is 16-dimensional and shows a good agreement with the exact solution, with an error smaller than 3% for density, temperature and major species. The hybrid approach also obtains a speed-up factor of about 500, when compared to the direct integration.

Singer & Pope (2004) [87] use the ISAT technique together with a splitting technique to solve a reaction-diffusion equation. The ISAT technique is used to solve pure reaction substep, whereas an implicit Crank-Nicolson finite difference technique is employed for the pure transport substep. The resulting numerical scheme, which is second order accurate in time and space, is applied to the simulation of a stoichiometric premixed hydrogen/air laminar flame using a reaction mechanism with 9 species and 19 reactions. The simulation results show that the numerical scheme is more sensitive to variations on ISAT error tolerance than in the ODE solver absolute error tolerance. This study also shows that ISAT allows to obtain a speed-up of 4.5 – 5, when compared to the direct integration of the governing equations for the reaction-diffusion model.

Liu & Pope (2005) [49] characterize the local and the global errors of the ISAT technique when used in conjunction with transported PDF methods. The object of study in this work is a nonpremixed turbulent methane/air flame experimentally addressed by Barlow & Frank (1998) [2]. The computational fluid dynamics package FLUENT is used to perform RANS simulations of the governing equations, with $k - \epsilon$ turbulence model and ISAT to efficiently solve the thermochemistry described by skeletal mechanism with 16 species and 41 reactions. Their work investigates the ISAT local error through the implementation of three different adaptive strategies, i.e., growth of the ellipsoids of accuracy. The analysis of the cumulative distribution function of local error shows the local error well controlled, but a large error is shown to be possible despite improbable. The global error is quantified and demonstrated to be small, when compared to statistical error, for tolerance values smaller than 10^{-4} . The global error is also shown to vary linearly with the ISAT error tolerance.

Singer et al. (2006) [88] perform the simulation of two-dimensional unsteady laminar reacting flows using ISAT technique. This work presents an operator splitting technique which used ISAT to solve the pure reaction substep and stabilized Runge-Kutta technique for pure transport substep. The numerical scheme is parallelized using a combination of OpenMP and MPI libraries and applied to the interaction of a laminar premixed methane/air flame with a counter-rotating vortex pair. The reaction mechanism used is the GRI mechanism version 3.0 [89], which has 53 species and 325 reactions. The simulation results show that an overall speed-up factor of approximately 2.5 – 3 times is achieved by the use of ISAT, when compared to the direct integration of the governing equations.

Lu et al. (2009) [50] develop parallelization strategies for ISAT technique. In essence, these parallelization strategies are smart ways to distribute the calculations tasks among various binary search trees. In a multi-processor environment calculation using parallel ISAT, the computational domain is decomposed into various sub-domains and each one of these are passed to a processor. Each one of these processors has its own binary search tree. Before or after a pure reaction fractional step, particles in one processor may be passed to one or more processors by distribution strategies to be solved there via serial ISAT. Three different distribution strategies have been tested. In the first strategy, there is no message passing, the evolution of each particle at a sub-domain is computed locally via serial ISAT. In the second strategy, all the particles at a group of sub-domains are randomly uniform distributed among the sub-domains of this group via message passing. Then serial ISAT is used to compute their evolution. In the third strategy, the particles of a group of sub-domains present a preference for some processors, e.g., those processors that they have not visited previously. Combinations of these strategies or adaptive strategies of the distribution are also possible. Numerical experiments using different parallelization strategies are performed in a methane/air partially stirred reactor, subject to different parametrical configurations. The adaptive strategy shows good parallel scalability and it is the only that yields a good performance for all parametric configurations tested, achieving a speed-up factor of up to 30 compared to the strategy with no message passing.

Lu & Pope (2009) [51] propose an improved version of the ISAT technique, which includes four search strategies for a query composition: the usual search in the ISAT tree; a list with the most recently used compositions; a list with the most frequently used compositions and the search in a binary search tree which has an ellipsoid associated to each node and leaf. Also, this improved ISAT verifies if a query composition lies inside the ellipsoid of accuracy by using the ellipsoid projection into an affine space. There is also defined an ellipsoid of inaccuracy, which is an upper bound for the region of accuracy. An error checking and correction criterion is introduced and allows the efficiently reduction of ISAT local error. The performance of the improved ISAT technique is compared to that of a previous version for two cases of methane/air combustion in partially stirred reactor. The first case uses a skeletal mechanism (16 species and 41 reactions), whereas the second uses the GRI mechanism version 3.0 [89] (53 species and 325 reactions). The simulation results show that the new algorithm demands less computational time and memory storage than the older version by factors of 2 and 5, respectively.

2.5

The State of the Art

The hybrid methodologies are those which combine two or more existing approaches for reduction reaction mechanisms. These sophisticated techniques envisage the best use of two or more well established techniques in order to achieve performance gains.

Among the different methodologies presented in this review, the hybrid approaches are surely the most promising, since they present excellent results, in terms of accuracy and computational cost. These virtues are associated to the combination of the advantages of well established techniques. The hybrid class can be considered in general as the state of the art in reduction of combustion chemical kinetics. The ICE-PIC technique combined with the ISAT storage/retrieval seems to be the most attractive reduction methodology available.

Pope & Ren (2009) [72] review the state of the art on efficient implementation of combustion thermochemistry in turbulent chemically reactive flows by the Turbulence and Combustion Group at Cornell. This review address the ICE-PIC technique to obtain a reduced models for chemically reactive flows; the coupling between thermochemistry and macroscopic transport in these reduced models; the development of efficient operator splitting schemes for chemically reactive flows; and the recent improvements in ISAT technique.

The remainder of this work is devoted to the presentation and to the study of an ISAT technique. Even if the chosen technique falls short to the state of the art, it is a fist stepping stone in more advanced developments.

3

Modelling of Stirred Reactors

In this chapter the fundamental aspects related to the modelling of stirred reactors are presented. These aspects cover basic definitions about the gas system, the principles of gas phase thermochemistry, the balance equations from continuum mechanics, two models for a spatially homogeneous transient reactor and a geometrical interpretation of the chemical reactors equations on the basis of the theory of dynamical systems. The presentation of the chemical transformation assumes that the continuum hypothesis is valid for the reactive gas mixture when such a mixture flows through a control volume.

3.1

Fundamental Definitions

The *molar fraction* of the i -th chemical species is defined as

$$X_i \equiv \frac{n_i}{n}, \quad (3.1)$$

where n_i is the number of moles of the i -th chemical species, n is the system total number of moles, i.e.,

$$n \equiv \sum_{i=1}^{n_s} n_i, \quad (3.2)$$

where n_s is the number of chemical species. It follows from the definition that X_i satisfies

$$0 \leq X_i \leq 1, \quad \text{and} \quad \sum_{i=1}^{n_s} X_i = 1. \quad (3.3)$$

The *mass fraction* of the i -th chemical species is defined as

$$Y_i \equiv \frac{m_i}{m}, \quad (3.4)$$

where m_i is the i -th chemical species mass and m is the system total mass, i.e.,

$$m \equiv \sum_{i=1}^{n_s} m_i. \quad (3.5)$$

It follows straightforward from the definition, that Y_i satisfies

$$0 \leq Y_i \leq 1, \quad \text{and} \quad \sum_{i=1}^{n_s} Y_i = 1. \quad (3.6)$$

The *molar mass* of the i -th chemical species, W_i , is defined as the mass of 1 mol of this species, i.e., N_A particles, where $N_A = 6.023 \times 10^{23}$ is the *Avogadro number*. The sum of the molar masses of all the species that compose a homogeneous gas mixture weighted by the molar fraction is the *mean molar mass* of the mixture,

$$\bar{W} \equiv \sum_{i=1}^{n_s} X_i W_i. \quad (3.7)$$

Mass fraction and molar fraction are two different concepts used to describe the amount of a chemical species in a gas mixture, and may be related with the help of \bar{W} and W_i ,

$$Y_i = \frac{W_i}{\bar{W}} X_i. \quad (3.8)$$

The *molar concentration* of the chemical species i is defined as

$$C_i \equiv \frac{n_i}{V}, \quad (3.9)$$

where V is the volume of the system, whereas the *mixture concentration* is defined as

$$C \equiv \sum_{i=1}^{n_s} C_i = \frac{n}{V}. \quad (3.10)$$

The *partial density* of the chemical species i is defined as

$$\rho_i \equiv \frac{m_i}{V}, \quad (3.11)$$

whereas the *mixture density*, or *density*, is defined as

$$\rho \equiv \sum_{i=1}^{n_s} \rho_i = \frac{m}{V}. \quad (3.12)$$

Density and concentration are intensive properties of a gas mixture, which are related via

$$\rho = \bar{W} C. \quad (3.13)$$

3.2

Gas Phase Thermochemistry

3.2.1

Equation of State for Perfect Gases

A perfect gas is a model to describe a gas that is composed by a set of point particles moving randomly that interact only through elastic collisions. This class of gases obeys an equation of state relating temperature, pressure and density called ideal gas law, which is given by

$$pV = nRT, \quad (3.14)$$

where p is the *pressure*, R is the *universal gas constant* and T is the *temperature*.

A consequence of the perfect gas model is that all the intensive thermodynamical properties are known function of the mixture temperature only. Herein it will be assumed that all the gas mixtures are composed by gases that behave as a perfect gas.

3.2.2

Stoichiometry

A gas mixture is said to be *stoichiometric* if the fuel and the oxidizer are in a proportion that are completely consumed during the reaction. If there is an excess of fuel, the mixture is called *fuel-rich*, and if there is an excess of oxidizer, it is called *fuel-lean* (Warnatz et al., 1999) [95].

The *equivalence ratio* is defined as

$$\Phi \equiv \frac{\frac{X_{Fu}}{X_{Ox}}}{\left(\frac{X_{Fu}}{X_{Ox}}\right)_{st}}, \quad (3.15)$$

where X_{Fu} is the fuel molar fraction, X_{Ox} is the oxidizer molar fraction and the subscript $_{st}$ notes stoichiometric conditions. By definition, Φ is smaller than one if the mixture is fuel-lean, greater than one if the mixture is fuel-rich and unitary if the mixture is stoichiometric, i.e.,

$$\begin{aligned} \Phi < 1 & \quad \text{fuel - lean mixture,} \\ \Phi = 1 & \quad \text{stoichiometric mixture,} \\ \Phi > 1 & \quad \text{fuel - rich mixture.} \end{aligned} \quad (3.16)$$

3.2.3

Reaction Mechanism

During a chemical transformation the molecular bonds holding atoms in a given molecule are broken and new bonds are formed with other molecules, leading to a conversion process between bond and kinetic energy. The number of atoms does not change in this transformation (Zel'dovich et al., 1985) [99].

A reaction mechanism with n_r elementary reactions and n_s chemical species can be represented in the general form



where \mathcal{M}_i is the symbol of the i -th chemical species and the integers ν'_{ij} and ν''_{ij} are, respectively, the forward and reverse stoichiometric coefficients of chemical species i in the j -th elementary reaction. The Table 3.1 presents a chemical kinetics mechanism, with 4 species (CO , O , CO_2 and O_2) and 3 reactions, for the description of carbon monoxide oxidation (Gardiner, 2000) [21].

Table 3.1: Reaction mechanism for carbon monoxide (CO) oxidation. In this table M represent a third body with a specific efficiency for each species ($f_{O_2} = 0.4$, $f_{CO} = 0.75$ and $f_{CO_2} = 1.5$).

Reaction	A_i (cm, mol, s)	β_i	E_i (cal/mol)
1: $O_2 + CO \rightleftharpoons CO_2 + O$	1.260×10^{13}	0.00	23682.94
2: $CO + O + M \rightleftharpoons CO_2 + M$	1.540×10^{15}	0.00	1510.70
3: $O + O + M \rightleftharpoons O_2 + M$	5.400×10^{13}	0.00	-899.69

Further information about reaction mechanisms can be obtained in the work of Orbegoso et al. (2009) [65], that presents a survey of recent chemical kinetics mechanisms available to model the combustion of simple fuels, such as hydrogen, natural gas, Syngas and liquefied petroleum gas.

3.2.4 Rate of Reaction

The transition from the initial to the final state is characterized by the chemical reaction rates for the various species of the reaction mechanism. The *net production rate* $\dot{\omega}_i$ of the i -th chemical species in a multistep mechanism is given by

$$\dot{\omega}_i = \sum_{j=1}^{n_r} \nu_{ij} r_j, \quad (3.18)$$

where the *overall stoichiometric coefficients* are

$$\nu_{ij} = \nu''_{ij} - \nu'_{ij}, \quad (3.19)$$

and the *overall reaction rate* of the j -th elementary reaction, r_j , is given by

$$r_j = r_j^+ - r_j^-, \quad (3.20)$$

where the *forward reaction rate* r_j^+ and the *reverse reaction rate* r_j^- are given by

$$r_j^+ = k_j^+ \prod_{i=1}^{n_s} C_i^{\nu'_{ij}}, \quad \text{and} \quad r_j^- = k_j^- \prod_{i=1}^{n_s} C_i^{\nu''_{ij}}, \quad (3.21)$$

with k_j^+ and k_j^- being the rate constants for the forward and reverse j -th elementary reaction.

The forward rate constant for the j -th elementary reaction is assumed to evolve according to an *Arrhenius law* (Williams, 1985) [96],

$$k_j^+ = A_j T^{\beta_j} \exp\left(-\frac{E_j}{RT}\right), \quad (3.22)$$

where A_j is the *pre-exponential factor*, of the j -th elementary reaction, which is representative of the molecular collision frequency at the average thermal velocity, β_j is *temperature exponent* of the j -th reaction and E_j is the *activation energy* of the j -th elementary reaction, which describes a barrier of energy that has to be overcome during the reaction.

The reverse rate constant for the j -th elementary reaction is related to the forward rate and its determination will be given in the following subsection.

3.2.5 Thermochemical Equilibrium

When the forward and the reverse reaction rate of the j -th elementary reaction approach each other, the concentration of the chemical species ceases to change and the system reaches a state of dynamic equilibrium (Zel'dovich et al., 1985) [99], which can be expressed as

$$0 = k_j^+ \prod_{i=1}^{n_s} C_i^{\nu_{ij}^+} - k_j^- \prod_{i=1}^{n_s} C_i^{\nu_{ij}^-}, \quad (3.23)$$

which yields

$$K_{c_j} \equiv \frac{k_j^+}{k_j^-} = \frac{\prod_{i=1}^{n_s} C_i^{\nu_{ij}^-}}{\prod_{i=1}^{n_s} C_i^{\nu_{ij}^+}} = \prod_{i=1}^{n_s} C_i^{\nu_{ij}}, \quad (3.24)$$

which defines the j -th elementary reaction *equilibrium constant in concentration units*, K_{c_j} . Note that it is also possible to define the j -th elementary reaction equilibrium constants in terms of pressure units,

$$K_{p_j} \equiv \prod_{i=1}^{n_s} p_i^{\nu_{ij}}, \quad (3.25)$$

and it is easy to show that the two equilibrium constants are related by

$$K_{c_j} = K_{p_j} \left(\frac{p^o}{RT} \right)^{\sum_{i=1}^{n_s} \nu_{ij}}, \quad (3.26)$$

where p^o is the *pressure at the standard state*.

From the definition of the *Gibbs free energy* (Warnatz et al., 1999) [95], it is possible to show that

$$K_{p_j} = \exp \left(\frac{\Delta S_j^o}{R} - \frac{\Delta H_j^o}{RT} \right), \quad (3.27)$$

where the *net change in entropy* ΔS_j^o and the *net change in enthalpy* ΔH_j^o in the j -th reaction are respectively given by

$$\Delta S_j^o \equiv \sum_{i=1}^{n_s} \nu_{ij} S_i^o, \quad (3.28)$$

and

$$\Delta H_j^o \equiv \sum_{i=1}^{n_s} \nu_{ij} H_i^o. \quad (3.29)$$

For all chemical species, the *enthalpy of formation* H_i^o and *entropy in standard state* S_i^o are assumed to be known functions of temperature and can be calculated, for example, using Chemkin-II package (Kee et al., 1989) [37].

3.3 Equations of Balance

Classically, the fundamental principles of balances (mass, momentum, chemical species and energy) are mathematically formulated in terms of partial differential equations. These fundamental principles are presented here without development, which may be found elsewhere Williams (1985) [96] or Law (2006) [45].

The balance equations of the total mass, momentum, species mass and energy read

$$\frac{\partial \rho}{\partial t} = \Gamma_{\rho}, \quad (3.30)$$

$$\frac{\partial(\rho \mathbf{u})}{\partial t} = \Gamma_{\mathbf{u}}, \quad (3.31)$$

$$\frac{\partial(\rho Y_i)}{\partial t} = \Gamma_{Y_i} + \Omega_i, \quad i = 1, \dots, n_s, \quad (3.32)$$

$$\frac{\partial(\rho h)}{\partial t} = \Gamma_h, \quad (3.33)$$

where t is the time; Γ_{ρ} represents the mass convection; \mathbf{u} is the velocity field; $\Gamma_{\mathbf{u}}$ accounts for the momentum convection, external surface and body forces; Γ_{Y_i} describes the convective and diffusive transport of the i -th chemical species; Ω_i is the i -th chemical species source term; h is the specific enthalpy and Γ_h accounts for all mechanisms of energy transport, i.e., conduction, convection and radiation. These equations are supplemented by the equation of state, Eq.(3.14), appropriate boundary and initial conditions.

3.4 Partially Stirred Reactor with IEM Model

A *partially stirred reactor* (PaSR) is a spatially homogeneous, transient, reactor model governed by the competition of chemical reactions, turbulent mixing and the *residence time* within the reactor, defined as

$$\tau_r \equiv \frac{\rho V}{\dot{m}}, \quad (3.34)$$

where \dot{m} is the *mass flow rate* entering the reactor. In such a reactor, a statistically steady state of “unmixedness” may be maintained. In this sense, this reactor is a chemical equivalent of the nondecaying homogeneous turbulent flow, in which energy is continuously supplied to the system in order to maintain the turbulence (Correa, 1993) [13].

A particular solution to such a reactor considers Monte-Carlo techniques, in which the reactive system consists of n_p stochastic particles, evolving adiabatically and at constant pressure. Under such hypothesis, $\Gamma_{\rho} = \Gamma_{\mathbf{u}} = 0$,

and the equation of state determines the density for a given temperature and mixture composition. The terms of enthalpy transport Γ_h and of the chemical species Γ_{Y_i} describe the turbulent transport micromixing process (Pope, 1985) [69]. Thus, under the hypothesis of linear relaxation of the properties towards the mean value, the balance equations for the the j -th stochastic particle ($j = 1, \dots, n_p$) of this system read

$$\frac{dh^{(j)}}{dt} = -\frac{h^{(j)} - \langle h \rangle}{\tau_m}, \quad (3.35)$$

$$\frac{dp^{(j)}}{dt} = 0, \quad (3.36)$$

$$\frac{dY_i^{(j)}}{dt} = -\frac{Y_i^{(j)} - \langle Y_i \rangle}{\tau_m} + \frac{\dot{\omega}_i^{(j)} W_i}{\rho}, \quad i = 1, \dots, n_s, \quad (3.37)$$

where the superscript (j) denote the j -th stochastic particle, τ_m is the *mixing time*, $\langle h \rangle$ and $\langle Y_i \rangle$ denote the *ensemble average* of h and Y_i respectively, where the ensemble average operator is defined as

$$\langle \psi \rangle \equiv \frac{1}{n_p} \sum_{j=1}^{n_p} \psi^{(j)}, \quad (3.38)$$

being ψ a generic property of the reactive system.

Another statistical quantity that is useful in the description of a system with stochastic particles is the *ensemble variance*, whereas the ensemble variance operator is defined as

$$\langle \psi'^2 \rangle \equiv \frac{1}{n_p} \sum_{j=1}^{n_p} (\psi^{(j)} - \langle \psi \rangle)^2, \quad (3.39)$$

and can be shown that

$$\langle \psi'^2 \rangle = \langle \psi^2 \rangle - \langle \psi \rangle^2. \quad (3.40)$$

Note that the micromixing process has been described in Eq.(3.37) by the interaction by exchange with the mean (IEM) model. More details about mixing models can be found in Fox (2003) [18]. The second term on the right hand side of Eq.(3.37) is the reaction rate of the i -th chemical species. The modelling of this nonlinear term has been described in section 3.2.4 and introduces stiffness on the chemical system, since the associated range of time scales spans over several orders of magnitude (Correa, 1993) [13].

3.5

Pairwise Mixing Stirred Reactor

According to Pope (1997) [70], for the purpose of testing a chemical kinetic reduction technique, it is desirable to devise a mixing model that leads to a

composition region accessed during the solution process which is “wider” than that provided by the IEM model.

Therefore, Pope (1997) [70] proposed the *pairwise mixing stirred reactor* (PMSR), which is designed to yield a much larger accessed region, and hence should provide a stringent test to the ability of the reduction technique to yield a reduction in computational time.

In the PMSR model the reactor consists of an even number n_p of particles. Given a time step, Δt , the model describes three types of events, for each discrete times $k\Delta t$, where k is an integer, *inflow*, *outflow* and *pairing*.

Initially, the particles are arranged in pairs (j_1, j_2) such that the particles $(1, 2), (3, 4), \dots, (n_p - 1, n_p)$ are partners. Given a specified residence time, τ_r , the inflow and outflow events consist of randomly selecting n_{in} pairs of particles and exchanging their thermodynamical properties by the properties of a prescribed inflow. The number of particles pairs to input the system is defined as

$$n_{in} \equiv \text{ceil} \left(\frac{1}{2} \frac{\Delta t}{\tau_r} n_p \right), \quad (3.41)$$

where $\text{ceil}(\cdot)$ denotes the ceil function of a real number, i.e., the smallest integer not less than a given real. Given a specified pairwise time, τ_p , the pairing event consists of randomly selecting a number of pairs of particles, different from the inflow particles, equal to

$$n_{pair} \equiv \text{ceil} \left(\frac{1}{2} \frac{\Delta t}{\tau_p} n_p \right), \quad (3.42)$$

for pairing. Then the chosen particles (inflow/outflow and pairing) are randomly shuffled. Between these discrete times, the pairs of particles (j_1, j_2) evolve according to the following mixing law

$$\frac{dh^{(j_1)}}{dt} = -\frac{h^{(j_1)} - h^{(j_2)}}{\tau_m}, \quad (3.43)$$

$$\frac{dh^{(j_2)}}{dt} = -\frac{h^{(j_2)} - h^{(j_1)}}{\tau_m}, \quad (3.44)$$

$$\frac{dp^{(j_1)}}{dt} = 0, \quad (3.45)$$

$$\frac{dp^{(j_2)}}{dt} = 0, \quad (3.46)$$

$$\frac{dY_i^{(j_1)}}{dt} = -\frac{Y_i^{(j_1)} - Y_i^{(j_2)}}{\tau_m} + \frac{\dot{\omega}_i^{(j_1)} W_i}{\rho}, \quad i = 1, \dots, n_s, \quad (3.47)$$

$$\frac{dY_i^{(j_2)}}{dt} = -\frac{Y_i^{(j_2)} - Y_i^{(j_1)}}{\tau_m} + \frac{\dot{\omega}_i^{(j_2)} W_i}{\rho}, \quad i = 1, \dots, n_s. \quad (3.48)$$

and the equation of state, Eq.(3.14).

3.6 The Geometry of Reactive Systems

In this section it is developed a geometric language to interpret a stirred reactor such as PaSR/IEM or PMSR. This approach is based on the theory of dynamical systems and allows one to identify the thermodynamical state of a reactive system as a vector and its evolution as a vector path on the systems phase space.

3.6.1 Composition Space

Given a reactive mixture in a stirred reactor, such as PaSR/IEM or PMSR, its thermodynamical state may be completely determined by the mass fraction Y_i ($i = 1, \dots, n_s$) of the n_s chemical species, the specific enthalpy h and pressure p . The thermodynamic state of the reactive mixture can be represented in a compact way by the *composition* vector defined as

$$\boldsymbol{\phi} \equiv (h, p, Y_1, \dots, Y_{n_s})^T, \quad (3.49)$$

where the superscript T denotes the transposition operation. One should note that, due to the invariance of the system number of atoms, which ensures the total conservation of the mass, the components of vector $\boldsymbol{\phi}$ are not linearly independent.

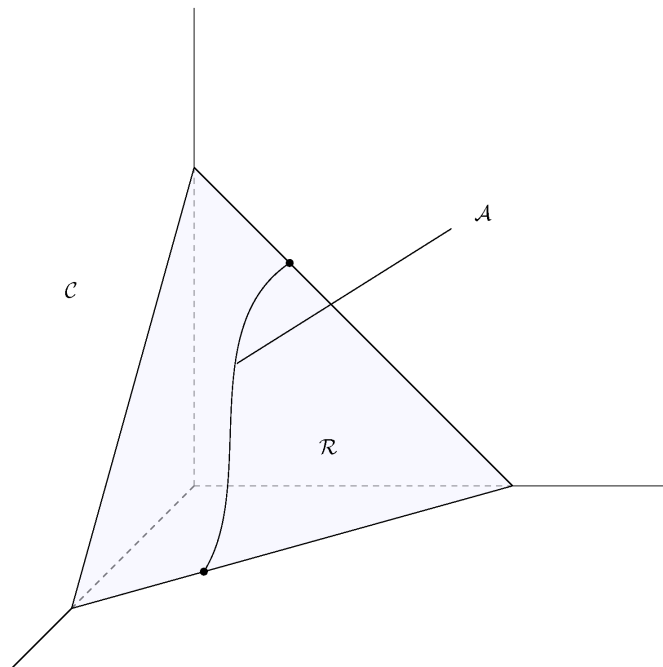


Figure 3.1: Sketch of the composition space and its subsets.

Defining $n_\phi \equiv n_s + 2$, the composition ϕ is a point in the n_ϕ -dimensional Euclidean space the so called *composition space* (\mathcal{C}), where the first direction is associated with the enthalpy, the second with the pressure and the other n_s are related to the chemical species. The region of the composition space defined by all physical realizable values of ϕ — those that respect elemental conservation — is called *realizable region* (\mathcal{R}). The locus in the realizable region defined by all composition ϕ that occurs in a given flow calculation is called *accessed region* (\mathcal{A}). By definition, the accessed region is a subset of the realizable region, which is a subset of the composition space. Figure 3.1 illustrates the structure of the composition space and its subsets.

3.6.2 Mixture Temperature

The composition vector ϕ completely defines the thermodynamical state of a reactive mixture in a partially stirred reactor. Thus, it is possible to determine the mixture temperature from the components of ϕ . Indeed, the mixture enthalpy is a function of the temperature given by

$$h(T) \equiv \sum_{i=1}^{n_s} Y_i h_i(T) \quad (3.50)$$

where the specific enthalpy of the i -th chemical species is given by

$$h_i(T) \equiv h_i^o + \int_{T^o}^T c_{p_i}(T') dT' \quad (3.51)$$

where h_i^o and c_{p_i} respectively are the specific enthalpy of formation and specific heat of i -th chemical species and T^o is the temperature at the standard state. In this work, h_i^o and c_{p_i} are computed using the **Chemkin-II** package by Kee et al. (1989) [37] and the system temperature is obtained from the Eq.(3.51) using the bisection method.

3.6.3 Reaction Mapping

Considering an ideal spatially homogeneous, transient, chemical reactor such as PaSR/IEM or PMSR, the evolution of the composition of each particle in the reactor can be written in a general framework according to the following set of ordinary differential equations

$$\frac{d\phi^{(j)}}{dt} = \mathbf{\Gamma}^{(j)}(t) + \mathbf{S}(\phi^{(j)}, t), \quad (3.52)$$

where $\mathbf{\Gamma}^{(j)}(t)$ is the rate of change due to micromixing transport and $\mathbf{S}(\phi^{(j)}, t)$ is the rate of change associated to the chemical reactions.

Integrating both sides of equation Eq.(3.52) from an initial time t_0 to a time t gives

$$\phi^{(j)}(t) = \phi_0^{(j)} + \int_{t_0}^t \mathbf{\Gamma}^{(j)}(t') dt' + \int_{t_0}^t \mathbf{S}(\phi^{(j)}, t') dt', \quad (3.53)$$

and defining the *reaction mapping*

$$\mathbf{R}(\phi_0^{(j)}, t) \equiv \phi^{(j)}(t), \quad (3.54)$$

as the solution of Eq.(3.52) after a time t starting from the initial composition $\phi^{(j)}(t_0) = \phi_0^{(j)}$.

The reaction mapping corresponds to a trajectory in composition space, which, for large values of t , tends to the equilibrium composition for the given enthalpy and pressure on $\phi_0^{(j)}$, such as shown in Figure 3.2.

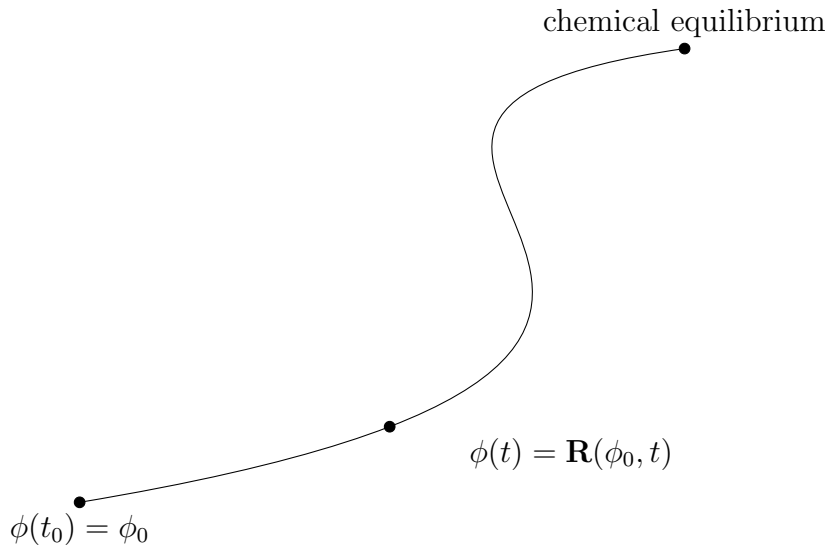


Figure 3.2: Sketch of a trajectory in composition space departing from an initial composition ϕ_0 until the chemical equilibrium.

3.6.4 Reaction Vector

For each particle with composition $\phi^{(j)}$, the reaction vector $\mathbf{S}(\phi^{(j)}, t)$ has its first and second components equal to zero and the next n_s components given by the mass rate of production of each species, i.e.,

$$\mathbf{S}(\phi^{(j)}, t) = \left(0, 0, \frac{\dot{\omega}_1^{(j)} W_1}{\rho}, \dots, \frac{\dot{\omega}_{n_s}^{(j)} W_{n_s}}{\rho} \right)^T. \quad (3.55)$$

3.6.5 Evolution Equations of PaSR/IEM

In the case of the IEM model the mixing vector can be written as

$$\mathbf{\Gamma}^{(j)}(t) = -\frac{1}{\tau_m} \left(h^{(j)} - \langle h \rangle, 0, Y_1^{(j)} - \langle Y_1 \rangle, \dots, Y_{n_s}^{(j)} - \langle Y_{n_s} \rangle \right)^T, \quad (3.56)$$

or, equivalently,

$$\mathbf{\Gamma}^{(j)}(t) = -\frac{\boldsymbol{\phi}^{(j)} - \langle \boldsymbol{\phi} \rangle}{\tau_m}, \quad (3.57)$$

where $\langle \boldsymbol{\phi} \rangle$ is the ensemble average composition vector is given by

$$\langle \boldsymbol{\phi} \rangle = (\langle h \rangle, 0, \langle Y_1 \rangle, \dots, \langle Y_{n_s} \rangle)^T, \quad (3.58)$$

such that the composition of the j -th stochastic particle evolves according to the following system of ODEs

$$\frac{d\boldsymbol{\phi}^{(j)}}{dt} = -\frac{\boldsymbol{\phi}^{(j)} - \langle \boldsymbol{\phi} \rangle}{\tau_m} + \mathbf{S}(\boldsymbol{\phi}^{(j)}, t). \quad (3.59)$$

3.6.6 Evolution Equations of PMSR

In the case of the PMSR the mixing vectors for the pair of particles (j_1, j_2) can be written as

$$\mathbf{\Gamma}^{j_1}(t) = -\frac{1}{\tau_m} \left(h^{(j_1)} - h^{(j_2)}, 0, Y_1^{(j_1)} - Y_1^{(j_2)}, \dots, Y_{n_s}^{(j_1)} - Y_{n_s}^{(j_2)} \right)^T, \quad (3.60)$$

$$\mathbf{\Gamma}^{j_2}(t) = -\frac{1}{\tau_m} \left(h^{(j_2)} - h^{(j_1)}, 0, Y_1^{(j_2)} - Y_1^{(j_1)}, \dots, Y_{n_s}^{(j_2)} - Y_{n_s}^{(j_1)} \right)^T, \quad (3.61)$$

or, equivalently,

$$\mathbf{\Gamma}^{j_1}(t) = -\frac{\boldsymbol{\phi}^{(j_1)} - \boldsymbol{\phi}^{(j_2)}}{\tau_m}, \quad (3.62)$$

$$\mathbf{\Gamma}^{j_2}(t) = -\frac{\boldsymbol{\phi}^{(j_2)} - \boldsymbol{\phi}^{(j_1)}}{\tau_m}, \quad (3.63)$$

such that the compositions of a pair of particles (j_1, j_2) evolves according to the following system of ODEs

$$\frac{d\boldsymbol{\phi}^{(j_1)}}{dt} = -\frac{\boldsymbol{\phi}^{(j_1)} - \boldsymbol{\phi}^{(j_2)}}{\tau_m} + \mathbf{S}(\boldsymbol{\phi}^{(j_1)}, t), \quad (3.64)$$

$$\frac{d\boldsymbol{\phi}^{(j_2)}}{dt} = -\frac{\boldsymbol{\phi}^{(j_2)} - \boldsymbol{\phi}^{(j_1)}}{\tau_m} + \mathbf{S}(\boldsymbol{\phi}^{(j_2)}, t). \quad (3.65)$$

4

Numerical Procedure

This chapter presents the numerical procedure used to solve Eq.(3.52), which consists of an operator splitting technique employed together with a backward differentiation formula method, used to integrate stiff systems of ordinary differential equations.

4.1

Operator Splitting Technique

In the simulation of stirred reactors, such as those presented in the preceding chapter, a system of equations similar to Eq.(3.52) must be solved for each particle in the reactor in order to predict the composition evolution. This system of equations has two terms, each of which associated to a different physical phenomena, micro-mixing and chemical reaction. To solve Eq.(3.52) for each particle in a stirred reactor it is used an operator splitting technique, also employed by Yang & Pope (1998a) [97] that allows the splitting of this system of equations into two systems, a pure mixing system

$$\frac{d\phi^{(j)}}{dt} = \mathbf{\Gamma}^{(j)}(t), \quad (4.1)$$

and a pure chemical reaction system

$$\frac{d\phi^{(j)}}{dt} = \mathbf{S}(\phi^{(j)}, t). \quad (4.2)$$

In the first fractional step, given an initial composition $\phi_0^{(j)}$ and a time step Δt , the pure mixing system, Eq.(4.1), is solved to determine $\phi_{mix}^{(j)}(t + \Delta t)$. In the next fractional step, the pure chemical reaction system, Eq.(4.2), is solved from an initial composition $\phi_{mix}^{(j)}(t + \Delta t)$ over a time step Δt to obtain $\phi^{(j)}(t + \Delta t)$. The overall process of integration via operator splitting technique can be represented as

$$\phi^{(j)}(t) \xrightarrow{\text{mixing}} \phi_{mix}^{(j)}(t + \Delta t) \xrightarrow{\text{reaction}} \phi^{(j)}(t + \Delta t). \quad (4.3)$$

The advantage of an operator splitting technique lies in the fact that each term in the evolution equation can be solved separately, using a specific efficient numerical method to treat the particular features inherent to the physical phenomenon modelled by the term (Fox, 2003) [18].

4.2 Integration of Mixing Vector

4.2.1 IEM Mixing Model

For the IEM model, Eq.(4.1), becomes

$$\frac{d\phi^{(j)}}{dt} = -\frac{\phi^{(j)} - \langle\phi\rangle}{\tau_m}, \quad (4.4)$$

which has an analytic solution, for an initial composition $\phi_0^{(j)}$, given by

$$\phi_{mix}^{(j)}(t) = \langle\phi\rangle + \zeta e^{-2t/\tau_m}, \quad (4.5)$$

where the vector ζ is given by

$$\zeta = \langle\phi\rangle - \phi_0^{(j)}. \quad (4.6)$$

4.2.2 PMSR Mixing Model

For PMSR model, the pure mixing step is the following pair of equations

$$\frac{d\phi^{(j_1)}}{dt} = -\frac{\phi^{(j_1)} - \phi^{(j_2)}}{\tau_m}, \quad (4.7)$$

$$\frac{d\phi^{(j_2)}}{dt} = -\frac{\phi^{(j_2)} - \phi^{(j_1)}}{\tau_m}, \quad (4.8)$$

which has an analytical solution, for a pair of initial compositions $\phi_0^{(j_1)}$ and $\phi_0^{(j_2)}$, given by

$$\phi_{mix}^{(j_1)}(t) = \zeta_1 + \zeta_2 e^{-2t/\tau_m}, \quad (4.9)$$

$$\phi_{mix}^{(j_2)}(t) = \zeta_1 - \zeta_2 e^{-2t/\tau_m}, \quad (4.10)$$

where the vectors ζ_1 and ζ_2 are given by

$$\zeta_1 = \frac{1}{2} \left(\phi_0^{(j_1)} + \phi_0^{(j_2)} \right), \quad (4.11)$$

$$\zeta_2 = \frac{1}{2} \left(\phi_0^{(j_1)} - \phi_0^{(j_2)} \right). \quad (4.12)$$

4.3

Integration of the Reaction Vector

For the PaSR/IEM model, Eq.(4.2), becomes

$$\frac{d\phi^{(j)}}{dt} = \mathbf{S}(\phi^{(j)}, t), \quad (4.13)$$

which is numerically integrated from a composition $\phi_{mix}^{(j)}$ using the CVODE solver that is part of the SUNDIALS suite by Hindmarsh et al. (2005) [28]. Similarly, from a pair of initial compositions $\phi_{mix}^{(j_1)}$ and $\phi_{mix}^{(j_2)}$, it is integrated the chemical reaction system for PMSR model, which is given by the following system of equations

$$\frac{d\phi^{(j_1)}}{dt} = \mathbf{S}(\phi^{(j_1)}, t), \quad (4.14)$$

$$\frac{d\phi^{(j_2)}}{dt} = \mathbf{S}(\phi^{(j_2)}, t). \quad (4.15)$$

The system of ordinary differential equations given by Eq.(4.2) is inherently nonlinear since its right hand side is proportional to the rate of reaction of the chemical species present in the reaction mechanism used to model the specified stirred reactor (Williams, 1985) [96].

If this system of equations is linearized around an equilibrium composition, the resulting system presents eigenvalues with real part of vastly different values, since the time scales associated with the elementary reaction in the reaction mechanism span over several orders of magnitude (Williams, 1985) [96]. Thus, the ratio between the eigenvalues maximum and minimum real part is very large, which is characteristic of a system of equations subject to a condition called *stiffness* (Shampine & Thompson, 2007) [85].

4.3.1

Backward Differentiation Formula

In order to numerically integrate a stiff system of ordinary differential equations, the CVODE solver has a family of implicit methods called *backward differentiation formula* (BDF). Assuming that the exact solution for the system given by Eq.(4.2) is known at the instants $t_{n-q}, t_{n-q+1}, \dots, t_{n-1}, t_n$, where q is the order of the method, this class of methods compute the approximated value of the function derivative at t_{n+1} using the values $\phi(t_{n-q}), \phi(t_{n-q+1}), \dots, \phi(t_{n-1}), \phi(t_n)$. Thus, the approximation precision increases with the method order.

The BDF method formula is given by

$$\boldsymbol{\phi}(t_{n+1}) = \sum_{j=0}^{q-1} \alpha_{j+1} \boldsymbol{\phi}(t_{n-j}) + \Delta t_n \mathbf{S}[\boldsymbol{\phi}(t_{n+1}), t_{n+1}], \quad (4.16)$$

where α_j are coefficients related to a particular method and the n -th time step is defined as

$$\Delta t_n \equiv t_n - t_{n-1}. \quad (4.17)$$

Since BDF methods are implicit, in order to find a value for $\boldsymbol{\phi}(t_{n+1})$, it is necessary to solve a nonlinear system of algebraic equations given by

$$\mathbf{N}[\boldsymbol{\phi}(t_{n+1})] = \mathbf{0}, \quad (4.18)$$

where

$$\mathbf{N}[\boldsymbol{\phi}(t_{n+1})] \equiv \sum_{j=0}^q \alpha_j \boldsymbol{\phi}(t_{n-j}) + \Delta t_n \mathbf{S}[\boldsymbol{\phi}(t_{n+1}), t_{n+1}]. \quad (4.19)$$

In the CVODE solver the system defined by Eq.(4.18) is solved iteratively using the Newton-Rapson method which defines the following iteration

$$\boldsymbol{\phi}^{m+1}(t_{n+1}) = \boldsymbol{\phi}^m(t_{n+1}) - \mathbf{J}^{-1}[\boldsymbol{\phi}^m(t_{n+1})] \mathbf{N}[\boldsymbol{\phi}^m(t_{n+1})], \quad (4.20)$$

where the superscript m denotes the m -th approximation of $\boldsymbol{\phi}(t_{n+1})$ and \mathbf{J} is the Jacobian matrix of \mathbf{N} , which is represented, in the canonical base, by the components

$$J_{ij}[\boldsymbol{\phi}(t_{n+1})] \equiv \frac{\partial N_i}{\partial \phi_j^n}[\boldsymbol{\phi}(t_{n+1})]. \quad (4.21)$$

Further details on this solution method may be found in Hindmarsh & Serban (2006) [29]. The reader interested in numerical analysis issues such as *convergence*, *order* and *stability* is referred to Hairer et al. (1996) [27].

4.3.2

Truncation Error Control

The calculations described in the section 4.3.1 are performed using a floating point arithmetic, which has finite precision, and are subject to truncation errors. The CVODE solver estimates the *local truncation error* in the computation of i -th component of $\boldsymbol{\phi}(t_n)$, $\phi_i(t_n)$, and store these values in the i -th component of the vector

$$\boldsymbol{\epsilon} = (\epsilon_1, \dots, \epsilon_{n_\phi})^T. \quad (4.22)$$

The control of the local truncation error is performed using two positive scalar parameters, ε_{rel} and ε_{abs} , which represent relative and absolute tolerances, respectively. Roughly speaking, for each component of the vector $\phi(t_n)$, one can think ε_{rel} as a value which defines the number of correct digits in a single time step. Conversely, ε_{abs} indicates a value which the number of correct digits in each component of the solution vector need not be smaller.

The vector that stores the local truncation error must satisfy the inequality

$$\|\epsilon\|_{wrms} \leq 1, \quad (4.23)$$

where the *weighted root mean square norm*, denoted by $\|\cdot\|_{wrms}$, is given by the expression

$$\|\epsilon\|_{wrms} \equiv \sqrt{\frac{1}{n_\phi} \sum_{i=1}^{n_\phi} \left(\frac{\epsilon_i}{w_i}\right)^2}, \quad (4.24)$$

where the *i*-th *error weight* is defined as

$$w_i = \varepsilon_{rel} \cdot |\phi_i(t_n)| + \varepsilon_{abs}. \quad (4.25)$$

The inequality defined by Eq.(4.23) provides a test to control the estimated local errors of truncation such that $|\epsilon_i|$ must be less than or equal w_i , i.e.,

$$|\epsilon_i| \leq \varepsilon_{rel} \cdot |\phi_i(t_n)| + \varepsilon_{abs}. \quad (4.26)$$

In order to $|\epsilon_i|$ satisfy the inequality given by Eq.(4.26) it is sufficient that

$$|\epsilon_i| \leq \varepsilon_{abs}, \quad \text{or} \quad \frac{|\epsilon_i|}{|\phi_i(t_n)|} \leq \varepsilon_{rel}. \quad (4.27)$$

The *global truncation error* results from the accumulation of the local errors of truncation and can exceed the local tolerances. So it is recommended to use conservative (small) values for ε_{rel} and ε_{abs} , i.e., of the order of 10^{-6} and 10^{-9} , respectively (Liu & Pope, 2005) [49].

5 In Situ Adaptive Tabulation

In this chapter is described the *in situ adaptive tabulation* (ISAT) technique proposed by Pope (1997) [70] that is used to reduce the computational cost associated to the solution of Eq.(4.2).

5.1 Linearized Reaction Mapping

Consider a composition ϕ^1 and an *initial composition* ϕ_0 , so that the series expansion of the reaction mapping of the composition around the initial one is

$$\mathbf{R}(\phi, t) = \mathbf{R}(\phi_0, t) + \mathbf{A}(\phi_0, t)\delta\phi + \mathcal{O}(\|\delta\phi\|_2^2), \quad (5.1)$$

where the *composition displacement* is given by

$$\delta\phi \equiv \phi - \phi_0, \quad (5.2)$$

the *mapping gradient matrix* is the $n_\phi \times n_\phi$ matrix $\mathbf{A}(\phi_0, t)$ which is represented in the canonical base by the components

$$A_{ij}(\phi_0, t) \equiv \frac{\partial R_i}{\partial \phi_{0j}}(\phi_0, t), \quad (5.3)$$

and $\mathcal{O}(\|\delta\phi\|_2^2)$ denotes terms that have order $\|\delta\phi\|_2^2$, where the Euclidean norm of a vector ψ , denoted by $\|\cdot\|_2$, is given by the expression

$$\|\psi\|_2 \equiv \sqrt{\sum_{i=1}^{n_\phi} \psi_i^2}. \quad (5.4)$$

The *linear approximation*

$$\mathbf{R}^l(\phi, t) \equiv \mathbf{R}(\phi_0, t) + \mathbf{A}(\phi_0, t)\delta\phi, \quad (5.5)$$

is second order accurate at a connected region of composition space centered at ϕ_0 . The shape of this region is unknown before the calculations, but the ISAT technique approximates this region by a hyper-ellipsoid, as will be shown in section 5.2.

¹ In this chapter the superscript ^(j) is omitted for the sake of notation simplicity.

The *local error* of the linear approximation is defined as the Euclidean norm of the difference between the reaction mapping at ϕ and the linear approximation for it around ϕ_0

$$\varepsilon \equiv \|\mathbf{R}(\phi, t) - \mathbf{R}^l(\phi, t)\|_2. \quad (5.6)$$

5.2

Ellipsoid of Accuracy

The accuracy of the linear approximation at ϕ_0 is controlled only if the local error is smaller than a positive *error tolerance* ε_{tol} , which is heuristically chosen. The *region of accuracy* is defined as the connected region of composition space centered at ϕ_0 where local error is not greater than ε_{tol} .

For instance, assume a *constant approximation* for the reaction mapping at ϕ , i.e., $\mathbf{R}^c(\phi, t) \equiv \mathbf{R}(\phi_0, t)$, instead of the linear approximation defined in Eq.(5.5). The local error to leading order is

$$\varepsilon = \|\mathbf{A}\delta\phi\|_2, \quad (5.7)$$

and thus the region of accuracy ($\varepsilon \leq \varepsilon_{tol}$) is

$$\delta\phi^T \mathbf{A}^T \mathbf{A} \delta\phi \leq \varepsilon_{tol}^2. \quad (5.8)$$

The *singular value decomposition* (SVD) states that the reaction gradient matrix has a factorization in the form

$$\mathbf{A} = \mathbf{U}\mathbf{\Sigma}\mathbf{V}^T, \quad (5.9)$$

where \mathbf{U} and \mathbf{V} are real square orthogonal matrices and $\mathbf{\Sigma}$ is a real square diagonal matrix with nonnegative elements on the diagonal (Golub & Van Loan, 1996) [22]. A real square matrix \mathbf{V} is orthogonal if, and only if, its transpose is equal to its inverse, i.e., $\mathbf{V}^T = \mathbf{V}^{-1}$. Therefore, Eq.(5.8) reads

$$\delta\phi^T \mathbf{V}\mathbf{\Sigma}^T \mathbf{\Sigma} \mathbf{V}^T \delta\phi \leq \varepsilon_{tol}^2, \quad (5.10)$$

which is a hyper dimensional quadratic form centered at ϕ_0 .

The matrix $\mathbf{\Sigma}^T \mathbf{\Sigma} = \mathbf{\Sigma}^2$ is diagonal, so its eigenvalues are σ_i^2 ($i = 1, \dots, n_\phi$) where the σ_i are the singular values of \mathbf{A} . Since all the eigenvalues of $\mathbf{\Sigma}^2$ are nonnegative, i.e., $\sigma_i^2 \geq 0$, the quadratic form above has the shape of a hyper-ellipsoid centered at ϕ_0 , which is dubbed *ellipsoid of accuracy* (EOA). A sketch of the region of accuracy for a constant approximation is shown in Figure 5.1.

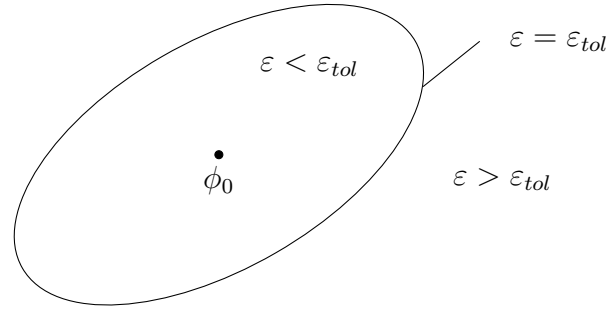


Figure 5.1: The region of accuracy for a constant approximation is a hyper-ellipsoid in composition space.

Therefore, the EOA is characterized by the center, ϕ_0 , the orthogonal matrix \mathbf{V} the diagonal matrix $\mathbf{\Sigma}$ and the error tolerance ε_{tol} . In fact, the columns of the matrix \mathbf{V} define the EOA principal directions and the half-length of the EOA in each principal direction is given by

$$l_i \equiv \frac{\varepsilon_{tol}}{\sigma_i}. \quad (5.11)$$

In cases when $\sigma_i \rightarrow 0^+$ or $\sigma_i \rightarrow \infty$, the hyper-ellipsoid degenerates. To avoid the situation where the region of accuracy is a degenerate hyper-ellipsoid, a modified version of the reaction gradient matrix, $\tilde{\mathbf{A}}$, is considered

$$\tilde{\mathbf{A}} \equiv \mathbf{U} \tilde{\mathbf{\Sigma}} \mathbf{V}^T, \quad (5.12)$$

where $\tilde{\mathbf{\Sigma}}$ is a diagonal matrix with elements given by

$$\tilde{\sigma}_i \equiv \min \left(\frac{\varepsilon_{tol}}{\kappa u_r}, \tilde{\tilde{\sigma}}_i \right), \quad (5.13)$$

where u_r is the *machine unit roundoff*², the lower bound κ is a positive real number such that $\kappa u_r < 2\varepsilon_{tol}$ and

$$\tilde{\tilde{\sigma}}_i \equiv \max(1/2, \sigma_i). \quad (5.14)$$

This modification ensures that the modified half-length of EOA, \tilde{l}_i , is bounded

$$\kappa u_r \leq \tilde{l}_i \leq 2\varepsilon_{tol}. \quad (5.15)$$

Also, the restriction imposed by Eq.(5.15) in EOA half-length defines a *band-pass filter*³ for chemical time scales, since the i -th singular value of reaction gradient matrix is related to i -th chemical species frequency through the rate of reaction of this species.

²The machine unit roundoff, u_r , is defined as the smallest floating point number such that $1.0 + u_r > 1.0$. Using double precision in a 32 bits digital computer, a typical value for u_r is 10^{-16} .

³A band-pass filter allows the passage of frequencies within a certain range and attenuates frequencies outside of this range.

It is noteworthy that the modification to avoid small singular values, Eq.(5.14), was proposed in the original work of Pope (1997) [70], whereas the change to avoid large singular values, Eq.(5.13), is a original contribution of the present work.

The product of the modified reaction gradient matrix transposed by itself is a symmetric positive defined matrix, and has a *Cholesky decomposition* of the form

$$\tilde{\mathbf{A}}^T \tilde{\mathbf{A}} = \mathbf{L}\mathbf{L}^T, \quad (5.16)$$

where \mathbf{L} is lower triangular matrix, (Golub & Van Loan, 1996) [22]. Thus, another natural way of describing the EOA is

$$\delta\boldsymbol{\phi}^T \mathbf{L}\mathbf{L}^T \delta\boldsymbol{\phi} \leq \varepsilon_{tol}^2. \quad (5.17)$$

Note that this decomposition is computed after performing the SVD given in Eq.(5.9) and recomposing $\tilde{\mathbf{A}}$ using Eq.(5.16).

The cost of the EOA representation, in terms of computer memory, involves storing three elements, the vector $\boldsymbol{\phi}_0$ and the matrices \mathbf{V} and $\tilde{\boldsymbol{\Sigma}}$, which requirements, respectively, scale as n_ϕ , n_ϕ^2 and n_ϕ ($\tilde{\boldsymbol{\Sigma}}$ is diagonal) floating point numbers. So, the total memory cost is $n_\phi^2 + 2n_\phi$.

On the other hand, the Cholesky representation, Eq.(5.17), stores only two elements, the vector $\boldsymbol{\phi}_0$ and the matrix \mathbf{L} . Each one, respectively, needing to store n_ϕ and $\frac{n_\phi(n_\phi+1)}{2}$ (\mathbf{L} is lower triangular) floating point numbers. So, the total memory cost is $\frac{1}{2}n_\phi^2 + \frac{3}{2}n_\phi$.

Both representations of the EOA are $\mathcal{O}(n_\phi^2)$, but using the Cholesky approach it is possible to save in memory storage $\frac{1}{2}n_\phi^2 + \frac{1}{2}n_\phi$ floating point positions. Thus the Cholesky representation is used in this work.

5.3

Hyper-ellipsoid Growth

In this section is discussed a geometric problem related to the adaptive step of ISAT technique. Consider the original hyper-ellipsoid centered at $\boldsymbol{\phi}_0$ and a *query composition*, $\boldsymbol{\phi}_q$, outside it, Figure 5.2. The problem is to determine a new hyper-ellipsoid of minimum hyper-volume, centered at $\boldsymbol{\phi}_0$, which encloses both the original hyper-ellipsoid and the point $\boldsymbol{\phi}_q$. A strategy to allow the growth of the hyper-ellipsoid proposed by Pope (2008) [71] is presented below.

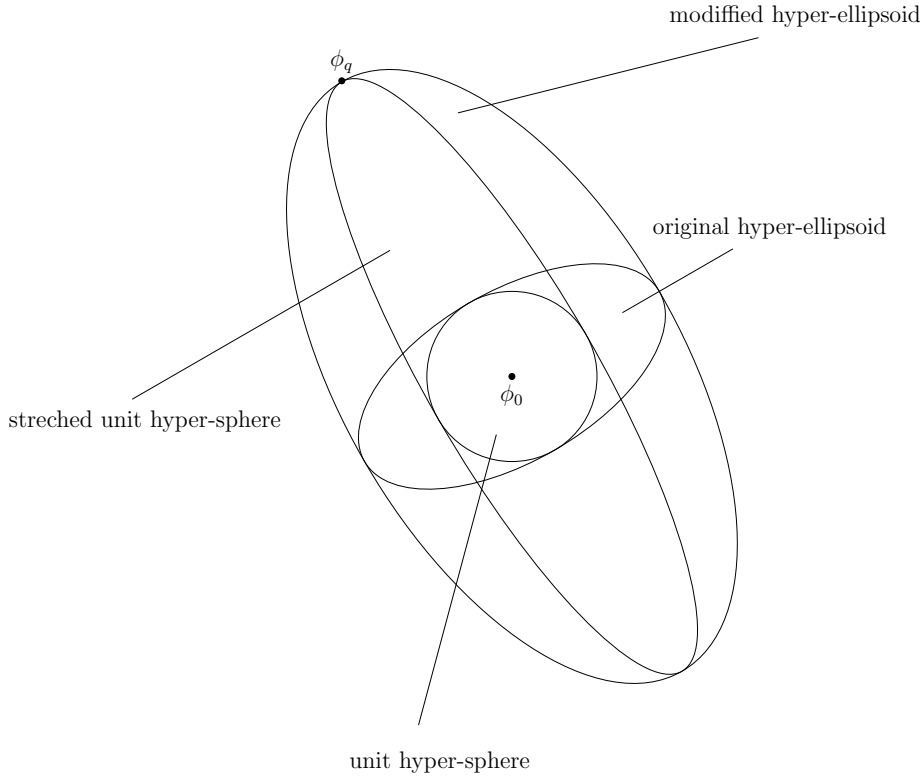


Figure 5.2: Growth process of the original hyper-ellipsoid.

Consider the affine transformation that maps a composition ϕ in \mathcal{C} into a transformed composition

$$\tilde{\phi} \equiv \frac{1}{\varepsilon_{tol}} \mathbf{L}^T \delta \phi. \quad (5.18)$$

It is obvious that $\tilde{\phi}$ also is in \mathcal{C} (see section 3.6.1) and, for any ϕ in the original hyper-ellipsoid, it is possible to see, with the help of Eq.(5.17), that

$$\|\tilde{\phi}\|_2^2 = \tilde{\phi}^T \tilde{\phi} = \frac{1}{\varepsilon_{tol}^2} \delta \phi^T \mathbf{L} \mathbf{L}^T \delta \phi \leq 1, \quad (5.19)$$

which is equivalent to

$$\tilde{\phi}_1^2 + \dots + \tilde{\phi}_{n_\phi}^2 \leq 1. \quad (5.20)$$

Therefore, it is possible to conclude that the transformation defined by Eq.(5.18) maps the original hyper-ellipsoid into the unit hyper-sphere in \mathcal{C} , as sketched in Figure 5.2. Likewise, applying this affine transformation to the query composition outside the EOA, ϕ_q , the modified query composition is obtained

$$\tilde{\phi}_q = \frac{1}{\varepsilon_{tol}} \mathbf{L}^T \delta \phi_q. \quad (5.21)$$

Now consider the linear transformation that stretches the unit hyper-sphere in \mathcal{C} in the direction of the vector $\tilde{\phi}_q$, as sketched in Figure 5.2.

This transformation is performed by the rank-one modification defined as

$$\mathbf{G} \equiv \mathbf{I} + \gamma \tilde{\boldsymbol{\phi}}_q \tilde{\boldsymbol{\phi}}_q^T, \quad (5.22)$$

where \mathbf{I} is the identity matrix and the constant γ , which is determined by the condition

$$\tilde{\boldsymbol{\phi}}_q^T \mathbf{G} \mathbf{G}^T \tilde{\boldsymbol{\phi}}_q = 1, \quad (5.23)$$

is given by

$$\gamma \equiv \left(\tilde{\phi}_q^{-1} - 1 \right) \tilde{\phi}_q^{-2}, \quad (5.24)$$

being $\tilde{\phi}_q = \|\tilde{\boldsymbol{\phi}}_q\|_2$.

To prove the last statement, suppose without loss of generality that the vector $\tilde{\boldsymbol{\phi}}_q$ is aligned with the first vector of an orthonormal basis $\{\hat{\mathbf{e}}_1, \dots, \hat{\mathbf{e}}_{n_\phi}\}$ in \mathcal{C} , i.e., $\tilde{\boldsymbol{\phi}}_q = \tilde{\phi}_q \hat{\mathbf{e}}_1$. Thus,

$$\hat{\boldsymbol{\phi}} \equiv \mathbf{G}^T \tilde{\boldsymbol{\phi}}, \quad (5.25)$$

reads as

$$\hat{\boldsymbol{\phi}} = \tilde{\boldsymbol{\phi}} + \left(\tilde{\phi}_q^{-1} - 1 \right) \tilde{\phi}_1 \hat{\mathbf{e}}_1, \quad (5.26)$$

which implies

$$\hat{\phi}_1 = \frac{\tilde{\phi}_1}{\tilde{\phi}_q} \quad \text{and} \quad \hat{\phi}_i = \tilde{\phi}_i \quad i = 2, \dots, n_\phi. \quad (5.27)$$

Thus, it is possible to see that

$$\|\hat{\boldsymbol{\phi}}\|_2^2 = \hat{\phi}_1^2 + \dots + \hat{\phi}_{n_\phi}^2 \quad (5.28)$$

$$= \frac{\tilde{\phi}_1^2}{\tilde{\phi}_q^2} + \tilde{\phi}_2^2 + \dots + \tilde{\phi}_{n_\phi}^2 \quad (5.29)$$

$$\leq \tilde{\phi}_1^2 + \tilde{\phi}_2^2 + \dots + \tilde{\phi}_{n_\phi}^2 \quad (5.30)$$

$$\leq 1, \quad (5.31)$$

or

$$\frac{\tilde{\phi}_1^2}{\tilde{\phi}_q^2} + \tilde{\phi}_2^2 + \dots + \tilde{\phi}_{n_\phi}^2 \leq 1, \quad (5.32)$$

which is a hyper-ellipsoid with semi-axis equal to the unit in all directions except the first where it is equal to $\tilde{\phi}_q$.

Returning to the original coordinate system, the modified hyper-ellipsoid equation, Figure 5.2, is given

$$\delta\phi^T \mathbf{LGG}^T \mathbf{L}^T \delta\phi \leq \varepsilon_{tol}^2, \quad (5.33)$$

and the new Cholesky matrix, \mathbf{L}' , can be obtained from

$$\mathbf{L}'\mathbf{L}'^T = (\mathbf{LG})(\mathbf{LG})^T. \quad (5.34)$$

5.4 Adaptive Tabulation Procedure

As illustrated in Figure 3.1, the accessed region in composition space is much smaller than the realizable region, since it consists of the union of a finite number of composition trajectories along the realizable region. Therefore, the adaptive tabulation method needs to treat the accessed region only, whose shape is unknown prior to the integration of the system of equations given by Eq.(3.52).

Initially the ISAT algorithm receives the time step Δt and the tolerance ε_{tol} . Then, in every time step, the ISAT algorithm receives a query composition ϕ_q and returns an approximation for the corresponding reaction mapping $\mathbf{R}(\phi_q, t)$. This approximation is obtained via numerical integration of Eq.(4.2) or by the linear approximation $\mathbf{R}^l(\phi_q, t)$.

During the chemically reactive flow calculation, some of the computed values are sequentially stored in a table for future use. This process is known as *in situ* tabulation.

In fact, the ISAT table created by the tabulation process includes the initial composition ϕ_0 , the reaction mapping $\mathbf{R}(\phi_0, t)$ and the mapping gradient matrix $\mathbf{A}(\phi_0, t)$. Using these elements it is possible to construct the linear approximation, Eq.(5.5).

As the calculation proceeds, new query composition, ϕ_q , are received by ISAT, the table is transversed until finds a ϕ_0 that is a composition “close” to ϕ_q . Depending on the accuracy, the linear approximation around ϕ_0 is returned or the reaction mapping of ϕ_q is obtained by direct integration of Eq.(4.2).

The ISAT table is a binary search tree, Figure 5.3, since this data structure allows searching for an information with a linear dependency on the complexity in the tree height. So, if the binary search tree is balanced, such as the one illustrated in Figure 5.3(a), the search complexity is only $\mathcal{O}(\log_2 n_{tab})$, where n_{tab} is the total number entries in the tree. A sequential search for the same information in a vector data structure costs $\mathcal{O}(n_{tab})$. Search for an information in a binary search tree that is not balanced, such as the one

shown in Figure 5.3(b), has the same cost as a sequential search in a vector. If $n_{tab} \gg 1$ than $\log_2 n_{tab} \ll n_{tab}$, justifying the option for the binary search tree as the storing table. For a deeper insight in tree data structures and searching algorithms see Knuth (1997) [38] and Knuth (1998) [39].

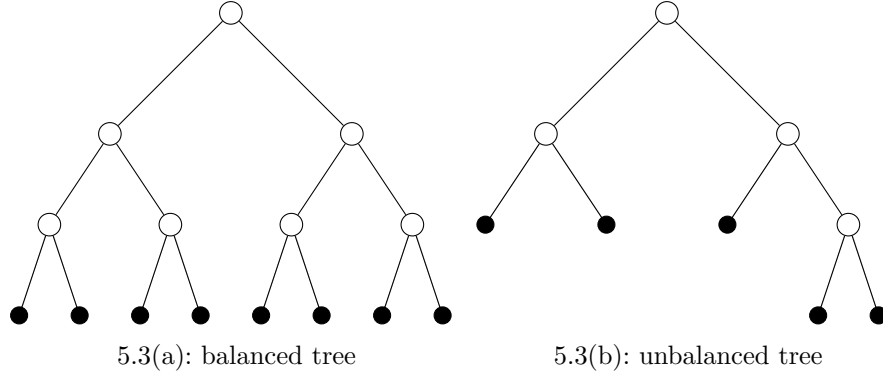


Figure 5.3: Sketch of the binary search trees created by ISAT algorithm (leaves are black and nodes white).

The binary search tree is basically formed by two types of elements, nodes and leaves. Each leaf of the tree stores the following data:

- ϕ_0 : initial composition;
- $\mathbf{R}(\phi_0, t)$: reaction mapping at ϕ_0 ;
- $\mathbf{A}(\phi_0, t)$: mapping gradient matrix at ϕ_0 ;
- \mathbf{L} : EOA Cholesky matrix.

Each node of the binary search tree has an associated *cutting plane*. This plane is defined by a *normal vector*

$$\mathbf{v} \equiv \phi_q - \phi_0, \quad (5.35)$$

and a scalar

$$a \equiv \mathbf{v}^T \left(\frac{\phi_q + \phi_0}{2} \right), \quad (5.36)$$

such that all composition ϕ with $\mathbf{v}^T \phi > a$ is deemed to be on the right of the cutting plane, all other compositions are on the left as sketched in Figure 5.4. The cutting plane construction defines a search criterion in the binary search tree.

If, during the calculation, a query point ϕ_q is encountered that is within the region of accuracy, (i.e. $\varepsilon \leq \varepsilon_{tol}$), but outside the estimate of EOA, then the EOA growth proceeds as detailed in section 5.3.

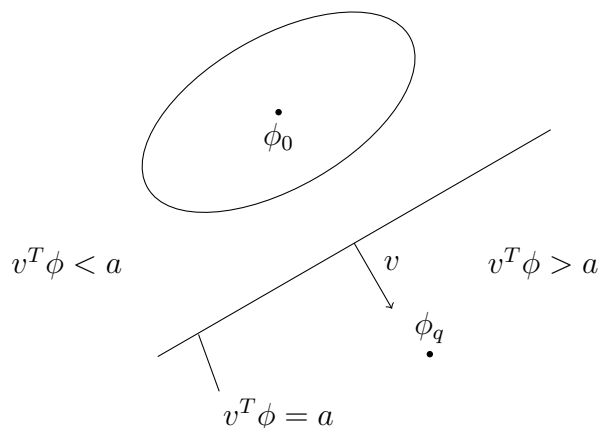


Figure 5.4: Sketch of cutting plane in relation to EOA position.

The first three items stored in the binary search tree leaf (ϕ_0 , $\mathbf{R}(\phi_0, t)$ and $\mathbf{A}(\phi_0, t)$) are computed once, whereas \mathbf{L} changes whenever the EOA is grown.

Once a query composition ϕ_q is received by ISAT table, the binary search tree is initialized as a single leaf ($\phi_0 = \phi_q$) and the exact value of the reaction mapping is returned.

The following steps are:

1. Given a query composition the tree is transversed until a leaf (ϕ_0) is found.
2. Equation (5.17) is used to determinate if ϕ_q is inside EOA or not.
3. If ϕ_q is inside EOA, the reaction mapping is given by the linear approximation, Eq.(5.5). This is the first of three outcomes, called *retrieve*.
4. If ϕ_q is outside EOA, direct integration is used to compute the reaction mapping, and the local error is measured by Eq.(5.6).
5. If the local error is smaller than tolerance, ε_{tol} , the EOA is grown according to the procedure presented in subsection 5.3 and the reaction mapping is returned. This outcome is called *growth*.
6. If local error is greater than the tolerance ε_{tol} and the maximum number of entries in the binary search tree is not reached, a new record is stored in the binary search tree based on ϕ_q and the reaction mapping is returned. The original leaf is replaced by a node with the left leaf representing the old composition ϕ_0 and the right leaf the new one ϕ_q as shown in Figure 5.5. This outcome is an *addition*.

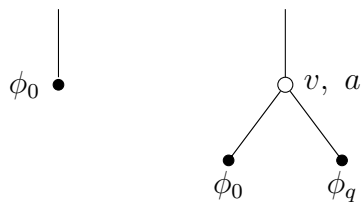


Figure 5.5: Binary search tree before and after the addition of a new node.

7. If the local error is greater than the tolerance ϵ_{tol} and the maximum number of entries in the binary search tree is reached, the reaction mapping is returned. This outcome is called *direct evaluation*.

A flowchart showing all steps of ISAT algorithm is presented in Figure 5.6.

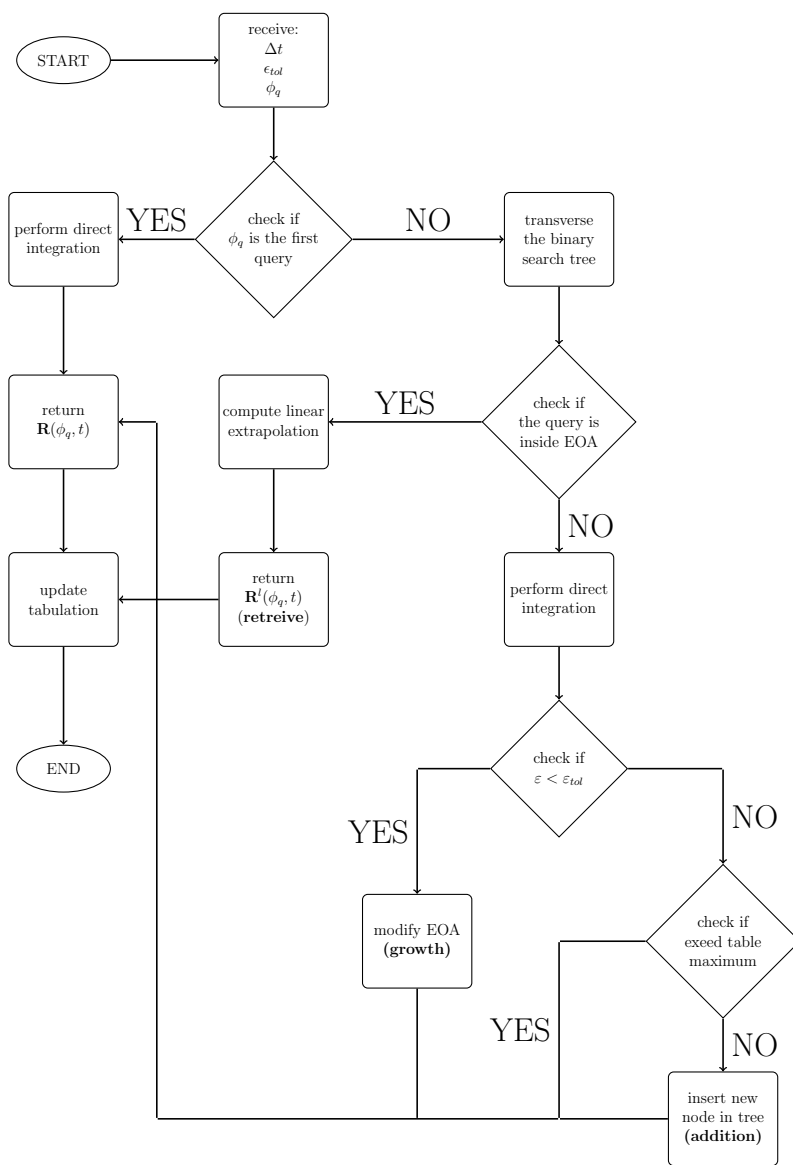


Figure 5.6: A flowchart showing all step of ISAT algorithm.

6

Results and Discussion

In this chapter are presented and discussed the results obtained in the simulations of pairwise mixing stirred reactors (PMSR) using detailed reaction mechanisms and *in situ* adaptive tabulation to solve the balance equations. All the simulations reported in this chapter were performed using double precision, in a workstation with an Intel Xeon processor with 8 cores of 2.53 GHz clock rate, 6 GB of RAM and 8 MB of cache, running Linux 2.6.32 operating system.

6.1

Code Verification

The PMSR model, the ISAT algorithm and the numerical procedures were implemented in an *in house* code written in ANSI C and Fortran 77 languages. This code uses the thermochemistry routines of Chemkin-II package by Kee et al. (1989) [37], the ODE integration routines of CVODE solver by Hindmarsh & Serban (2006) [29], the numerical linear algebra routines of the GSL package by Galassi et al. (2008) [20] and the random number generation algorithm by L'Ecuyer (1996) [47]. In order to ensure the reliability of the developed code, this section presents verification tests that were conducted.

All verification tests reported in this section use time step of $\Delta t = 0.1$ ms; solver relative tolerance of $\varepsilon_{rel} = 10^{-6}$; and solver absolute tolerance of $\varepsilon_{abs} = 10^{-9}$. Also, these tests are run for $K = 500$ time steps.

6.1.1

Numerical Integration Verification Test

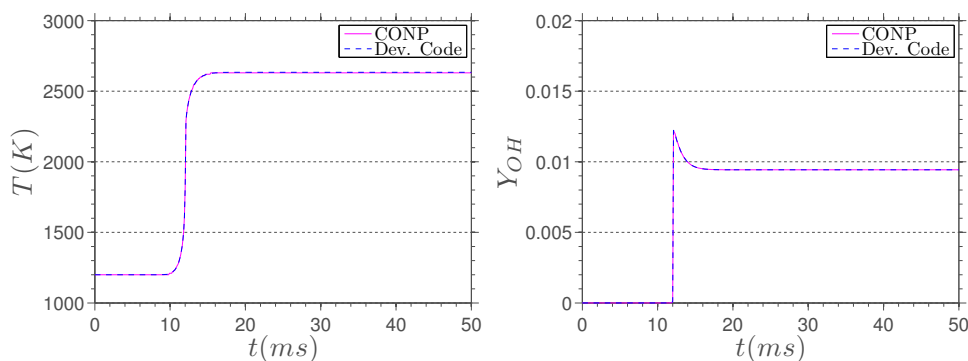
The first verification test aims to evaluate the correct implementation of the numerical integration routines. For this purpose, the results of the developed code are compared with those obtained with the CONP code by Kee et al. (1989) [37] in the simulation of an adiabatic constant pressure system.

In this test the reaction of a stoichiometric ($\Phi = 1$) mixture of CH_4 /Air at $T_0 = 1200$ K and $p_0 = 1$ atm is considered. The skeletal reaction mechanism shown in Table 6.1, (Yang & Pope, 1998a) [97], with 16 species and 40 reactions, is used to describe the CH_4 combustion with air chemical kinetics. This is the same reaction mechanism used by Pope (1997) [70].

Table 6.1: Skeletal reaction mechanism for methane/air combustion.

	Reaction		A_i (cm, mol, s)	β_i	E_i (cal/mol)
1:	$H + O_2 \rightleftharpoons OH + O$		1.59×10^{17}	-0.927	16874.0
2:	$O + H_2 \rightleftharpoons OH + H$		3.87×10^4	2.700	6262.0
3:	$OH + H_2 \rightleftharpoons H_2O + H$		2.16×10^8	1.510	3430.0
4:	$OH + OH \rightleftharpoons O + H_2O$		2.10×10^8	1.400	-397.0
5:	$H + H + M \rightleftharpoons H_2 + M$		6.40×10^{17}	-1.000	0.0
6:	$H + OH + M \rightleftharpoons H_2O + M$		8.40×10^{21}	-2.000	0.0
7:	$H + O_2 + M \rightleftharpoons HO_2 + M$		7.00×10^{17}	-0.800	0.0
8:	$HO_2 + H \rightleftharpoons OH + OH$		1.50×10^{14}	0.000	1004.0
9:	$HO_2 + H \rightleftharpoons H_2 + O_2$		2.50×10^{13}	0.000	693.0
10:	$HO_2 + O \rightleftharpoons O_2 + OH$		2.00×10^{13}	0.000	0.0
11:	$HO_2 + OH \rightleftharpoons H_2O + O_2$		6.02×10^{13}	0.000	0.0
12:	$H_2O_2 + M \rightleftharpoons OH + OH + M$		1.00×10^{17}	0.000	45411.0
13:	$CO + OH \rightleftharpoons CO_2 + H$		1.51×10^7	1.300	-758.0
14:	$CO + O + M \rightleftharpoons CO_2 + M$		3.01×10^{14}	0.000	3011.0
15:	$HCO + H \rightleftharpoons H_2 + CO$		7.23×10^{13}	0.000	0.0
16:	$HCO + O \rightleftharpoons OH + CO$		3.00×10^{13}	0.000	0.0
17:	$HCO + OH \rightleftharpoons H_2O + CO$		1.00×10^{14}	0.000	0.0
18:	$HCO + O_2 \rightleftharpoons HO_2 + CO$		4.20×10^{12}	0.000	0.0
19:	$HCO + M \rightleftharpoons H + CO + M$		1.86×10^{17}	-1.000	16993.0
20:	$CH_2O + H \rightleftharpoons HCO + H_2$		1.26×10^8	1.620	2175.0
21:	$CH_2O + O \rightleftharpoons HCO + OH$		3.50×10^{13}	0.000	3513.0
22:	$CH_2O + OH \rightleftharpoons HCO + H_2O$		7.23×10^5	2.460	-970.0
23:	$CH_2O + O_2 \rightleftharpoons HCO + HO_2$		1.00×10^{14}	0.000	39914.0
24:	$CH_2O + CH_3 \rightleftharpoons HCO + CH_4$		8.91×10^{-13}	7.400	-956.0
25:	$CH_2O + M \rightleftharpoons HCO + H + M$		5.00×10^{16}	0.000	76482.0
26:	$CH_3 + O \rightleftharpoons CH_2O + H$		8.43×10^{13}	0.000	0.0
27:	$CH_3 + OH \rightleftharpoons CH_2O + H_2$		8.00×10^{12}	0.000	0.0
28:	$CH_3 + O_2 \rightleftharpoons CH_3O + O$		4.30×10^{13}	0.000	30808.0
29:	$CH_3 + O_2 \rightleftharpoons CH_2O + OH$		5.20×10^{13}	0.000	34895.0
30:	$CH_3 + HO_2 \rightleftharpoons CH_3O + OH$		2.28×10^{13}	0.000	0.0
31:	$CH_3 + HCO \rightleftharpoons CH_4 + CO$		3.20×10^{11}	0.500	0.0
32:	$CH_4 + H \rightleftharpoons CH_3 + H_2$		7.80×10^6	2.110	7744.0
33:	$CH_4 + O \rightleftharpoons CH_3 + OH$		1.90×10^9	1.440	8676.0
34:	$CH_4 + O_2 \rightleftharpoons CH_3 + HO_2$		5.60×10^{12}	0.000	55999.0
35:	$CH_4 + OH \rightleftharpoons CH_3 + H_2O$		1.50×10^6	2.130	2438.0
36:	$CH_4 + HO_2 \rightleftharpoons CH_3 + H_2O_2$		4.60×10^{12}	0.000	17997.0
37:	$CH_3O + H \rightleftharpoons CH_2O + H_2$		2.00×10^{13}	0.000	0.0
38:	$CH_3O + OH \rightleftharpoons CH_2O + H_2O$		5.00×10^{12}	0.000	0.0
39:	$CH_3O + O_2 \rightleftharpoons CH_2O + HO_2$		4.28×10^{-13}	7.600	-3528.0
40:	$CH_3O + M \rightleftharpoons CH_2O + H + M$		1.00×10^{14}	0.000	25096.0

The evolution of the system temperature/ OH mass fraction are shown in Figure 6.1, where it is possible to verify the excellent agreement of the results of the developed code with those obtained with the CONP code by Kee et al. (1989) [37]. These results allow to conclude that the numerical integration routines of the developed code are capable of reproducing the baseline results. The results for the other chemical species, not shown here for the sake of brevity, exhibit a similar agreement.

6.1(a): Evolution of T .6.1(b): Evolution of Y_{OH} .Figure 6.1: Evolution of T and Y_{OH} for the first verification test.

6.1.2

Error Control Verification Test

The second verification test evaluates the capacity of the ISAT routines to control the errors. For this purpose, the test analyzes how the error incurred by the ISAT behaves as the value of the ISAT error tolerance is changed.

In this test the PMSR reported in the work of Pope (1997) [70] is considered. This PMSR has its parameters are shown in Table 3.1 and, initially, all of its stochastic particles have their composition set to the adiabatic constant pressure equilibrium of a stoichiometric ($\Phi = 1$) mixture of CH_4/Air ($T_{eq} = 2376$ K) at $T_0 = 300$ K and $p_0 = 1$ atm. At every time step, three inflow streams at atmospheric pressure and with mass flow rates in the ratio 0.85 : 0.05 : 0.1 enter the reactor. The first stream is air (79% N_2 and 21% O_2) at $T_{in} = 300$ K, the second one is CH_4 at $T_{in} = 300$ K, whereas the third stream composition is the same as the particles which initially are within the PMSR. The thermochemistry of these mixtures is also described by the skeletal reaction mechanism of Table 6.2, (Yang & Pope, 1998a) [97].

Table 6.2: PMSR parameters used in the code verification tests.

number of particles	N	100
residence time (ms)	τ_r	10
mixing time (ms)	τ_m	1
pairwise time (ms)	τ_p	1

Note that Pope (1997) [70] does not provide details on the actual composition of each particle entering the reactor. Indeed, this three stream problem may be treated in several ways, for instance, each incoming particle may have the same composition, or each incoming particle may be prescribed with the composition of a given stream. Here the first, simpler, possibility is used.

In the simulation of the PMSR described above an ISAT binary search tree with a maximum of 1,000 entries is used as well as an ISAT lower bound of $\kappa = 1$.

The error metric used by Pope (1997) [70] to measure the error incurred by ISAT technique is the *global error* over $K = 500$ time steps, which is defined as

$$\epsilon_G \equiv \frac{1}{KN_p} \sum_{k=1}^K \sum_{j=1}^{N_p} \|\phi^{(j)}(k\Delta t)_{ISAT} - \phi^{(j)}(k\Delta t)_{DI}\|_2, \quad (6.1)$$

where the subscripts DI and $ISAT$ denote DI and ISAT calculations, respectively. This is the error metric used in this verification test to evaluate the capacity of the ISAT routines control de errors incurred by the algorithm. In order to seek the two time series used to compute ϵ_G exhibit a small statistical dispersion, at least in the beginning of the computation, the same seed values are used for the random process describing mixing and outflow.

The behavior of the ISAT global error as function of the error tolerance for the developed code and for the reference PMSR of Pope (1997) [70] (described above) is shown in Figure 6.2. The results show that the linear trend of ϵ_G with ε_{tol} obtained by Pope (1997) [70] is not recovered, but, instead, a nearly constant value of ϵ_G , of the order of 10^{-1} , occurs when ε_{tol} is decreased. Such a behavior could be explained by the uncertainty of the particle composition adopted Pope (1997) [70] at the inflow. Another possible explanation for the observed discrepancy is the use of a scaling matrix (Pope, 1997) [70] to construct the ellipsoid of accuracy, Eq.(5.16). This scaling matrix could be responsible for the decrease of the error measure of the enthalpy. As will be show in the next section, the expected error behavior is

recovered under more controlled situations. Note also that the monotonically decreasing behavior of ϵ_G exhibit by Pope (1997) [70] seems rather surprising for such a small number of stochastic particles, which is expected to lead to large bias errors.

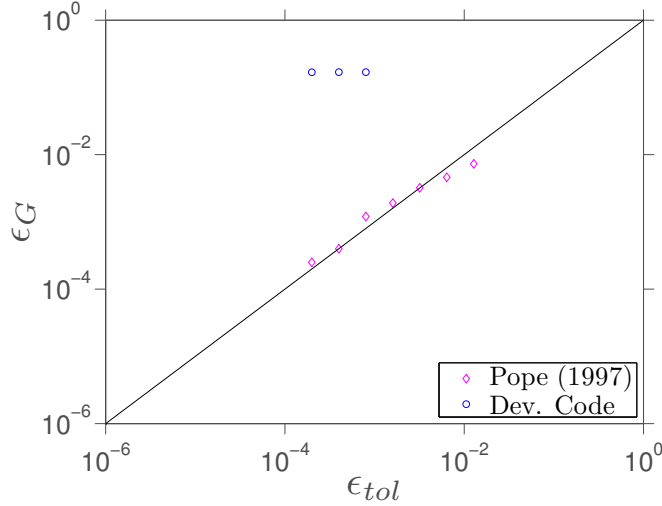


Figure 6.2: Behavior of the ISAT global error as function of the error tolerance for the second verification test.

6.2 Analysis of ISAT Accuracy

In order to assess the accuracy of the ISAT technique implementation, this section defines the error metrics used to estimate the uncertainties in ISAT calculations. Also, this section presents a study which aims to compare the calculation results obtained by the ISAT technique with those issued from the direct integration (DI), which uses `CVODE` solver to perform the numerical integration of the evolution equation in a PMSR.

6.2.1 Error Metrics

The *absolute global error* of the ISAT calculation over a time interval $\Delta\tau$ is defined as

$$\epsilon_g \equiv \frac{1}{\Delta\tau} \int_t^{t+\Delta\tau} \|\mathbf{B}[\langle\phi\rangle(t')_{DI} - \langle\phi\rangle(t')_{ISAT}]\|_2 dt', \quad (6.2)$$

where \mathbf{B} is a scaling matrix. In this work \mathbf{B} is a identity matrix except by the first entry, which is chosen equal to inverse of the equilibrium enthalpy of the mixture that feeds the reactor. This metric is a global measure of error imposed by the ISAT technique on the solution of the system of ODE's that governs the problem under study.

A metric that represents a local measure of the error incurred by ISAT technique is the *relative local error* of a property ψ , which is defined as

$$\varepsilon_{r,\psi} \equiv \left| \frac{\psi_{DI}(t) - \psi_{ISAT}(t)}{\psi_{DI}(t)} \right|. \quad (6.3)$$

Two other metrics, which are used to measure the global error are the *mean relative error* of ψ over an interval $\Delta\tau$, defined as

$$\langle \varepsilon_{r,\psi} \rangle_M \equiv \frac{1}{\Delta\tau} \int_t^{t+\Delta\tau} \varepsilon_{r,\psi}(t') dt', \quad (6.4)$$

and the *maximum relative error* of ψ over an interval $\Delta\tau$, defined as

$$\langle \varepsilon_{r,\psi} \rangle_\infty \equiv \sup_{t' \in [t, t+\Delta\tau]} \{ \varepsilon_{r,\psi}(t') \}. \quad (6.5)$$

Those metrics were chosen in order to provide measures that are, in a sense, more global than that of Eq.(6.1) and, thus, could be easily applied to more complicated problems, such as those involving transport.

6.2.2

PMSR with a CO/O_2 Mixture

Consider a PMSR initially filled with a fuel-lean ($\Phi = 0.7$) mixture of CO/O_2 at $T_0 = 2948.5$ K and $p_0 = 1$ atm. At every time step, a fuel-lean ($\Phi = 0.7$) mixture of CO/O_2 enters the reactor at $T_{in} = 300$ K and $p_{in} = 1$ atm. The constant pressure and enthalpy equilibrium state associated to the inflow mixture is reached at $T_{eq} = 2948.5$ K. The reaction of CO with O_2 , which chemical kinetics is described by the reaction mechanism given in Table 3.1, involves 4 species and 3 reactions.

Influence of the time scale ratio

Two configurations of time scales are studied for this PMSR, which are presented in Table 6.3. For the first configuration of time scales, which defines the first test case, $\tau_m/\tau_r = 1/2$ and $\tau_p/\tau_r = 1/2$, so that the pairwise/mixing time scales are of the same order of magnitude as the residence time, thus allowing to obtain partially stirred reactor (PaSR) conditions. For the second test case, which is defined by the second configuration of time scales presented in the Table 6.3, $\tau_m/\tau_r = 1/10$ and $\tau_p/\tau_r = 1/10$, so that the pairwise/mixing time scales are small when compared with the residence time. Thus, the reactor should behave almost like a perfect stirred reactor (PSR), where the processes of mixing and pairing occur instantaneously. Note that the same seed is used to the pairwise mixing and outflow statistical processes in the DI and ISAT calculations.

Table 6.3: Parameters used in the simulation of a CO/O_2 mixture in a PMSR.

		Case 1	Case 2
number of particles	N	1024	1024
residence time (μs)	τ_r	200	1000
mixing time (μs)	τ_m	100	100
pairwise time (μs)	τ_p	100	100

This study uses a binary search tree with a maximum of 50,000 entries; time step of $\Delta t = 10 \mu s$; solver relative tolerance of $\varepsilon_{rel} = 10^{-6}$; solver absolute tolerance of $\varepsilon_{abs} = 10^{-9}$; ISAT error tolerance of $\varepsilon_{tol} = 10^{-3}$; and ISAT lower bound of $\kappa = 1$.

Figures 6.3 and 6.4 show the comparison between DI and ISAT computational results for the temporal evolution of the first two statistical moments of the reduced temperature (defined in appendix A) in both cases. The dimensionless time, τ^* , shown in these figures is also defined in appendix A.

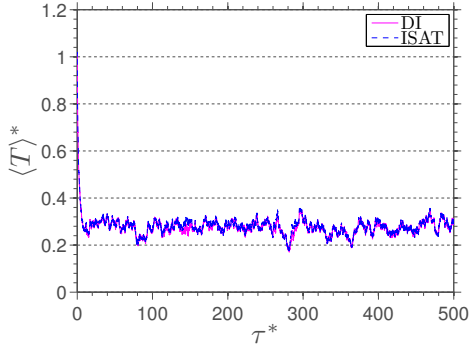
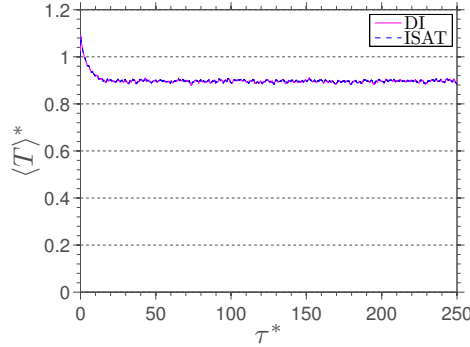
6.3(a): Evolution of $\langle T \rangle^*$ for case 1.6.3(b): Evolution of $\langle T \rangle^*$ for case 2.

Figure 6.3: Comparison between DI and ISAT results of ensemble average of reduced temperature for cases 1 and 2.

For case 1 results, which span over a range of 500 residence times, one can observe an excellent qualitative agreement for the ensemble average/variance of the reduced temperature. The ensemble average value rapidly drops from the initial value to reach the statistically steady state regime around $\langle T \rangle^* = 0.3$. The ensemble variance rapidly grows, then decreases until it reaches the statistically steady state value around $\langle T'^2 \rangle^* = 0.13$. The analysis of the two figures shows that the statistically steady state regime is reached after $\tau^* = 10$ residence times.

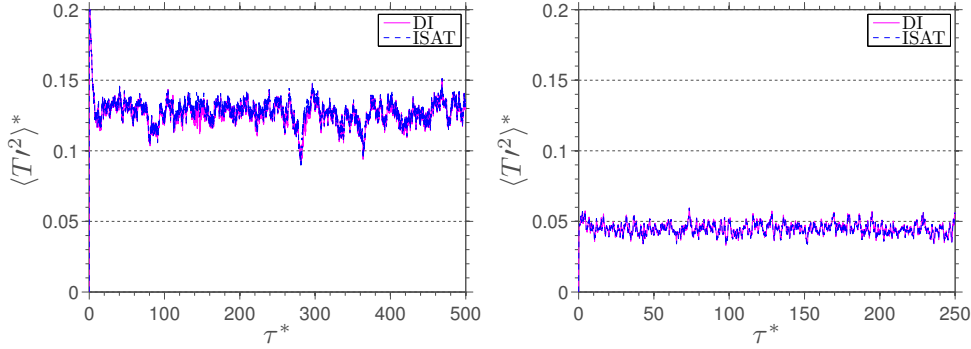
6.4(a): Evolution of $\langle T'^2 \rangle^*$ for case 1.6.4(b): Evolution of $\langle T'^2 \rangle^*$ for case 2.

Figure 6.4: Comparison between DI and ISAT results of ensemble variance of reduced temperature for cases 1 and 2.

In case 2, where a range of 250 residence times is computed, one can also observe an excellent qualitative agreement for the ensemble average/variance of reduced temperature. Again, the overall history of the PMSR is the same for DI and ISAT. Similar results, not shown here, were obtained for the other thermochemical properties of the reactors.

Aiming to quantify the discrepancies between the values obtained via DI and ISAT, Figures 6.5 and 6.6 present the evolution of the relative local errors of the statistical moments of T^* and Y_O , Eq.(6.3). Concerning the errors associated to the mean physical quantities in case 1, one can observe a large statistical variation due to stochastic nature of the PMSR model, with amplitudes reaching 13%. In case 2, relative errors of the order of 1% can be observed.

Table 6.4: Mean and maximum relative errors for cases 1 and 2, using a binary search tree with 50k entries.

ψ	Case 1		Case 2	
	$\langle \varepsilon_{r,\psi} \rangle_M$	$\langle \varepsilon_{r,\psi} \rangle_\infty$	$\langle \varepsilon_{r,\psi} \rangle_M$	$\langle \varepsilon_{r,\psi} \rangle_\infty$
$\langle T \rangle^*$	1.0 %	13.4 %	0.0 %	0.1 %
$\langle Y_O \rangle$	1.2 %	19.1 %	0.1 %	1.0 %
$\langle T'^2 \rangle^*$	1.0 %	12.2 %	0.5 %	2.0 %
$\langle Y_O'^2 \rangle$	0.9 %	13.0 %	0.5 %	3.2 %

In Table 6.4 are presented error metrics associated to the statistical moments of T^* and Y_O . One can observe that the mean error of the average properties is smaller than 1.2% in case 1, and of 0.1% in case 2 only. The mean error of T^* and Y_O ensemble variances is rather large in case 1. Concerning the maximum error, the extrema are 19.1% and 3.2% for cases 1 and 2, respectively.

Such high values for the maximum errors could be explained by the existence, in ISAT table, of compositions which are tabulated during the transient regime. An approximation for a reaction mapping, which is in statistically steady state regime, computed around one of these compositions incurs in large errors.

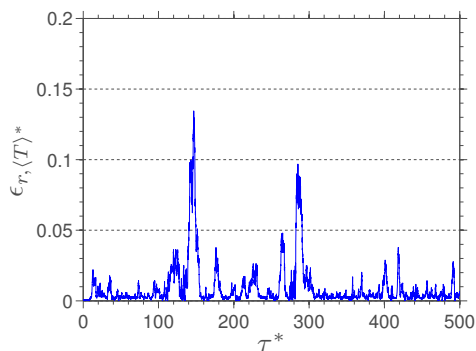
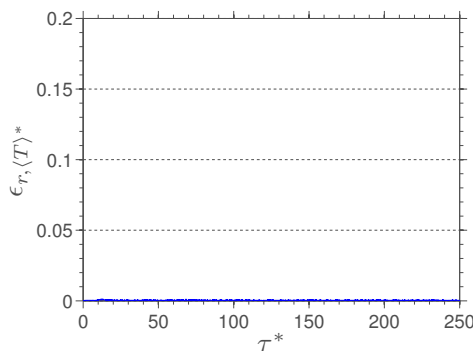
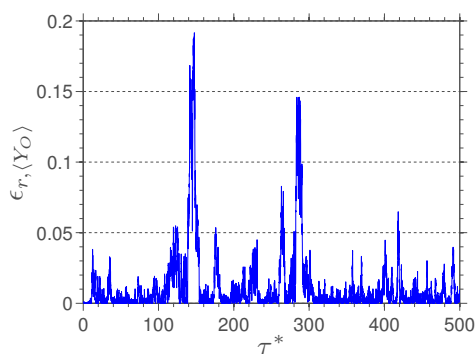
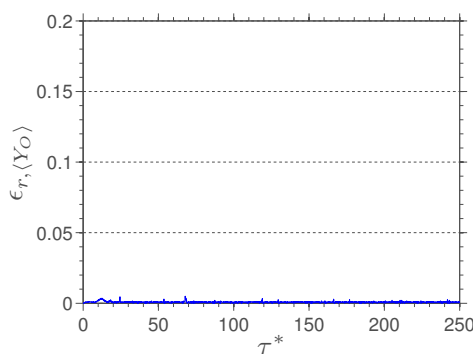
6.5(a): Evolution of $\varepsilon_{r,\langle T \rangle^*}$ for case 16.5(b): Evolution of $\varepsilon_{r,\langle T \rangle^*}$ for case 26.5(c): Evolution of $\varepsilon_{r,\langle Y_O \rangle}$ for case 16.5(d): Evolution of $\varepsilon_{r,\langle Y_O \rangle}$ for case 2

Figure 6.5: Evolution of relative local error for ensemble average of the reduced temperature and of the O mass fraction for cases 1 and 2.

The difference among cases is due to the behavior of each reactor at the statistically steady state regime. Indeed, the behavior of the reactor of case 2 is governed by a competition between the chemical and residence times mostly, therefore the thermodynamical properties steady state probability density function is spread over a smaller range than in case 1, where the mixing and pairing time scales are large. This behavior is illustrated in Figures 6.7 and 6.8, which present the comparison between DI and ISAT computations of the mean histograms, averaged over the last 50 residence times, of the reduced temperature and the O mass fraction for cases 1 and 2. These figures underscore the influence of the controlling parameters of the PMSR, i.e., the time scales ratios, on the thermochemical conditions prevailing within each reactor.

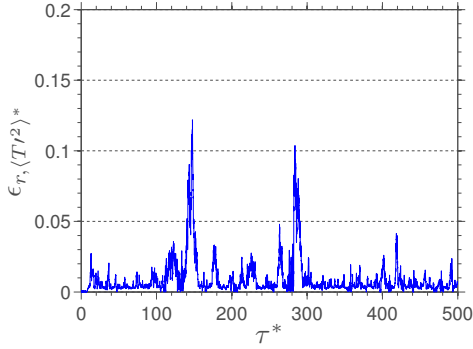
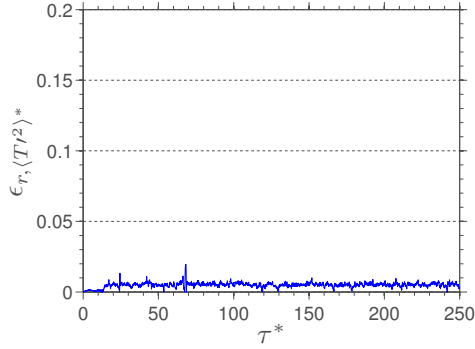
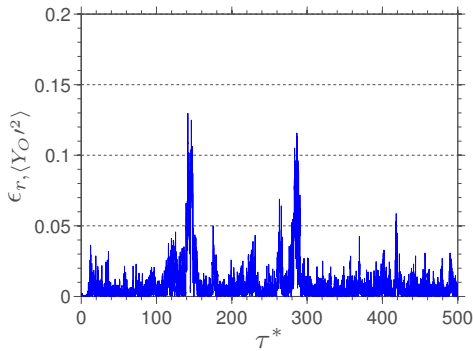
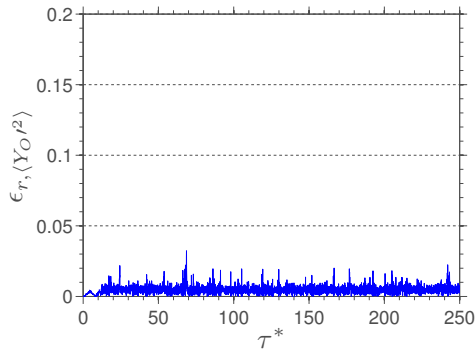
6.6(a): Evolution of $\varepsilon_{r,\langle T'^2 \rangle^*}$ for case 16.6(b): Evolution of $\varepsilon_{r,\langle T'^2 \rangle^*}$ for case 26.6(c): Evolution of $\varepsilon_{r,\langle Y_O'^2 \rangle}$ for case 16.6(d): Evolution of $\varepsilon_{r,\langle Y_O'^2 \rangle}$ for case 2

Figure 6.6: Evolution of relative local error for ensemble variance of the reduced temperature and of the O mass fraction for cases 1 and 2.

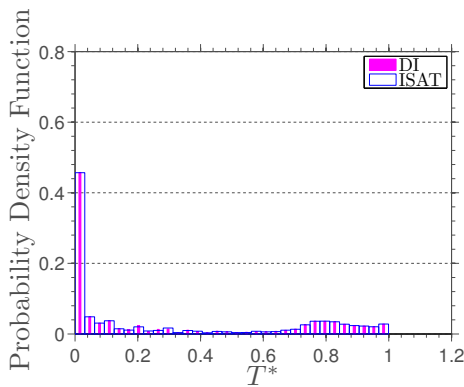
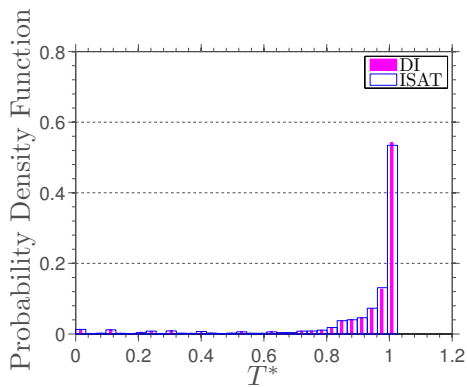
6.7(a): PDF of T^* for case 1.6.7(b): PDF of T^* for case 2.

Figure 6.7: Comparison between DI and ISAT computations of the mean histograms (over the last 50 residence times) of the reduced temperature for cases 1 and 2.

Indeed, the temperature within the reactor of case 2 is such that almost only burned gases are found. On the other hand, case 1 reactor is characterized by a bimodal temperature distribution with a large probability of finding $T^* = 0.04$ and a broader temperature distribution leaning toward the burned gases. Such a distribution, as it could be expected, is reflected on the Y_O one, which also exhibits a bimodal distribution.

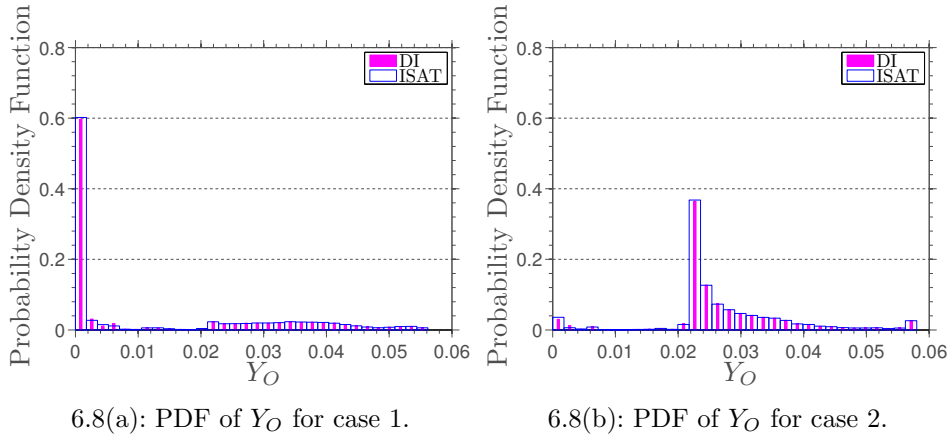


Figure 6.8: Comparison between DI and ISAT computations of the mean histograms (over the last 50 residence times) of the O mass fraction for cases 1 and 2.

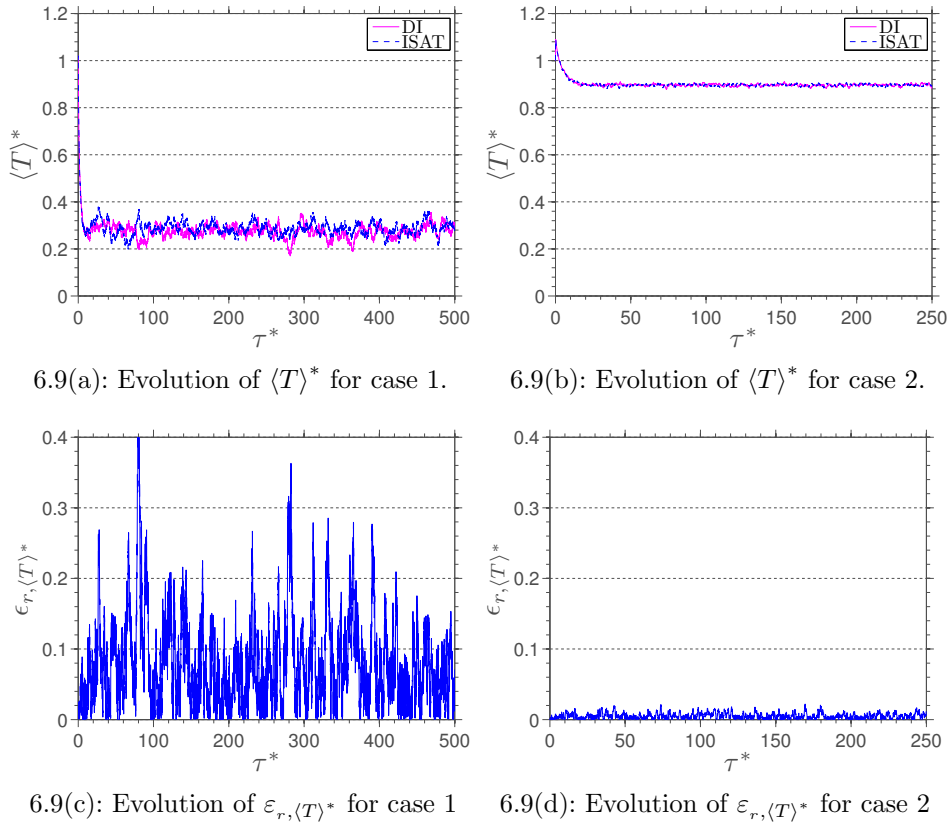


Figure 6.9: Comparison between DI and ISAT results (using different seeds) of reduced temperature ensemble average and the corresponding relative local errors for cases 1 and 2.

Influence of the statistical process seed

All the results for cases 1 and 2 shown above use the same seed value for the random number generator in DI and ISAT calculations. However, since the mixing model is statistical in nature, it could be expected that the seed value may influence the ISAT behavior. Therefore, if DI calculation seed is kept fixed and ISAT seed is changed, the results for $\langle T \rangle^*$ and $\varepsilon_{r, \langle T \rangle^*}$ are modified. This can be seen in Figure 6.9, where one can observe an increase in the relative local error of $\langle T \rangle^*$ for both cases.

The analysis of graphs in Figure 6.9 indicates that 1024 particles are not sufficient to guarantee the statistical independence of the results. This hypothesis is also confirmed if one observe the Figure 6.10, where it is possible to see discrepancies in DI and ISAT mean histograms of T^* for both cases.

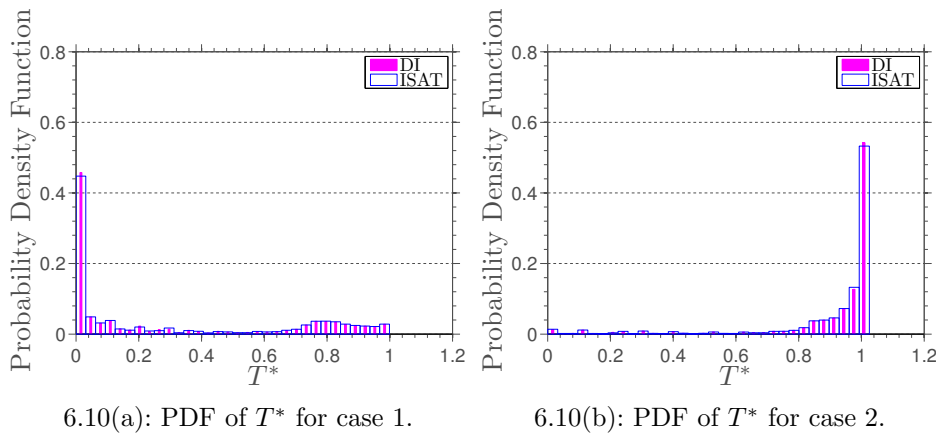


Figure 6.10: Comparison between DI and ISAT computations (using different seeds) of the mean histograms (over the last 50 residence times) of the reduced temperature for cases 1 and 2 .

On the other hand, these histograms qualitatively are not much different from those shown in Figure 6.7. Thus, one can conclude that although the results have not guaranteed their statistical independence with a sample of 1024 particles, they do not vary much with a sample of this size. Possibly a sample of 4096¹ particles is sufficient to ensure the independence of the results.

Influence of the ISAT error tolerance

In the early development of the ISAT technique (Pope, 1997) [70] it was noted that the choice of the tolerance could affect the accuracy of the problem solution. In order to investigate the effect of the tolerance on the present results, Figure 6.11 presents the absolute global error, defined in section 6.2.1,

¹Powers of 4, such as $1024 = 4^5$ and $4096 = 4^6$, are commonly used in statistics since they are always perfect squares, which facilitates the construction of histograms.

as a function of the ISAT error tolerance for cases 1 and 2. When the same statistical seed is used, for both cases, ε_g decreases monotonically as ε_{tol} is reduced. However, if different statistical seeds are used, one can note a limit where ε_g does not decrease if ε_{tol} is reduced. This saturation in ε_g value indicates that decrease ε_{tol} value below 10^{-3} is not effective in cases where the statistical seeds are different.

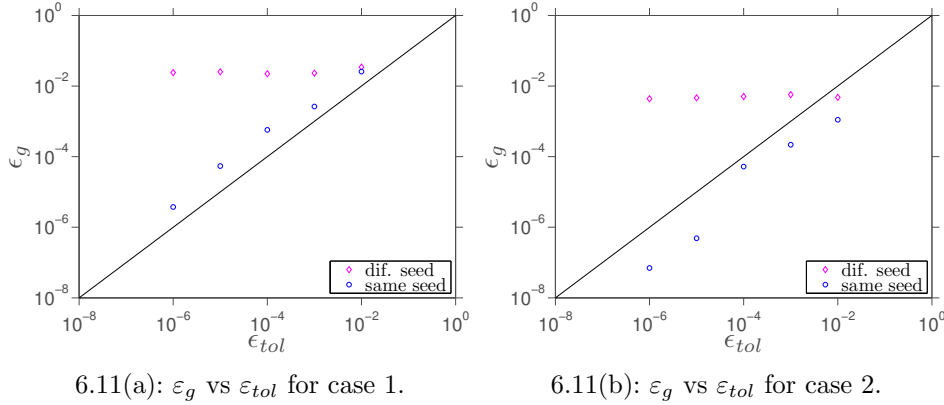


Figure 6.11: Absolute global errors for cases 1 and 2 as function of the error tolerance, using a binary search tree with 50k entries.

From the analysis of the global and local error metrics it is possible to characterize an ISAT table with 50k entries as one with an excellent qualitative reproduction of the results, in which the local errors are less than 20% and the global errors are smaller than 1%.

Influence of the ISAT lower bound

Tests were also made to characterize the influence of the ISAT lower bound, κ , on the accuracy of the algorithm. Again equal statistical seed are used for DI and ISAT calculations. Table 6.5 shows the values of absolute global error as function of ε_{tol} and κ for a test case similar to case 1, but simulated only for 100 residence times. The analysis of this data reveals that, in general, for a fixed value of κ , the error decreases monotonically as ε_{tol} is reduced.

Moreover, one can note that, for a fixed value of ε_{tol} , the error remains approximately of the same order of magnitude, except for the pair $\varepsilon_{tol} = 10^{-6}$ and $\kappa = 10^9$. In this case, the lengths of the half-axes of the EOA are limited within a range that varies only two orders of magnitude, Eq.(5.15), which leads to a bad initial estimate for the region of accuracy of the ISAT.

Table 6.5: Absolute global error as function of ε_{tol} and κ .

κ	ε_{tol}				
	10^{-2}	10^{-3}	10^{-4}	10^{-5}	10^{-6}
10^0	3.3×10^{-3}	2.4×10^{-4}	5.0×10^{-5}	4.1×10^{-6}	3.4×10^{-7}
10^3	3.3×10^{-3}	2.4×10^{-4}	5.0×10^{-5}	4.1×10^{-6}	3.4×10^{-7}
10^5	3.3×10^{-3}	2.4×10^{-4}	5.0×10^{-5}	4.1×10^{-6}	3.3×10^{-7}
10^6	3.3×10^{-3}	2.4×10^{-4}	5.0×10^{-5}	4.1×10^{-6}	2.9×10^{-7}
10^7	3.3×10^{-3}	2.4×10^{-4}	5.0×10^{-5}	3.5×10^{-6}	4.0×10^{-7}
10^8	3.3×10^{-3}	2.4×10^{-4}	3.7×10^{-5}	1.2×10^{-6}	5.4×10^{-7}
10^9	3.3×10^{-3}	2.4×10^{-4}	3.7×10^{-5}	3.2×10^{-5}	2.4×10^{-2}

From these results it may be concluded that the filter of chemical time scales, characterized by κ and originally proposed in this work, does not offer any significant advantage in terms of accuracy of the overall ISAT technique. The effect of this parameter on the side of the binary search tree or the speed-up of the computation are not investigated, although should deserve attention in future works.

6.2.3

PMSR with a CH_4/Air Mixture

The third studied case consists of a PMSR initially filled with the combustion products of a stoichiometric ($\Phi = 1$) mixture of CH_4/Air at $T_0 = 2100$ K and $p_0 = 1$ atm. At every time step, a stoichiometric ($\Phi = 1$) mixture of CH_4/Air enters the reactor at $T_{in} = 300$ K and $p_{in} = 1$ atm. The constant pressure and enthalpy equilibrium state associated to this mixture is reached at $T_{eq} = 2225.5$ K. The reaction of CH_4 with air chemical kinetics is described by GRI mechanism version 3.0 [89], with 53 species and 325 reactions. A discussion of the accuracy of such a mechanism is developed by Orbegoso et al. (2009) [65].

The time scales associated to this PMSR are presented in the Table 6.6. For this choice of time scales, where the ratio between the time of pairwise/mixing and the residence time are the order of one quarter, the reactor is expected to behave like a partially stirred reactor.

This simulation uses a binary search tree with a maximum of 60,000 entries; time step of $\Delta t = 0.1$ ms; solver relative tolerance of $\varepsilon_{rel} = 10^{-6}$; solver absolute tolerance of $\varepsilon_{abs} = 10^{-9}$; ISAT error tolerance of $\varepsilon_{tol} = 10^{-3}$; and ISAT lower bound of $\kappa = 1$. Different seed are used for the DI and ISAT calculations, it can thus be expected that rather large errors result.

Table 6.6: Parameters for a PMSR of CH_4/Air that behaves like a partially stirred reactor.

number of particles	N	1024
residence time (ms)	τ_r	4
mixing time (ms)	τ_m	1
pairwise time (ms)	τ_p	1

The comparison between DI and ISAT computational results for the first two statistical moments of the reduced temperature and OH mass fraction for case 3 are presented in Figures 6.12 and 6.13. One can note reasonable and good agreements for reduced temperature and OH mass fraction statistics, respectively. The results of case 3 show large discrepancy for the reduced temperature than that obtained in case 1. The kinetic mechanism of methane is much more complex than the mechanism used to model the carbon monoxide system in case 1, which would in principle lead to a PMSR with methane to assume a wider range of possible thermodynamic states. Thus, it could be expected that the present binary search tree with 60k entries (almost similar to that used in case 1) would yield comparatively lower accuracy.

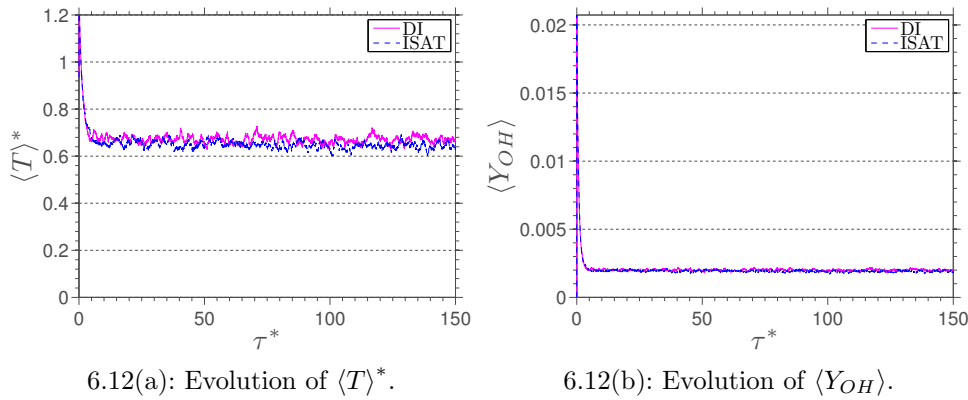


Figure 6.12: Comparison between DI and ISAT results of the ensemble average of the reduced temperature and OH mass fraction for case 3.

It is noteworthy that a binary search tree with 60k entries uses almost all available memory of the workstation used in this work. Thus, for practical purposes, it is the largest tree that can be used to simulate a PMSR with this methane combustion mechanism and 1024 particles.

In Figure 6.14 one can observe the evolution of the relative local error of the statistical moments of T^* and Y_{OH} for case 3. Compared with the results of case 1, the errors of case 3 present more oscillations. The other error metrics for this case are presented in Table 6.7, where it can be noted that the higher

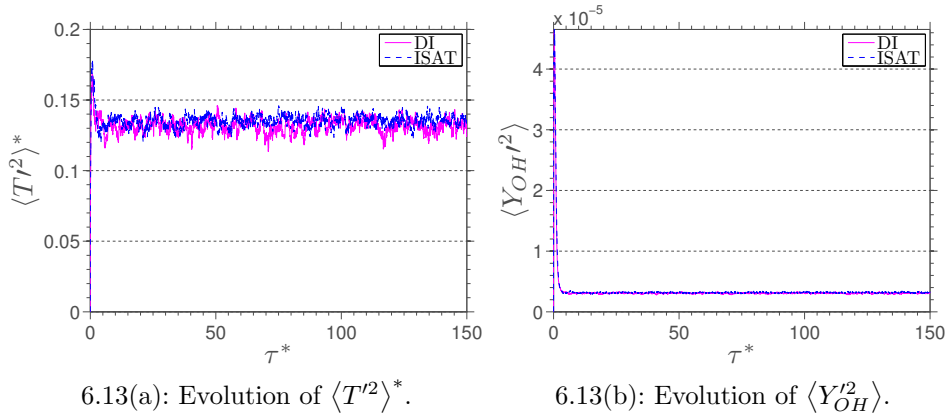


Figure 6.13: Comparison between DI and ISAT results of the ensemble variance of the reduced temperature and OH mass fraction for case 3.

values for average and maximum relative errors in case 3 are 5% and 21%, respectively. Also, the absolute global error for this case is 2.4×10^{-3} , an order of magnitude larger than the values obtained in cases 1 and 2 also using $\varepsilon_{tol} = 10^{-3}$.

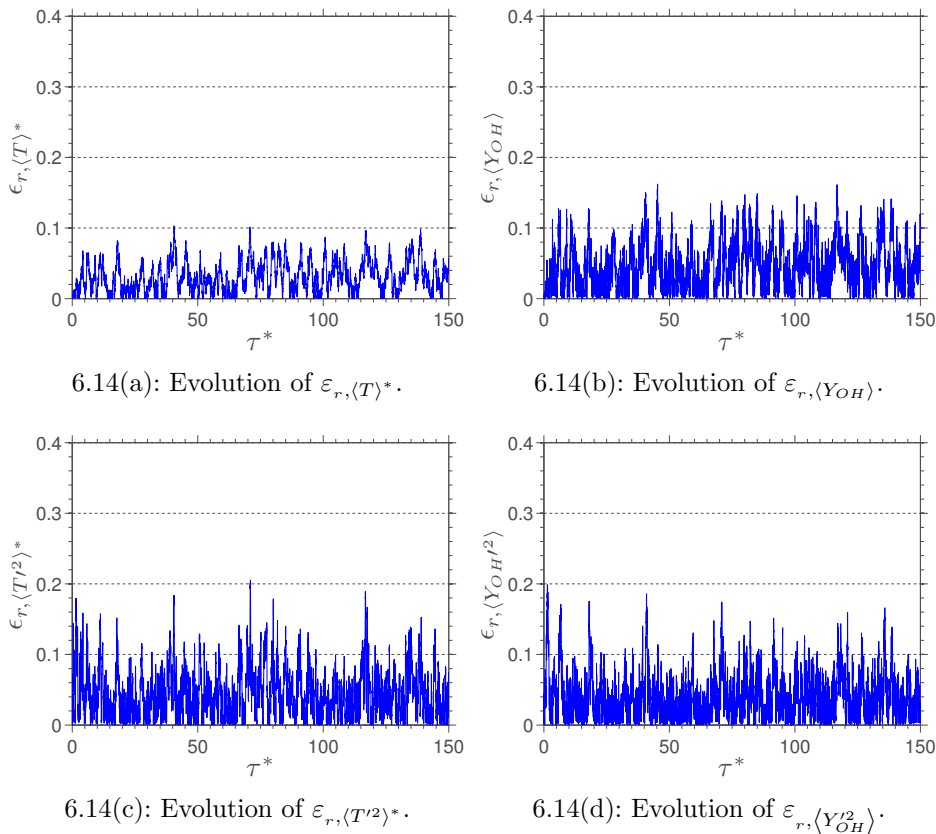


Figure 6.14: Evolution of relative local error of the first two statistical moments of the reduced temperature and OH mass fraction for case 3.

Table 6.7: Mean and maximum relative errors for case 3, using a binary search tree with 60k entries.

ψ	$\langle \varepsilon_{r,\psi} \rangle_M$	$\langle \varepsilon_{r,\psi} \rangle_\infty$
$\langle T \rangle^*$	3 %	10 %
$\langle Y_{OH} \rangle$	5 %	16 %
$\langle T'^2 \rangle^*$	5 %	21 %
$\langle Y_{OH}^2 \rangle$	4 %	20 %

Finally, Figure 6.15 presents the comparison between DI and ISAT computations of the mean histograms, averaged over the last 50 residence times, of the reduced temperature and the HCO mass fraction for case 3.

The temperature PDF presents a bimodal distribution with large probability of finding $T^* = 1$ and a broader temperature distribution leaning to the fresh gases. On the other hand, the PDF of Y_{HCO} shows a distribution essentially concentrated in the fresh gases region, and nearly homogeneous elsewhere. This behavior illustrates the fact that HCO , an intermediate species, appears in low concentration at the burned gases.

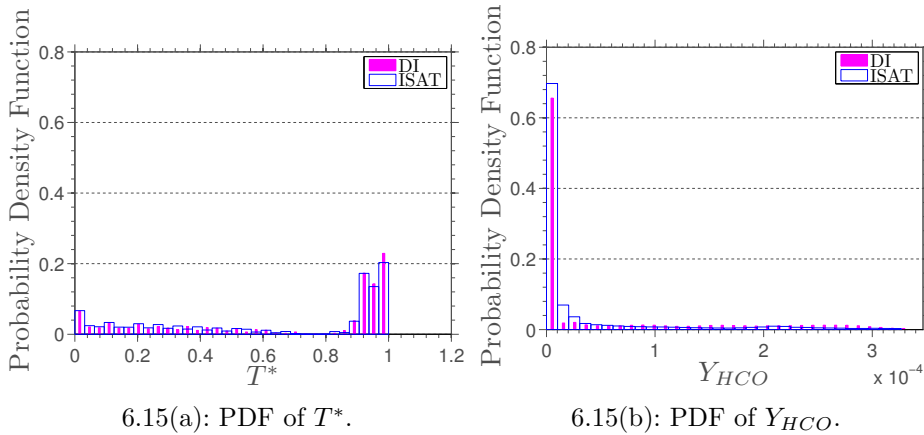


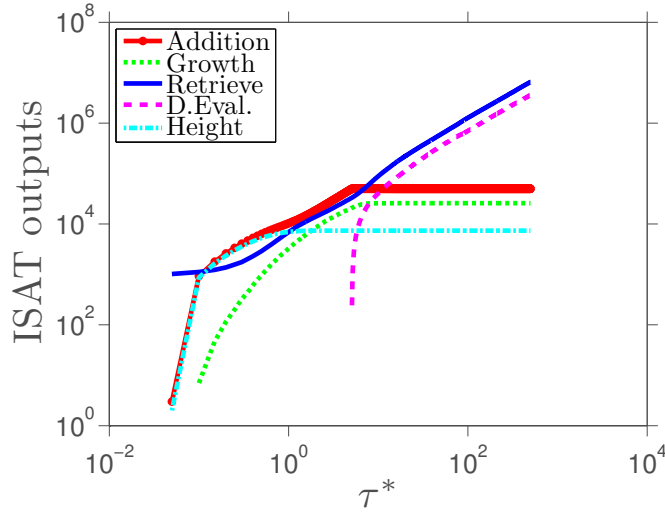
Figure 6.15: Comparison between DI and ISAT computations of the mean histograms (over the last 50 residence times) of the reduced temperature and HCO mass fraction for case 3.

6.3 Analysis of ISAT Performance

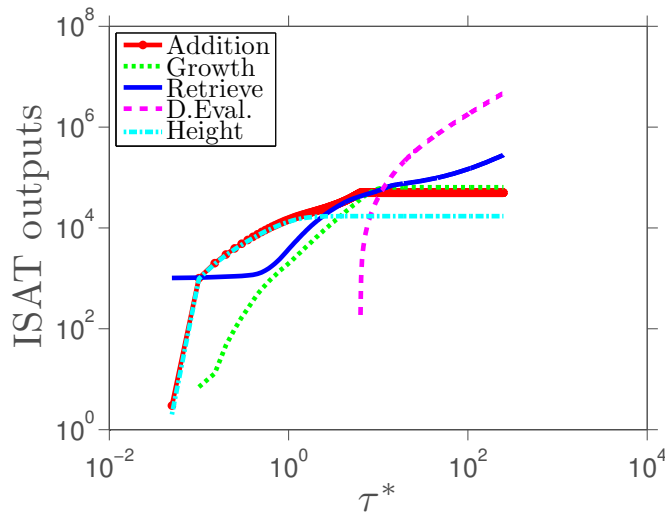
In order to assess the performance of the ISAT technique implementation, this section presents the evolution of the ISAT algorithm outputs (number of additions, growths, retrieves and direct evaluations), the evolution of the height of the ISAT binary search tree and the corresponding rates of change.

6.3.1 ISAT Performance for CO/O_2 Mixtures

The comparison of evolution of the ISAT algorithm outputs and of the height of the ISAT binary search tree as well as the corresponding rates of change, for cases 1 and 2, which parameters are given in Table 6.3, are presented in Figures 6.16 and 6.17.



6.16(a): Case 1.

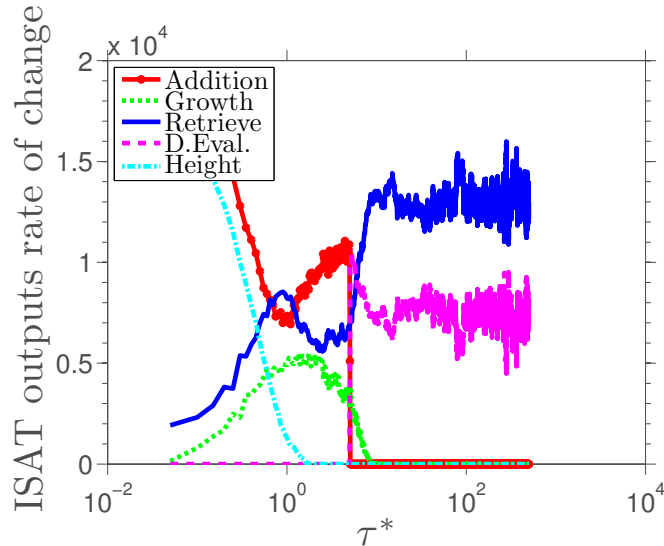


6.16(b): Case 2.

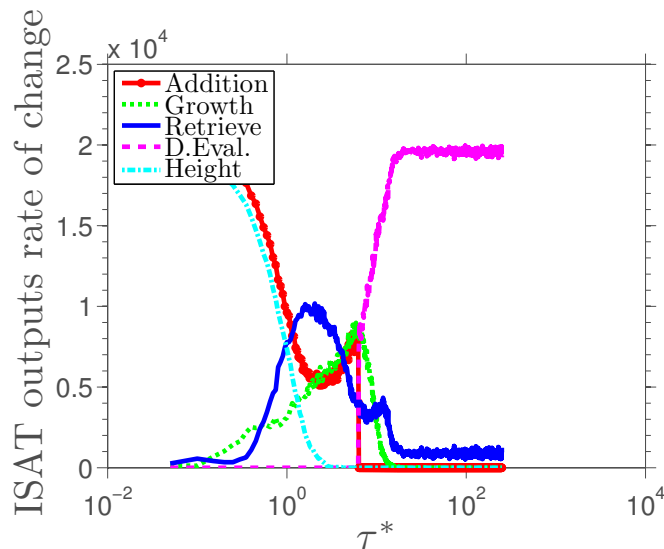
Figure 6.16: Evolution of the ISAT algorithm outputs and of the height of ISAT binary search tree for cases 1 and 2.

First one can observe that the number of additions, in both cases, reaches the maximum allowed value in the binary search tree, 50k. Therefore, the additions curve reaches a steady state after $\tau^* = 5.1$ and $\tau^* = 1.3$ residence times in cases 1 and 2, respectively. Note that these residence times correspond to 101 and 126 PMSR events (see section 3.5), which indicates that the ISAT table is saturated earlier when the mixing is slow.

Figures 6.16 and 6.17 also show the evolution of the height of the binary tree, which reaches steady state after 35 PMSR events ($\tau^* = 1.8$ residence time) in the first case and 81 PMSR events ($\tau^* = 0.8$ residence time) in the second case.



6.17(a): Case 1.



6.17(b): Case 2.

Figure 6.17: Evolution of the rates of change of each ISAT algorithm outputs and of the height of the ISAT binary search tree for cases 1 and 2.

It is also noteworthy that in both cases the tree height is one or two orders of magnitude smaller than the total number of entries in the tree ($\sim 7k$ in case 1 and $\sim 17k$ in case 2). This difference between height and total entries in the tree ensures the efficiency of the process of searching for a new query, which may be performed up to seven and three times faster in cases 1 and 2 than a vector search (see section 5.4 for details).

In case 1, Figures 6.16 and 6.17 show that the number of growths presents a sharp rate of change around, $\tau^* = 2$ residence times, whereas, in case 2, this occurs around $\tau^* = 6$ times of residence. In both cases, growth steady state occurs after $\tau^* = 10$ residence times. For case 1, the number of growths is always smaller than the process of additions. This indicates that an increase of the ellipsoids of accuracy, to form a better estimate for the region of accuracy, is not observed. However, this behavior might be circumstantial to the reaction mechanism of the carbon monoxide. This point will not be examined further here.

Figure 6.16 shows that, after tree saturation occurs, the number of retrieves and direct evaluations exceed the number of additions in both cases. In case 1 there is a higher occurrence of the retrieve event, whereas in case 2 direct evaluation prevails. The number of retrieves exhibits a linear limit behavior in both cases. The ISAT behavior for the second case reflects the fact that the binary tree of this case is poor, i.e., contains too few compositions in the region eventually accessed by the calculation. As a consequence, the number of direct evaluations vastly outnumbers the ISAT operations.

As discussed in the appendix B, a necessary condition for a calculation using the ISAT technique to be faster than the same calculation using DI is that the number of retrieves exceed the number of additions by a certain factor, which depends on the specific time of each output. Accordingly the metrics presented in Table B.1, this factor is 9 for CO/O_2 mixtures. From Figure 6.16 it is possible to see that, in case 1, the number of recoveries approximately exceeds the number of additions by a factor of 130, while in case 2 this factor is only 6. Therefore, as case 2 factor is less than 9, ISAT calculations are not expected to be faster than DI procedure.

As can be seen in Table 6.8, where a comparison of computational time is shown, cases 1 and 2 are computed using DI in 4.0 ks and 2.0 ks respectively, whereas with the use of the ISAT, for $\varepsilon_{tol} = 10^{-3}$, the same cases spent 2.3 ks and 2.1 ks, respectively. Speed-up factors of 1.7 (case 1) and 1.0 (case 2) are obtained, where the speed-up factor is defined as the ratio between the computational time spent by DI and the computational time spent by ISAT.

Table 6.8 also allows to compare the computational time spent by DI and ISAT for different values of error tolerance. An increase in processing time is obtained as ISAT error tolerance is reduced, which is to be expected, given the fact that lower values of ε_{tol} correspond to a smaller region of accuracy. Indeed, as ε_{tol} is decreased, it is less likely that ISAT returns a retrieve, which is the ISAT output with lower computational cost. In case 1, for all values of ε_{tol} , the ISAT technique offers an advantage in terms of processing time when compared

Table 6.8: Comparison between the computational time spent by DI and ISAT in cases 1 and 2 and the corresponding speed-up factors.

ε_{tol}	Case 1		Case 2	
	time spent (ks)	speed-up	time spent (ks)	speed-up
DI	~ 4.0		~ 2.0	
10^{-2}	~ 1.9	~ 2.1	~ 2.1	~ 1.0
10^{-3}	~ 2.3	~ 1.7	~ 2.1	~ 1.0
10^{-4}	~ 2.4	~ 1.7	~ 2.2	~ 0.9
10^{-5}	~ 2.5	~ 1.6	~ 2.2	~ 0.9
10^{-6}	~ 2.6	~ 1.5	~ 2.2	~ 0.9

to the process of direct integration, reducing on average the processing time in 42%. On the other hand, in case 2, no reduction in processing time is seen. As discussed above, this behavior is natural, once the necessary condition for efficiency of the algorithm is not reached.

Aiming to analyze the asymptotic behavior of the ISAT speed-up, case 1 is also simulated for 50,000 time steps. This computation with ISAT spends 204.7 ks, while if DI was used the same calculation would spend ~ 1024.0 ks (speed-up factor of 5.0). Therefore, in this asymptotic case, ISAT spends approximately 80% less time than DI. The pioneer work of Pope (1997) [70] reports an asymptotic speed-up factor of 1000, but this significant factor is not observed in the study developed here.

6.3.2

ISAT Performance for CH_4/Air Mixtures

The evolution of the ISAT algorithm outputs, height of the ISAT binary search tree and the corresponding rates of change, for case 3, with the parameters shown in Table 6.6, are presented in Figures 6.18 and 6.19. As in cases 1 and 2 the number of additions reaches the maximum allowed value in the binary search tree, 60k for this case. The additions curve reaches a steady state after 160 PMSR events, which corresponds to $\tau^* = 3.2$ residence times.

The maximum height of the binary search tree for case 3 is $\sim 7k$ as in case 2. Here the steady state of the tree height is observed at $\tau^* = 1.28$ residence time, or 64 PMSR events, as can be seen in Figures 6.18 and 6.19.

The behavior of the number of growths is quite similar to that of case 1, where the greater rate of change occurs near $\tau^* = 2$ residence times but, now, the steady state it reached before $\tau^* = 10$ residence times. For case 3, however, the number of growths is not always smaller than the number of additions.

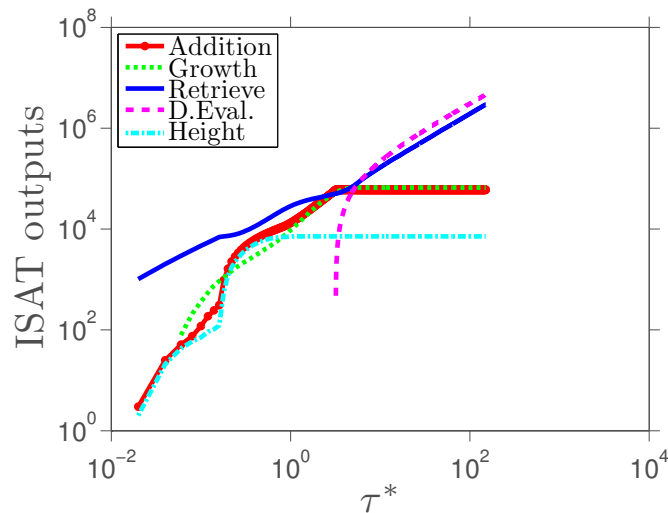


Figure 6.18: Evolution of the ISAT algorithm outputs and of the height of the ISAT binary search tree for case 3.

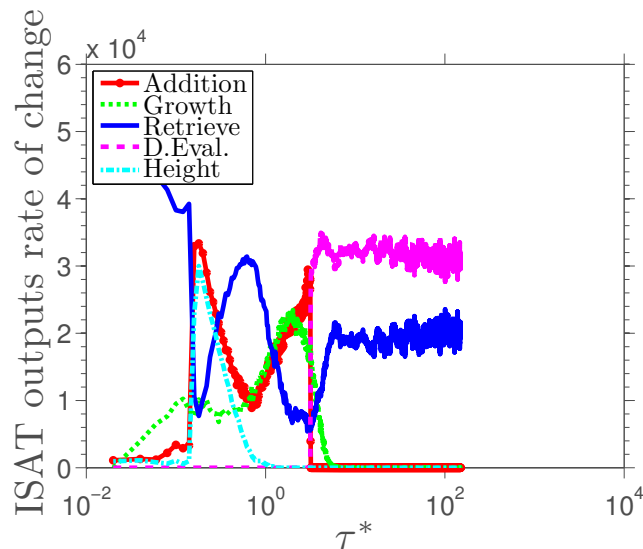


Figure 6.19: Evolution of the rates of change of each ISAT algorithm outputs and of the height of the ISAT binary search tree for case 3.

Initially the growths exceed additions by nearly an order of magnitude. After $\tau^* = 0.2$ residence time the additions exceeded the number of growths, to be overcome again once steady state is reached. This behavior is an indicative that the ellipsoids of accuracy show a considerable period of adaptation, which allows to access with precision a larger portion of the realizable region. This may explain the small discrepancy between the calculations obtained via ISAT and DI presented in section 6.3.1.

As in the previous cases, after the tree saturation, the number of retrieves and direct evaluations exceed the number of additions. The number of direct evaluations overcomes the total number of retrieves in approximately 60%, which is not negligible, but it is far from the large difference that occurs in

case 2. This indicates that the binary search tree covers a significant portion of the realizable region in the composition space.

From Figure 6.18 one can estimate as 49 the factor by which the number of additions must exceed at least the number of additions if the ISAT technique is to be more efficient than direct integration.

For case 3, the computational time spent by DI and ISAT is 689.3 ks and 454.5 ks, respectively. Therefore, a speed-up of 1.5 is observed. For this case, other values of the ISAT error tolerance were not tested, since each simulation using the ISAT requires a few days of processing time.

During the simulation of case 3, the evolution of the PMSR was computed during $\tau^* = 150$ residence times, which corresponds to 7500 PMSR events. Considering that the reactor has 1024 particles, it is possible to note that the system of governing equations defined by Eq.(4.2) is solved 7,680,000 times. In this case ISAT technique allows to save 34% in terms of computational time.

For problems that require solving Eq.(4.2) several times, one should speculate that the ISAT technique would provide an even better performance improvement, since more retrieves are expected and the time per operation of the former is small, when compared to direct integration specific time.

6.4

Analysis of ISAT Memory Usage

In order to assess the memory usage of the ISAT technique implementation, this section presents an analysis of the memory demanded by the ISAT technique. The amount of memory effectively used in the test cases defined in the section 6.2 is discussed.

6.4.1

ISAT Memory Complexity

In the simulations that use the ISAT technique, almost all of the memory used is intended for storage of the binary search tree. Therefore, it is desirable to know how to express the memory cost of a binary search tree, such as the one used in ISAT, in terms of the size of the problem under study. In the case of PMSR, the size of the problem is given by n_ϕ , which is the dimension of the vector of unknowns.

The operator $\#(\text{data})$ receives as input a data type `data` and returns its memory cost in bytes. The memory cost is generally machine dependent. For instance, in the workstation used in this work, an `integer` and a `double` data types respectively have $\#(\text{integer}) = 4$ bytes and $\#(\text{double}) = 8$ bytes.

The standard `vector` and standard `matrix` of the ANSI C language have their memory cost given by

$$\#(\mathbf{vector}) = n_\phi \times \#(\mathbf{double}), \quad (6.6)$$

and

$$\#(\mathbf{matrix}) = n_\phi^2 \times \#(\mathbf{double}), \quad (6.7)$$

respectively, whereas the `GSL` package (Galassi et al., 2008) [20] uses its own data structure for vectors and matrices with memory cost given by

$$\#(\mathbf{vector}) = 5 \times \#(\mathbf{integer}) + n_\phi \times \#(\mathbf{double}), \quad (6.8)$$

and

$$\#(\mathbf{matrix}) = 6 \times \#(\mathbf{integer}) + n_\phi^2 \times \#(\mathbf{double}). \quad (6.9)$$

Although `GSL` has a high memory cost for basic data structures, such as vectors and matrices, it offers a variety of numerical routines that are robust, stable and well implemented, which justified the choice of this package in the present work.

As seen in section 5.4, each node of the binary search tree stores two elements (\mathbf{v} and a) and each leaf stores four elements (ϕ_0 , $\mathbf{R}(\phi_0, t)$, $\mathbf{A}(\phi_0, t)$ and \mathbf{L}).

From the development presented in section 5.2, it is possible to see that matrix \mathbf{L} is lower triangular and requires only $\frac{n_\phi(n_\phi+1)}{2}$ floating point positions. But the `GSL` package does not offer any option of compact matrix storage, which implies that the ISAT implementation presented in this work also uses n_ϕ^2 floating point positions to store the components of the matrix \mathbf{L} .

It follows that the cost of memory of a `node` and a `leaf` are respectively given by

$$\#(\mathbf{node}) = \#(\mathbf{vector}) + \#(\mathbf{double}), \quad (6.10)$$

and

$$\#(\mathbf{leaf}) = 2 \times \#(\mathbf{vector}) + 2 \times \#(\mathbf{matrix}). \quad (6.11)$$

Therefore, the memory cost of the ISAT binary search tree (`bst`) reads

$$\#(\mathbf{bst}) = n_L \times \#(\mathbf{leaf}) + n_N \times \#(\mathbf{node}), \quad (6.12)$$

where n_L and n_N are respectively equal to the number of leaves and nodes in the tree.

6.4.2

ISAT Memory Cost for CO/O_2 Mixtures

Cases 1 and 2 previously studied are both modeled by a reaction mechanism with 4 species and use a binary search tree with 50,000 entries for ISAT simulations. Hence, $n_\phi = 6$, $n_N = 50,000$ and $n_L = 50,001$.

In Table 6.9 is presented a comparison between the memory cost of some of the data types previously presented for cases 1 and 2. The second column presents the amount of memory spent by the ISAT implementation reported in this work (which uses GSL structures) and the third column shows the same information for a hypothetical ISAT implementation (which uses standard ANSI C structures and compact matrix storage strategy). From the data in the table, one can see that for the real implementation $\#(\mathbf{bst}) \cong 40$ Mbytes, whereas for the hypothetical one holds $\#(\mathbf{bst}) \cong 22$ Mbytes. These values lead to the conclusion that the hypothetical implementation would be about 45% more efficient in terms of memory cost than the real approach for cases 1 and 2.

Table 6.9: Comparison between the memory cost of some data types in cases 1 and 2 using two different implementations of the ISAT technique.

	GSL (bytes)	ANSI C (bytes)	difference
$\#(\mathbf{vector})$	68	48	$\sim 29\%$
$\#(\mathbf{matrix})$	312	288	$\sim 8\%$
$\#(\mathbf{node})$	76	56	$\sim 26\%$
$\#(\mathbf{leaf})$	760	405	$\sim 47\%$

6.4.3

ISAT Memory Cost for CH_4/Air Mixtures

Case 3 is modeled by a reaction mechanism with 53 species and uses a binary search tree with 60,000 entries for ISAT simulations. Thus, $n_\phi = 55$, $n_N = 60,000$ and $n_L = 60,001$.

The Table 6.10 presents a comparison analogous to that of Table 6.9, but now for case 3. The data of this allows one to see that for the real implementation holds $\#(\mathbf{bst}) \cong 3.3$ Gbytes, and for the hypothetical implementation $\#(\mathbf{bst}) \cong 1.8$ Gbytes. The analysis of these values leads one to conclude that, for case 3, the hypothetical implementation would spend about 47% less memory than the real implementation.

Table 6.10: Comparison between the memory cost of some data types in case 3 using two different implementations of the ISAT technique.

	GSL (bytes)	ANSI C (bytes)	difference
#(vector)	460	440	~ 4 %
#(matrix)	24224	24200	~ 0 %
#(node)	468	448	~ 4 %
#(leaf)	49368	26620	~ 46 %

Furthermore, it is noteworthy that the values of memory usage reported in case 3 are not negligible, when compared to the total memory available on the workstation. This underscores what is perhaps the greatest weakness of the ISAT technique, its huge expense of memory.

7

Conclusions and Suggestions

This chapter summarizes and highlights the main conclusions and contributions of this dissertation and suggest some paths for future works.

7.1

Contributions of this Dissertation

This dissertation presented and discussed some of the challenges that are encountered in the development of models for the numerical simulation of turbulent chemically reactive flows in industrial problems.

A literature review concerning the available techniques to reduce the size of a reaction mechanism and efficiently solve models for turbulent chemically reactive flows with detailed combustion thermochemistry is provided.

The chosen and implemented technique dubbed *in situ* adaptive tabulation (ISAT) is described in detail. Also, the ISAT technique was assessed for its accuracy, performance and memory usage in the numerical simulation of chemically reactive flows in homogeneous reactors using detailed thermochemistry mechanisms.

An *in house* modular code written in ANSI C and Fortran 77 languages which implements the ISAT algorithm and the PMSR reactor model was developed in this work and has undergone series of verification tests. The results of the verification tests allowed to characterize the code in terms of computational performance and from the numerical analysis and computer programming point of view. The code is available under request on the email americo.cunhajr@gmail.com.

The ISAT technique shows good accuracy from a global point of view, with the absolute global error smaller than 1% for the reactor configurations studied. The analysis of ISAT accuracy also allows to identify the effect of the statistical seed on the control of the absolute global error, which decreases monotonically as ISAT error tolerance is reduced, when the simulations use the same statistical seed for ISAT and DI calculations. On the other hand, when different seeds are used, a limit value for ISAT error tolerance is observed.

Concerning the local error, ISAT technique achieves maximum error values of the instantaneous properties of the reactor of up to 20%, which could be unacceptable, depending on the application envisaged.

A strategy to avoid that the ellipsoid of accuracy degenerates as a single point is proposed. This modification in the half-lengths of ISAT ellipsoids constitutes a filter for chemical times scales. However, the performed tests shown that this modification does not offer any advantage in terms of ISAT technique accuracy.

In terms of performance, the ISAT technique allows to reduce the computational time of the simulations in all cases tested. For the test cases with the carbon monoxide/oxygen thermochemistry speed-up factors of 5.0 (case 1) and 1.0 (case 2) were achieved, whereas for case 3, which considers a system with a methane/air mixture, the algorithm allows to save 34% in terms of computational time. Moreover, the ISAT technique presented, in the cases studied the desired feature of speed-up factor increases with the complexity of the system analyzed.

Regarding the memory usage, ISAT technique is, as it could be expected, very demanding. In the simulation of the methane/air mixture using a binary search tree with 60,000 entries, the algorithm demanded 3.3 Gbytes of storage. This work confirms that memory expense is the major drawback of the ISAT technique.

Part of the results of this work were published in conference paper (Cunha and Figueira da Silva, 2010) [14], adjoined to this dissertation in appendix C.

The main results of this dissertation are being summarized in a paper, (Cunha and Figueira da Silva, in preparation), and will be submitted for publication in *Journal of Brazilian Society of Mechanical Sciences and Engineering*.

7.2

Suggestions for Further Works

A natural extension of this work is the characterization of the ISAT technique in the simulation of chemically reacting mixtures different from those used in this work. For example, it could be interesting to evaluate the ISAT behavior for a mixture of hydrogen with oxygen, which may be described by the reaction mechanism of Li et al. (2004) [48]; or a mixture of natural gas with air, which could be modeled by the mechanism of Le Cong & Dagaut (2008) [46].

Another natural extension of this work would be to incorporate the improvements of ISAT technique proposed by Lu & Pope (2009) [51] in the code developed. Also, performance gains would be possible if a parallelization strategy is implemented, such as those strategies proposed by Lu et al. (2009) [50].

A more sophisticated application would be the coupling of a detailed reaction mechanism, using the ISAT technique, with the hybrid LES/PDF model by Andrade (2009) [1] for description of turbulent combustion. This model currently uses a hybrid approach that combines large eddy simulation (LES), for description of fluid dynamics, and the transport of the PDF with a single step global kinetic for modeling the combustion. The incorporation of a detailed reaction mechanism would allow a better description of combustion, at the expense of a significant increase in computation time, which is not negligible in the case of a LES models. In this context, ISAT could be a viable option that may be able to decrease, to an acceptable level, the simulation time. It is also worth considering that LES calculations also spend a lot of memory, so that the coupling of LES with a detailed reaction mechanism with dozens of species, such as the GRI version 3.0 [89], is not yet feasible.

Finally, it is worth stressing that this study conducted verification tests of ISAT algorithm and PMSR reactor model only. No validation attempt was developed due to the difficulty of obtaining experimental data for such a homogeneous reactor configuration. This validation could be performed if carefully designed direct numerical simulations were available, or in more challenging flow problems, for instance.

Bibliography

- [1] ANDRADE, F. O. **Contribution to the Large Eddy Simulation of a Turbulent Premixed Flame Stabilized in a High Speed Flow**. Rio de Janeiro, 2009. Doctoral Thesis, Pontifícia Universidade Católica do Rio de Janeiro. (in Portuguese).
- [2] BARLOW, R. S.; FRANK, J. H. Effects of Turbulence on Species Mass Fractions in Methane/Air Jet Flames. **Symposium (International) on Combustion**, v. 27, n. 1, p. 1087–1095, 1998. doi:10.1016/S0082-0784(98)80510-9.
- [3] BAUKAL JR, C. E.; SCHWARTZ, R. E. **The John Zink Combustion Handbook**. Boca Raton: CRC Press, 2001. 750 p.
- [4] BERKOOZ, G.; HOLMES, P.; LUMLEY, J. The Proper Orthogonal Decomposition in the Analysis of Turbulent Flows. **Annual Reviews of Fluid Mechanics**, v. 25, n. 1, p. 539–575, 1993. doi:10.1146/annurev.fl.25.010193.002543.
- [5] BLASCO, J. A.; FUEYO, N.; LARROYA, J. C.; DOPAZO, C.; CHEN, J.-Y. A Single-Step Time-Integrator of a Methane–Air Chemical System Using Artificial Neural Networks. **Computers & Chemical Engineering**, v. 23, n. 9, p. 1127–1133, 1999. doi:10.1016/S0098-1354(99)00278-1.
- [6] BODENSTEIN, M.; LIND, S. C. Geschwindigkeit der Bildung des Bromwasserstoffs aus Seinen Elementen. **Zeitschrift für Physikalische Chemie**, v. 57, p. 168–192, 1907. (in German).
- [7] BODENSTEIN, M.; LÜTKEMEYER, H. Die Photochemische Bildung von Bromwasserstoff und die Bildungsgeschwindigkeit der Brommolekel aus den Atomen. **Zeitschrift für Physikalische Chemie**, v. 114, p. 208–236, 1924. (in German).

- [8] BRAD, R.; TOMLIN, A.; FAIRWEATHER, M. ; GRIFFITHS, J. The Application of Chemical Reduction Methods to a Combustion System Exhibiting Complex Dynamics. **Proceedings of the Combustion Institute**, v. 31, n. 1, p. 455–463, 2007. doi:10.1016/j.proci.2006.07.026.
- [9] CHEN, J.-Y. **A General Procedure for Constructing Reduced Reaction Mechanisms with Given Independent Relations**. Livermore: Sandia National Laboratories, 1987. Technical Report SAND 87-8782.
- [10] CHEN, J.-Y.; CHANG, W.-C.; KOSZYKOWSKI, M. Numerical Simulation and Scaling of NO_x Emissions from Turbulent Hydrogen Jet Flames with Various Amounts of Helium Dilution. **Combustion Science and Technology**, v. 110-111, n. 1, p. 505–529, 1995. doi:10.1080/00102209508951938 .
- [11] CHEN, J.-Y.; KOLLMANN, W.; DIBBLE, R. W. PDF Modeling of Turbulent Nonpremixed Methane Jet Flames. **Combustion Science and Technology**, v. 64, n. 4-6, p. 315–346, 1989. doi:10.1080/00102208908924038 .
- [12] CHRISTO, F. C.; MASRI, A. R.; NEBOT, E. M. Artificial Neural Network Implementation of Chemistry with PDF Simulation of H_2/CO_2 Flames. **Combustion and Flame**, v. 106, n. 4, p. 406–427, 1996. doi:10.1016/0010-2180(95)00250-2.
- [13] CORREA, S. M. Turbulence-Chemistry Interactions in the Intermediate Regime of Premixed Combustion. **Combustion and Flame**, v. 93, n. 1-2, p. 41–60, 1993. doi:10.1016/0010-2180(93)90083-F.
- [14] CUNHA, A. B.; FIGUEIRA DA SILVA, L. F. **Characterization of an Adaptive Technique to Reduce Combustion Thermochemistry**. In: Proceedings of ENCIT 2010, 2010.
- [15] DALLY, B. B.; MASRI, A. R.; BARLOW, R. S.; FIECHTNER, G. J. Instantaneous and Mean Compositional Structure of Bluff-Body Stabilized Nonpremixed Flames. **Combustion and Flame**, v. 114, n. 1-2, p. 119–148, 1998. doi:10.1016/S0010-2180(97)00280-0.
- [16] EMPRESA DE PESQUISA ENERGÉTICA. **Brazilian Energy Balance 2009: Year 2008**. Rio de Janeiro: Empresa de Pesquisa Energética, 2009. 274 p. Technical report.

- [17] FIORINA, B.; GICQUEL, O.; VEYNANTE, D. Turbulent Flame Simulation Taking Advantage of Tabulated Chemistry Self-Similar Properties. **Proceedings of the Combustion Institute**, v. 32, n. 2, p. 1687–1694, 2009. doi:10.1016/j.proci.2008.06.004.
- [18] FOX, R. O. **Computational Models for Turbulent Reacting Flows**. Cambridge: Cambridge University Press, 2003. 419 p.
- [19] FRANK-KAMENETSKII, D. A. Conditions for the Applicability of the Bodenstein Method in Chemical Kinetics. **Zhurnal Fizicheskoy Himii**, v. 14, p. 695–700, 1940. (in Russian).
- [20] GALASSI, M.; DAVIES, J.; THEILER, J.; GOUGH, B.; JUNGMAN, G.; BOOTH, M.; ROSSI, F. **GNU Scientific Library Version 1.12**. GNU Press, Boston, 2008.
- [21] GARDINER, W. C. **Gas Phase Combustion Chemistry**. New York: Springer, 2000. 543 p.
- [22] GOLUB, G. H.; VAN LOAN, C. F. **Matrix Computations**. 3rd. ed., Baltimore: John Hopkins University Press, 1996. 694 p.
- [23] GOUSSIS, D.; LAM, S. A Study of Homogeneous Methanol Oxidation Kinetics Using CSP. **Symposium (International) on Combustion**, v. 24, n. 1, p. 113–120, 1992. doi:10.1016/S0082-0784(06)80018-4.
- [24] GRAHAM, M. D.; KEVREKIDIS, I. G. Alternative Approaches to the Karhunen–Loève Decomposition for Model Reduction and Data Analysis. **Computers & Chemical Engineering**, v. 20, n. 5, p. 495–506, 1996. doi:10.1016/0098-1354(95)00040-2.
- [25] GRIFFITHS, J. Reduced Kinetic Models and their Application to Practical Combustion Systems. **Progress in Energy and Combustion Science**, v. 21, n. 1, p. 25–107, 1995. doi:10.1016/0360-1285(94)00022-V.
- [26] GURNEY, K. **An Introduction to Neural Networks**. London: UCL Press, 1997. 234 p.
- [27] HAIRER, E.; WANNER, G. **Solving Ordinary Differential Equations II: Stiff and Differential-Algebraic Problems**. 2nd. ed., Berlin: Springer, 1996. 614 p.

- [28] HINDMARSH, A. C.; BROWN, P.; GRANT, K.; LEE, S.; SERBAN, R.; SHUMAKER, D. E.; WOODWARD, C. S. **SUNDIALS: Suite of Nonlinear and Differential/Algebraic Equation Solvers.** *ACM Transactions on Mathematical Software*, v. 31, n. 3, p. 363–396, 2005. doi:10.1145/1089014.1089020.
- [29] HINDMARSH, A. C.; SERBAN, R. **User Documentation for CVODE v2.5.0.** Livermore: Lawrence Livermore National Laboratory, 2006. 145 p. Technical Report UCRL-SM-208108.
- [30] HOLMES, P.; LUMLEY, J. L.; BERKOOZ, G. **Turbulence, Coherent Structures, Dynamical Systems and Symmetry.** Cambridge: Cambridge University Press, 1998. 420 p.
- [31] HUGHES, K. J.; FAIRWEATHER, M.; GRIFFITHS, J. F.; PORTER, R.; TOMLIN, A. S. The Application of the QSSA via Reaction Lumping for the Reduction of Complex Hydrocarbon Oxidation Mechanisms. *Proceedings of the Combustion Institute*, v. 32, n. 1, p. 543–551, 2009. doi:10.1016/j.proci.2008.06.064.
- [32] IHME, M.; SCHMITT, C.; PITSCH, H. Optimal Artificial Neural Networks and Tabulation Methods for Chemistry Representation in LES of a Bluff-Body Swirl-Stabilized Flame. *Proceedings of the Combustion Institute*, v. 32, n. 1, p. 1527–1535, 2009. doi:10.1016/j.proci.2008.06.100.
- [33] JOLLIFFE, I. T. **Principal Component Analysis.** 2nd. ed., Berlin-Verlag: New York, 2002. 487 p.
- [34] KECK, J. Rate-Controlled Constrained-Equilibrium Theory of Chemical Reactions in Complex Systems. *Progress in Energy and Combustion Science*, v. 16, n. 2, p. 125–154, 1990. doi:10.1016/0360-1285(90)90046-6.
- [35] KECK, J. C.; GILLESPIE, D. Rate-Controlled Partial-Equilibrium Method for Rreating Reacting Gas Mixtures. *Combustion and Flame*, v. 17, n. 2, p. 237–241, 1971. doi:10.1016/S0010-2180(71)80166-9.
- [36] KEE, R.; GRCAR, J.; SMOOKE, M.; MILLER, J. **PREMIX: A Fortran Program for Modeling Steady Laminar One-dimensional Premixed Flames.** Livermore: Sandia National Laboratories, 1985. Technical Report SAND85-8240.

- [37] KEE, R. J.; RUPLEY, F. M.; MILLER, J. A. **CHEMKIN-II: A Fortran Chemical Kinetics Package for the Analysis of Gas-Phase Chemical Kinetics**. Livermore: Sandia National Laboratories, 1989. 127 p. Technical Report SAND 89-8009.
- [38] KNUTH, D. E. **The Art of Computer Programming, Volume 1: Fundamental Algorithms**. 3rd. ed., Boston: Addison-Wesley Professional, 1997. 672 p.
- [39] KNUTH, D. E. **The Art of Computer Programming, Volume 3: Sorting and Searching**. 2nd. ed., Boston: Addison-Wesley Professional, 1998. 800 p.
- [40] KÖNIG, K.; MAAS, U. Sensitivity of Intrinsic Low-Dimensional Manifolds with Respect to Kinetic Data. **Proceedings of the Combustion Institute**, v. 30, n. 1, p. 1317–1323, 2005. doi:10.1016/j.proci.2004.08.217.
- [41] KÖNIG, K.; MAAS, U. On-Demand Generation of Reduced Mechanisms Based on Hierarchically Extended Intrinsic Low-Dimensional Manifolds in Generalized Coordinates. **Proceedings of the Combustion Institute**, v. 32, n. 1, p. 553–560, 2009. doi:10.1016/j.proci.2008.05.039.
- [42] LAM, S. H. **Singular Perturbation for Stiff Equations Using Numerical Methods**. In: Casci, C.; Bruno, C., editors, *Recent Advances in the Aerospace Sciences*, p. 3–19. New York: Plenum Press, 1985.
- [43] LAM, S. H. Using CSP to Understand Complex Chemical Kinetics. **Combustion Science and Technology**, v. 89, n. 5-6, p. 375–404, 1993. doi:10.1080/00102209308924120.
- [44] LAM, S. H.; GOUSSIS, D. A. The CSP Method for Simplifying Kinetics. **International Journal of Chemical Kinetics**, v. 26, n. 4, p. 461–486, 1994. doi:10.1002/kin.550260408.
- [45] LAW, C. K. **Combustion Physics**. New York: Cambridge University Press, 2006. 722 p.
- [46] LE CONG, T.; DAGAUT, P. Oxidation of H_2/CO_2 Mixtures and Effect of Hydrogen Initial Concentration on the Combustion of CH_4 and CH_4/CO_2 Mixtures: Experiments and Modeling. **Proceedings of the Combustion Institute**, v. 32, n. 1, p. 427–435, 2008. doi:10.1016/j.proci.2008.05.079.

- [47] L'ECUYER, P. Maximally Equidistributed Combined Tausworthe Generators. **Mathematics of Computation**, v. 65, n. 213, p. 203–213, 1996. doi:10.1090/S0025-5718-96-00696-5.
- [48] LI, J.; ZHAO, Z.; KAZAKOV, A.; DRYER, F. L. An Updated Comprehensive Kinetic Model of Hydrogen Combustion. **International Journal of Chemical Kinetics**, v. 36, n. 10, p. 566–575, 2004. doi:10.1002/kin.20026.
- [49] LIU, B. J. D.; POPE, S. B. The Performance of *In Situ* Adaptive Tabulation in Computations of Turbulent Flames. **Combustion Theory Modelling**, v. 9, n. 4, p. 549–568, 2005. doi:10.1080/13647830500307436.
- [50] LU, L.; LANTZ, S. R.; REN, Z.; POPE, S. B. Computationally Efficient Implementation of Combustion Chemistry in Parallel PDF Calculations. **Journal of Computational Physics**, v. 228, n. 15, p. 5490–5525, 2009. doi:10.1016/j.jcp.2009.04.037.
- [51] LU, L.; POPE, S. B. An Improved Algorithm for *In Situ* Adaptive Tabulation. **Journal of Computational Physics**, v. 228, n. 2, p. 361–386, 2009. doi:10.1016/j.jcp.2008.09.015.
- [52] LU, T.; LAW, C. K. A Directed Relation Graph Method for Mechanism Reduction. **Proceedings of the Combustion Institute**, v. 30, n. 1, p. 1333–1341, 2005. doi:10.1016/j.proci.2004.08.145.
- [53] LU, T.; LAW, C. K. Linear Time Reduction of Large Kinetic Mechanisms with Directed Relation Graph: n-heptane and iso-octane. **Combustion and Flame**, v. 144, n. 1-2, p. 24–36, 2006. doi:10.1016/j.combustflame.2005.02.015.
- [54] LU, T.; LAW, C. K. Systematic Approach To Obtain Analytic Solutions of Quasi Steady State Species in Reduced Mechanisms. **The Journal of Physical Chemistry A**, v. 110, n. 49, p. 13202–13208, 2006. doi:10.1021/jp064482y.
- [55] LU, T.; LAW, C. K. Toward Accommodating Realistic Fuel Chemistry in Large-Scale Computations. **Progress in Energy and Combustion Science**, v. 35, n. 2, p. 192–215, 2009. doi:10.1016/j.peccs.2008.10.002.
- [56] LUTZ, A. E.; KEE, R. J.; MILLER, J. A. **SENKIN: A Fortran Program for Predicting Homogenous Gas Phase Chemical Kinetics with Sensitivity Analysis**. Livermore: Sandia National Laboratories, 1987. 30 p. Technical Report SAND 87-8248.

- [57] MAAS, U.; POPE, S. B. Implementation of Simplified Chemical Kinetics Based on Intrinsic Low-Dimensional Manifolds. **Symposium (International) on Combustion**, v. 24, n. 1, p. 103–112, 1992. doi:10.1016/S0082-0784(06)80017-2.
- [58] MAAS, U.; POPE, S. B. Simplifying Chemical Kinetics: Intrinsic Low-Dimensional Manifolds in Composition Space. **Combustion and Flame**, v. 88, n. 3-4, p. 239–264, 1992. doi:10.1016/0010-2180(92)90034-M.
- [59] MASRI, A. R.; BILGER, R. W.; DIBBLE, R. W. Turbulent Nonpremixed Flames of Methane Near Extinction: Mean Structure from Raman Measurements. **Combustion and Flame**, v. 71, n. 3, p. 245–266, 1988. doi:10.1016/0010-2180(88)90062-4.
- [60] MORR, A.; HEYWOOD, J. Partial Equilibrium Model for Predicting Concentration of CO in Combustion. **Acta Astronautica**, v. 1, n. 7-8, p. 949–966, 1974. doi:10.1016/0094-5765(74)90062-9.
- [61] MÜLLER, U.; PETERS, N.; NÁN, A. L. Global Kinetics for n-heptane Ignition at High pressures. **Symposium (International) on Combustion**, v. 24, n. 1, p. 777–784, 1992. doi:10.1016/S0082-0784(06)80095-0.
- [62] NAJM, H. N.; LEE, J. C.; VALORANI, M.; GOUSSIS, D. A.; FRENKLACH, M. Adaptive Chemical Model Reduction. **Journal of Physics: Conference Series**, v. 16, n. 1, p. 101–106, 2005. doi:10.1088/1742-6596/16/1/012.
- [63] NIEMANN, H.; SCHMIDT, D.; MAAS, U. An Efficient Storage Scheme for Reduced Chemical Kinetics Based on Orthogonal Polynomials. **Journal of Engineering Mathematics**, v. 31, n. 2-3, p. 131–142, 1997. doi:10.1023/A:1004206200192.
- [64] OKINO, M. S.; MAVROVOUNIOTIS, M. L. Simplification of the Mathematical Models of Chemical Reaction Systems. **Chemical Review**, v. 98, n. 2, p. 391–408, 1998. doi:10.1021/cr950223l.
- [65] ORBEGOSO, E. M. M.; NOVGORODCEV JR, A. R.; FIGUEIRA DA SILVA, L. F. **On the Predictability of Chemical Kinetic Mechanisms for the Description Combustion of Gaseous Fuels**. In: Proceedings of COBEM 2009, 2009.

- [66] PEPIOT-DESJARDINS, P.; PITSCHE, H. An Efficient Error-Propagation-Based Reduction Method for Large Chemical Kinetic Mechanisms. **Combustion and Flame**, v. 154, n. 1-2, p. 67–81, 2008. doi:10.1016/j.combustflame.2007.10.020.
- [67] PETERS, N. Multiscale Combustion and Turbulence. **Proceedings of the Combustion Institute**, v. 32, n. 1, p. 1–25, 2009. doi:10.1016/j.proci.2008.07.044.
- [68] PINNAU, R. **Model Reduction via Proper Orthogonal Decomposition**. In: Schilders, W. H. A.; van der Vorst, H. A.; Rommes, J., editors, *Model Order Reduction: Theory, Research Aspects and Applications*, p. 95–109. Berlin Heidelberg: Springer-Verlag, 2008.
- [69] POPE, S. B. PDF Methods for Turbulent Reactive Flows. **Progress in Energy and Combustion Science**, v. 11, n. 2, p. 119–192, 1985. doi:10.1016/0360-1285(85)90002-4.
- [70] POPE, S. B. Computationally Efficient Implementation of Combustion Chemistry Using *In Situ* Adaptive Tabulation. **Combustion Theory and Modelling**, v. 1, n. 1, p. 41–63, 1997. doi:10.1080/713665229.
- [71] POPE, S. B. **Algorithms for Ellipsoids**. Ithaca: Cornell University, 2008. 47 p. Technical Report FDA-08-01.
- [72] POPE, S. B.; REN, Z. Efficient Implementation of Chemistry in Computational Combustion. **Flow Turbulence Combustion**, v. 82, n. 4, p. 437–453, 2009. doi:10.1007/s10494-008-9145-3.
- [73] QIN, Z.; LISSIANSKI, V. V.; YANG, H.; GARDINER, W. C.; DAVIS, S. G.; WANG, H. Combustion Chemistry of Propane: A Case Study of Detailed Reaction Mechanism Optimization. **Symposium (International) on Combustion**, v. 28, n. 2, p. 1663–1669, 2000. doi:10.1016/S0082-0784(00)80565-2.
- [74] RABITZ, H.; KRAMER, M.; DACOL, D. Sensitivity Analysis in Chemical Kinetics. **Annual Review of Physical Chemistry**, v. 34, n. 1, p. 419–461, 1983. doi:10.1146/annurev.pc.34.100183.002223.
- [75] RATHINAM, M.; PETZOLD, L. A New Look at Proper Orthogonal Decomposition. **SIAM Journal of Numerical Analysis**, v. 41, n. 5, p. 1893–1925, 2003. doi:10.1137/S0036142901389049.

- [76] REN, Z. **Modelling Combustion with Detailed Chemistry**. Ithaca, 2006. 225 p. Ph.D. Thesis, Cornell University.
- [77] REN, Z.; POPE, S. B. Entropy Production and Element Conservation in the Quasi-Steady-State Approximation. **Combustion and Flame**, v. 137, n. 1-2, p. 251–254, 2004. doi:10.1016/j.combustflame.2004.02.002.
- [78] REN, Z.; POPE, S. B. Species Reconstruction Using Pre-Image Curves. **Proceedings of the Combustion Institute**, v. 30, n. 1, p. 1293–1300, 2005. doi:10.1016/j.proci.2004.07.017.
- [79] REN, Z.; POPE, S. B. Reduced Description of Complex Dynamics in Reactive Systems. **Journal of Physical Chemistry A**, v. 111, n. 34, p. 8464–8474, 2007. doi:10.1021/jp0717950.
- [80] REN, Z.; POPE, S. B.; VLADIMIRSKY, A.; GUCKENHEIMER, J. M. The Invariant Constrained Equilibrium Edge Preimage Curve Method for the Dimension Reduction of Chemical Kinetics. **The Journal of Chemical Physics**, v. 124, n. 11, p. 114111, 2006. doi:10.1063/1.2177243.
- [81] REN, Z.; POPE, S. B.; VLADIMIRSKY, A.; GUCKENHEIMER, J. M. Application of the ICE-PIC Method for the Dimension Reduction of Chemical Kinetics Coupled with Transport. **Proceedings of the Combustion Institute**, v. 31, p. 473–481, 2007. doi:10.1016/j.proci.2006.07.106.
- [82] RIBERT, G.; GICQUEL, O.; DARABIHA, N. ; VEYNANTE, D. Tabulation of Complex Chemistry Based on Self-Similar Behavior of Laminar Premixed Flames. **Combustion and Flame**, v. 146, n. 4, p. 649–664, 2006. doi:10.1016/j.combustflame.2006.07.002.
- [83] SAXENA, V.; POPE, S. B. PDF Calculations of Major and Minor Species in a Turbulent Piloted Jet Flame. **Proceedings of the Combustion Institute**, v. 27, n. 1, p. 1081–1086, 1998. doi:10.1016/S0082-0784(98)80509-2.
- [84] SAXENA, V.; POPE, S. B. PDF Simulations of Turbulent Combustion Incorporating Detailed Chemistry. **Combustion and Flame**, v. 117, n. 1-2, p. 340–350, 1999. doi:10.1016/S0010-2180(98)00081-9.
- [85] SHAMPINE, L. F.; THOMPSON, S. Stiff Systems. **Scholarpedia**, v. 2, n. 3, p. 2855, 2007.
http://www.scholarpedia.org/article/Stiff_equations.

- [86] SINGER, M. A.; GREEN, W. Using Adaptive Proper Orthogonal Decomposition to Solve the Reaction–Diffusion Equation. **Applied Numerical Mathematics**, v. 59, n. 2, p. 272–279, 2009. doi:10.1016/j.apnum.2008.02.004.
- [87] SINGER, M. A.; POPE, S. B. Exploiting ISAT to Solve the Reaction-Diffusion Equation. **Combustion Theory Modelling**, v. 8, n. 2, p. 361–383, 2004. doi:10.1088/1364-7830/8/2/009.
- [88] SINGER, M. A.; POPE, S. B.; NAJM, H. Modeling Unsteady Reacting Flow with Operator-Splitting and ISAT. **Combustion and Flame**, v. 147, n. 1-2, p. 150–162, 2006. doi:10.1016/j.combustflame.2006.06.007.
- [89] SMITH, G. P.; GOLDEN, D. M.; FRENKLACH, M.; MORIARTY, N. W.; EITENEER, B.; GOLDENBERG, M.; BOWMAN, C. T.; HANSON, R. K.; SONG, S.; GARDINER, W. C.; LISSIANSKI, V. V.; QIN, Z.
http://www.me.berkeley.edu/gri_mech/.
- [90] TANG, Q.; POPE, S. B. Implementation of Combustion Chemistry by *In Situ* Adaptive Tabulation of Rate-Controlled Constrained Equilibrium Manifolds. **Proceedings of the Combustion Institute**, v. 29, n. 1, p. 1411–1417, 2002. doi:10.1016/S1540-7489(02)80173-0.
- [91] TONSE, S. R.; MORIARTY, N. W.; BROWN, N. J.; FRENKLACH, M. PRISM: Piece-Wise Reusable Implementation of Solution Mapping. An Economical Strategy for Chemical Kinetics. **Israel Journal of Chemistry**, v. 39, n. 1, p. 97–106, 1999.
- [92] TURÁNYI, T.; TOMLIN, A. S.; PILLING, M. J. On the Error of the Quasi-Steady-State Approximation. **The Journal of Physical Chemistry**, v. 97, p. 163–172, 1993. doi:10.1021/j100103a028.
- [93] TURÁNYI, T.; TÓTH, J. Comments to an Article of Frank-Kamenetskii on the Quasi-Steady-State Approximation. **Acta Chimica Hungarica - Models in Chemistry**, v. 129, n. 6, p. 903–914, 1992.
- [94] TURÁNYI, T. Application of Repro-Modeling for the Reduction of Combustion Mechanisms. **Symposium (International) on Combustion**, v. 25, n. 1, p. 949–955, 1994. doi:10.1016/S0082-0784(06)80731-9.

- [95] WARNATZ, J.; MASS, U. ; DIBBLE, R. W. **Combustion: Physical and Chemical Fundamentals, Modeling and Simulation, Experiments, Pollutant Formation**. 4th. ed., Berlin: Springer-Verlag, 2006. 378 p.
- [96] WILLIAMS, F. A. **Combustion Theory**. 2nd. ed., Cambridge: Wesley, 1985. 680 p.
- [97] YANG, B.; POPE, S. B. An Investigation of the Accuracy of Manifold Methods and Splitting Schemes in the Computational Implementation of Combustion Chemistry. **Combustion and Flame**, v. 112, n. 1-2, p. 16–32, 1998. doi:10.1016/S0010-2180(97)81754-3.
- [98] YANG, B.; POPE, S. B. Treating Chemistry in Combustion with Detailed Mechanisms—*In Situ* Adaptive Tabulation in Principal Directions—Premixed Combustion. **Combustion and Flame**, v. 112, n. 1, p. 85–112, 1998. doi:10.1016/S0010-2180(97)81759-2.
- [99] ZEL'DOVICH, Y. B.; BARENBLATT, G. I.; LIBROVICH, V. B.; MAKHVILADZE, G. M. **The Mathematical Theory of Combustion and Explosions**. Moscou: Consultants Bureau, 1985. 595 p.

A Dimensionless Parameters

The procedure of construction of the dimensionless parameters associated with a chemically reactive flow in a stirred reactor is presented in this appendix.

A.1 Dimensionless Time

Among all the characteristic time scales associated with a stirred reactor, the residence time τ_r , defined by Eq.(3.34), is the most important, since it indicates the age of the fluid particles. The dimensionless time is defined as

$$\tau^* \equiv \frac{t}{\tau_r}. \quad (\text{A.1})$$

A.2 Reduced Temperature

Consider the temperature T of a reactive mixture in a partially stirred reactor, an inflow value T_{in} and the equilibrium value T_{eq} associated with the inflow state. The reduced temperature is defined as

$$T^* \equiv \frac{T - T_{in}}{T_{eq} - T_{in}}. \quad (\text{A.2})$$

A.3 Ensemble Average of Reduced Temperature

The ensemble average of reduced temperature is defined as

$$\langle T \rangle^* \equiv \langle T^* \rangle, \quad (\text{A.3})$$

which reads as

$$\langle T \rangle^* = \left\langle \frac{T - T_{in}}{T_{eq} - T_{in}} \right\rangle, \quad (\text{A.4})$$

where the ensemble average operator is defined by Eq.(3.38).

Recalling that the ensemble average operator commutes with the arithmetic operations on quantities and the ensemble average of a constant is the constant itself, the previous equation is equivalent to

$$\langle T \rangle^* = \frac{\langle T \rangle - T_{in}}{T_{eq} - T_{in}}. \quad (\text{A.5})$$

A.4

Ensemble Variance of Reduced Temperature

From the definition of ensemble average, Eq.(3.38), and ensemble variance, Eq.(3.39), it follows that

$$\begin{aligned} \langle T'^2 \rangle &= \frac{1}{n_p} \sum_{j=1}^{n_p} [T^{(j)} - \langle T \rangle]^2 \\ &= \frac{1}{n_p} \sum_{j=1}^{n_p} \left\{ [T^{(j)}]^2 - 2T^{(j)} \langle T \rangle + \langle T \rangle^2 \right\} \\ &= \frac{1}{n_p} \sum_{j=1}^{n_p} [T^{(j)}]^2 - 2 \langle T \rangle \left[\frac{1}{n_p} \sum_{j=1}^{n_p} T^{(j)} \right] + \langle T \rangle^2 \left[\frac{1}{n_p} \sum_{j=1}^{n_p} 1 \right] \\ &= \langle T^2 \rangle - 2 \langle T \rangle^2 + \langle T \rangle^2, \end{aligned} \quad (\text{A.6})$$

which is equivalent to

$$\langle T'^2 \rangle = \langle T^2 \rangle - \langle T \rangle^2. \quad (\text{A.7})$$

Thus, with the help of Eq.(A.7), it is natural to define the ensemble variance of reduced temperature as

$$\langle T'^2 \rangle^* \equiv \langle T^2 \rangle^* - [\langle T \rangle^*]^2. \quad (\text{A.8})$$

The first term on the right hand side of Eq.(A.8) can be developed as

$$\begin{aligned} \langle T^2 \rangle^* &= \langle [T^*]^2 \rangle \\ &= \left\langle \left(\frac{T - T_{in}}{T_{eq} - T_{in}} \right)^2 \right\rangle \\ &= \left\langle \frac{T^2 - 2TT_{in} + T_{in}^2}{(T_{eq} - T_{in})^2} \right\rangle \\ &= \frac{\langle T^2 \rangle - 2 \langle T \rangle T_{in} + T_{in}^2}{(T_{eq} - T_{in})^2}, \end{aligned} \quad (\text{A.9})$$

whereas the second one expands as

$$\begin{aligned} [\langle T \rangle^*]^2 &= \left(\frac{\langle T \rangle - T_{in}}{T_{eq} - T_{in}} \right)^2 \\ &= \frac{\langle T \rangle^2 - 2 \langle T \rangle T_{in} + T_{in}^2}{(T_{eq} - T_{in})^2}, \end{aligned} \quad (\text{A.10})$$

which yields

$$\langle T'^2 \rangle^* = \frac{\langle T^2 \rangle - \langle T \rangle^2}{(T_{eq} - T_{in})^2}. \quad (\text{A.11})$$

B Analysis of ISAT Efficiency

In this appendix is presented an analysis of the ISAT technique efficiency compared to the procedure of direct integration (DI) using a classical numerical technique.

B.1 Necessary Condition for Efficiency

If the ISAT technique is to be more efficient than the DI procedure, the computational time spent by the ISAT must be smaller than computational time spent by DI. The computational time spent by ISAT is the sum of the computational time spent at each of its possible outputs. Therefore, the efficiency condition can be stated as

$$n_A \tau_A + n_G \tau_G + n_R \tau_R + n_{DE} \tau_{DE} < n_{DI} \tau_{DI}, \quad (\text{B.1})$$

or

$$n_A \frac{\tau_A}{\tau_{DI}} + n_G \frac{\tau_G}{\tau_{DI}} + n_R \frac{\tau_R}{\tau_{DI}} + n_{DE} \frac{\tau_{DE}}{\tau_{DI}} < n_{DI}, \quad (\text{B.2})$$

where n_A is the number of additions; n_G is the number of growths; n_R is the number of retrieves; n_{DE} is the number of direct evaluations; n_{DI} is the number of direct integrations; τ_A is the average time spent at each addition; τ_G is the average time spent at each growth; τ_R is the average time spent at each retrieve; τ_{DE} is the average time spent at each direct evaluation; τ_{DI} is the average time spent at each direct integration.

B.2 Empirical Metrics

Table B.1 presents some empirical metrics for average time spent at each output of ISAT technique and DI in the simulation of a PMSR filled with a carbon monoxide mixture such as the one studied in section 6.2.2. These metrics are obtained from the ratio between the total time spent at each ISAT output and the number of records of the corresponding output along a simulation. One can observe that the computational cost of growth and direct evaluation have the same order of magnitude as direct integration. The retrieve is the

output that has a computational cost two orders of magnitude smaller than the direct integration. Also, one can note that addition is the most expensive output, where the computational cost is an order of magnitude larger than the computational cost of direct evaluation/integration.

Table B.1: Empirical metrics for the computational time spent at each output of ISAT algorithm and DI.

Output	Metrics (μs)
additon	$\sim 10^4$
growth	$\sim 10^3$
retrieve	$\sim 10^0$
direct evaluation	$\sim 10^3$
direct integration	$\sim 10^3$

B.3 Addition/Retrieve Relation

Based on the observations of the last section, it is reasonable to assume that

$$\frac{\tau_G}{\tau_{DI}} \approx 1, \quad \frac{\tau_{DE}}{\tau_{DI}} \approx 1, \quad \text{and} \quad \frac{\tau_R}{\tau_{DI}} \ll 1. \quad (\text{B.3})$$

Therefore, it is possible to simplify Eq. (B.2) so that

$$n_A \frac{\tau_A}{\tau_{DI}} + n_G + n_{DE} < n_{DI}. \quad (\text{B.4})$$

Since the number of direct integration is equal to the sum of ISAT outputs, i.e.,

$$n_{DI} = n_A + n_G + n_R + n_{DE}, \quad (\text{B.5})$$

Eq. (B.4) reads

$$n_A \frac{\tau_A}{\tau_{DI}} + n_G + n_{DE} < n_A + n_G + n_R + n_{DE}, \quad (\text{B.6})$$

which can be simplified to

$$\frac{n_R}{n_A} > \frac{\tau_A}{\tau_{DI}} - 1. \quad (\text{B.7})$$

Respecting the assumptions made on its deduction, Eq. (B.7) provides a necessary, but not sufficient, condition for ISAT efficiency. This means that if the number of retrieves does not exceed the number of additions by $\tau_A/\tau_{DI} - 1$, then the ISAT technique is not efficient. Based on Table B.1 the right hand side of Eq. (B.7) should be larger than 9 for carbon monoxide mixtures.

C

Conference Paper

In this appendix is shown the paper by Cunha and Figueira da Silva (2010) [14], presented in the *13th Brazilian Congress of Thermal Sciences and Engineering*, which summarizes part of the results of this dissertation.

CHARACTERIZATION OF AN ADAPTIVE TECHNIQUE TO REDUCE COMBUSTION THERMOCHEMISTRY

Americo Barbosa da Cunha Junior

Luís Fernando Figueira da Silva

Departamento de Engenharia Mecânica

Pontifícia Universidade Católica do Rio de Janeiro

Rua Marquês de São Vicente, 225, Gávea, Rio de Janeiro - RJ, Brasil - 22453-900

americo.cunhajr@gmail.com — luisfer@esp.puc-rio.br

Abstract.

*The study of combustion requires the description of the thermochemistry of elementary reactions. Modern detailed chemical kinetic description of hydrocarbon mixtures combustion with air involves tens of species and hundreds of elementary reactions. Since each of these elementary reactions evolve at timescales which may span over several orders of magnitudes, the resulting model is inherently stiff. These characteristics imply that the numerical integration of the detailed thermochemical evolution equations is the most expensive task when a detailed description of combustion chemistry is sought, for instance, in computational fluid dynamics models. This work presents a technique, dubbed *in situ* adaptive tabulation (ISAT), which has been implemented in order to reduce the integration time of the system of equations governing the thermochemical evolution of reactive mixtures. The technique is tested in a modification of the classical Partially Premixed Reactor (PaSR) called Pairwise Mixing Stirred Reactor (PMSR) and the results obtained characterize the efficiency of the algorithm, demonstrating a reduction of up to 46% in computational time when compared to the direct integration of the governing equations.*

Keywords: *combustion modelling, thermochemistry reduction, adaptive tabulation*

1. INTRODUCTION

Computational models to predict the behavior of an industrial device that uses combustion on its operation may require the solution of partial differential equations that represent the balance of mass, momentum, chemical species and energy. These models may include a detailed kinetic mechanism for the description of the physicochemical phenomena involved. Typically, such reaction mechanisms for mixtures of hydrocarbons with air involve tenths of species, hundreds of elementary reactions and timescales that vary up to nine orders of magnitude Williams (1985).

The challenge numerical simulation of these models, is related to the reaction rate of chemical species, which is difficult to model and imposes stiffness to system, since it has a nonlinear nature and presents a strong dependence with the size of the reaction mechanism. Therefore, the numerical solution of a detailed reaction mechanism is computationally demanding, which justifies the development of techniques that allow for the reduction of the computational cost associated.

This work presents a technique, dubbed *in situ* adaptive tabulation (ISAT), Pope (1997), which has been implemented in order to reduce the integration time of the system of equations governing the evolution of reactive mixtures. The methodology consists in progressively creating a table which stores solutions and initial conditions for the system of governing equations. A search is performed along this table whenever the integration of these equations is required and a tabulated solution is recovered. If the information recovered from the table is satisfactory, in a sense implicit to the technique, a linear extrapolation gives an adequate approximate solution. This approximate solution has a local error which is second order accurate in time, thus ensuring that the global error is of first order. A characterization of this technique is presented which details benefits and the shortcomings of this technique when applied to simple and complex reactive systems.

2. MATHEMATICAL FORMULATION

In this section the mathematical formulation of the problem is briefly described, further details may be found in Pope (1997) or Cunha Jr (2010).

2.1 The Geometry of Reactive Systems

To study a reduction technique for combustion thermochemistry is desirable to consider a physical system in which the behavior depends primarily on the processes of transport and reaction of the chemical species. Thus,

consider a transient spatially homogeneous reactive mixture evolving adiabatically and at constant pressure in a continuous flow reactor. The thermodynamical state of a fluid particle in the reactor may be completely determined by the mass fraction Y_i ($i = 1, \dots, n_s$) of the n_s chemical species, the specific enthalpy h and pressure p , which can be lumped in the *composition* vector defined as

$$\phi \equiv (h, p, Y_1, \dots, Y_{n_s})^T, \quad (1)$$

where the superscript T denotes the transposition operation. One should note that, due to the invariance of the system number of atoms, which ensures the total conservation of the mass, the components of vector ϕ are not linearly independent.

In the framework of the transported probability density function (PDF) models Pope (1985), a reactive system may be described by an ensemble (j) of stochastic particles, which mimic the behavior of the fluid system.

The evolution of the composition of each particle in a reactor can be written in a general framework according to the following set of ordinary differential equations

$$\frac{d\phi^{(j)}}{dt} = -\mathbf{\Gamma}^{(j)}(t) + \mathbf{S}(\phi^{(j)}, t), \quad (2)$$

where $\mathbf{\Gamma}^{(j)}(t)$ is the rate of change due to mixing and $\mathbf{S}(\phi^{(j)}, t)$ is the rate of change associated to the chemical reactions. One may integrate Eq.(2) from an initial time t_0 to a time t

$$\phi^{(j)}(t) = \phi_0^{(j)} - \int_{t_0}^t \mathbf{\Gamma}^{(j)}(t') dt' + \int_{t_0}^t \mathbf{S}(\phi^{(j)}, t') dt', \quad (3)$$

and define the *reaction mapping*

$$\mathbf{R}(\phi_0^{(j)}, t) \equiv \phi^{(j)}(t), \quad (4)$$

as the solution of Eq.(2) after a time t starting from the initial composition $\phi^{(j)}(t_0) = \phi_0^{(j)}$. The reaction mapping corresponds to a trajectory in *composition space*, which, for large values of t , tends to the equilibrium composition for the given enthalpy and pressure on $\phi_0^{(j)}$. The composition space is the $(n_s + 2)$ -dimensional Euclidean space where where the first direction is associated with the enthalpy, the second with the pressure and the other n_s are related to the chemical species.

2.2 Pairwise Mixing Stirred Reactor

The classical *Partially Stirred Reactor* (PaSR), used by Correa (1993), describes $\mathbf{\Gamma}(t)$ by the interaction by exchange with the mean (IEM) micromixing model but, for the purpose of testing a thermochemistry reduction technique, it is desirable to employ a mixing model that leads to a composition region accessed during the solution process which is “wider” than that provided by the IEM model. A modified version of PaSR model called *Pairwise Mixing Stirred Reactor* (PMSR), Pope (1997), is designed to yield a much larger accessed region, and, hence, should provide a stringent test to the ability of ISAT technique to yield a reduction in computational time.

In the PMSR model the reactor consists of an even number n_p of particles, initially arranged in pairs (j_1, j_2) such that the particles $(1, 2), (3, 4), \dots, (n_p - 1, n_p)$ are partners. Given a time step, Δt , for each discrete times $k\Delta t$, where k is an integer, the model is characterized by three types of events: *inflow*, *outflow* and *pairing*. The inflow and outflow events consist of randomly selecting $n_{in} \equiv \text{ceil}(0.5\Delta t/\tau_r n_p)$ pairs of particles, being τ_r the residence time within the reactor, and exchanging the thermodynamical properties by the properties of a prescribed inflow. The pairing event consists of randomly selecting for pairing a number of pairs of particles, different from the inflow particles, equal to $n_{pair} \equiv \text{ceil}(0.5\Delta t/\tau_p n_p)$, being τ_p the pairwise time. Then the chosen particles (inflow/outflow and pairing) are randomly shuffled. Between these discrete times, the pairs of particles (j_1, j_2) evolve according to the following mixing law

$$\frac{d\phi^{(j_1)}}{dt} = -\frac{\phi^{(j_1)} - \phi^{(j_2)}}{\tau_m} + \mathbf{S}(\phi^{(j_1)}, t), \quad (5)$$

$$\frac{d\phi^{(j_2)}}{dt} = -\frac{\phi^{(j_2)} - \phi^{(j_1)}}{\tau_m} + \mathbf{S}(\phi^{(j_2)}, t). \quad (6)$$

2.3 Numerical Integration

An operator splitting technique Yang and Pope (1998) is employed to solve Eq.(2). The overall process of integration via operator splitting technique can be represented as

$$\phi^{(j)}(t) \xrightarrow{\text{mixing}} \phi_{mix}^{(j)}(t + \Delta t) \xrightarrow{\text{reaction}} \phi^{(j)}(t + \Delta t), \quad (7)$$

where given an initial composition $\phi_0^{(j)}$ and a time step Δt , the first fractional step integrates the pure mixing system,

$$\frac{d\phi^{(j)}}{dt} = -\mathbf{\Gamma}^{(j)}(t), \quad (8)$$

to obtain $\phi_{mix}^{(j)}(t + \Delta t)$. Then, the pure chemical reaction system,

$$\frac{d\phi^{(j)}}{dt} = \mathbf{S}(\phi^{(j)}, t). \quad (9)$$

is solved from an initial composition $\phi_{mix}^{(j)}(t + \Delta t)$ over a time step Δt and gives $\phi^{(j)}(t + \Delta t)$.

The operator splitting technique allows to solve each term in the evolution equation, Eq.(2), separately, using specific efficient numerical methods to treat the particular features inherent to the physical phenomenon modeled by each term Fox (2003).

2.4 Linearized Reaction Mapping

Consider a composition ϕ^1 and an *initial composition* ϕ_0 , so that the series expansion of the reaction mapping of the composition around the initial one is

$$\mathbf{R}(\phi, t) = \mathbf{R}(\phi_0, t) + \mathbf{A}(\phi_0, t)\delta\phi + \mathcal{O}(\|\delta\phi\|^2), \quad (10)$$

where $\delta\phi \equiv \phi - \phi_0$, the *mapping gradient matrix* is the $n_\phi \times n_\phi$ matrix $\mathbf{A}(\phi_0, t)$ with components given by

$$A_{ij}(\phi_0, t) \equiv \frac{\partial R_i}{\partial \phi_{0j}}(\phi_0, t), \quad (11)$$

the $\mathcal{O}(\|\delta\phi\|^2)$ denotes terms that have order $\|\delta\phi\|^2$ and $\|\cdot\|$ denotes the Euclidean norm of a vector.

The *linear approximation* $\mathbf{R}^l(\phi, t)$ is obtained by neglecting the high order terms of Eq.(10) and is second order accurate at a connected region of composition space centered at ϕ_0 . The shape of this region is unknown before the calculations, but the ISAT algorithm approximates this region by a hyper-ellipsoid, as will be shown in section 2.5 The *local error* of this linear approximation is defined as the Euclidean norm of the difference between the reaction mapping at ϕ and the linear approximation for it around ϕ_0 ,

$$\varepsilon \equiv \|\mathbf{R}(\phi, t) - \mathbf{R}^l(\phi, t)\|. \quad (12)$$

2.5 Ellipsoid of Accuracy

The accuracy of the linear approximation at ϕ_0 is controlled only if the local error is smaller than a positive *error tolerance* ε_{tol} , which is heuristically chosen. The *region of accuracy* is defined as the connected region of the composition space centered at ϕ_0 where local error is not greater than ε_{tol} . As shown in Pope (1997), this

¹ From now on the superscript (j) is omitted for the sake of notation simplicity.

region is approximated by a hyper-ellipsoid centered at ϕ_0 which is dubbed *ellipsoid of accuracy* (EOA), and is mathematically represented by the following equation

$$\delta\phi^T \mathbf{L}\mathbf{L}^T \delta\phi \leq \varepsilon_{tol}^2, \quad (13)$$

where the EOA Cholesky matrix \mathbf{L} is lower triangular, Golub and Van Loan (1996).

The adaptive step of ISAT algorithm involves the solution of the following geometric problem: given a hyper-ellipsoid centered at ϕ_0 and a *query composition*, ϕ_q , outside it, determine a new hyper-ellipsoid of minimum hyper-volume, centered at ϕ_0 , which encloses both the original hyper-ellipsoid and the point ϕ_q . The solution of this problem is presented by Pope (2008) and is not shown here for sake of brevity.

2.6 In Situ Adaptive Tabulation

Initially the ISAT algorithm receives the time step Δt and the tolerance ε_{tol} . Then, in every time step, the ISAT algorithm receives a query composition ϕ_q and returns an approximation for the corresponding reaction mapping $\mathbf{R}(\phi_q, t)$. This approximation is obtained via numerical integration of Eq.(9) or by the linear approximation $\mathbf{R}^l(\phi_q, t)$.

During the reactive flow calculation, the computed values are sequentially stored in a table for future use. This process is known as *in situ* tabulation. The ISAT table, which is created by the tabulation process, includes the initial composition ϕ_0 , the reaction mapping $\mathbf{R}(\phi_0, t)$ and the mapping gradient matrix $\mathbf{A}(\phi_0, t)$. Using these elements it is possible to construct the linear approximation. As the calculation proceeds, a new query composition, ϕ_q , is received by ISAT, the table is transversed until a ϕ_0 is found that is close to ϕ_q . Depending on the accuracy, the linear approximation around ϕ_0 is returned or the reaction mapping of ϕ_q is obtained by direct integration of Eq.(9).

The ISAT table is a binary search tree, since this data structure allows for searching an information in $\mathcal{O}(\log_2 n_{tab})$ operations, where n_{tab} is the total number entries in the tree, if the tree is balanced Knuth (1998). The binary search tree is basically formed by two types of elements, nodes and leaves. Each leaf of the tree stores the following data:

- ϕ_0 : initial composition;
- $\mathbf{R}(\phi_0, t)$: reaction mapping at ϕ_0 ;
- $\mathbf{A}(\phi_0, t)$: mapping gradient matrix at ϕ_0 ;
- \mathbf{L} : EOA Cholesky matrix.

Each node of the binary search tree has an associated *cutting plane*. This plane is defined by a *normal vector*

$$\mathbf{v} \equiv \phi_q - \phi_0, \quad (14)$$

and a scalar

$$a \equiv \mathbf{v}^T \left(\frac{\phi_q + \phi_0}{2} \right), \quad (15)$$

such that all composition ϕ with $\mathbf{v}^T \phi > a$ are located to the right of the cutting plane, all other compositions are on the left, as sketched in Figure 1. The cutting plane construction defines a search criterion in the binary search tree.

If, during the calculation, a query point ϕ_q is encountered that is within the region of accuracy, i.e. $\varepsilon \leq \varepsilon_{tol}$, but outside the estimate of EOA, then the EOA growth proceeds as detailed in Pope (2008). The first three items stored in the binary search tree leaf [ϕ_0 , $\mathbf{R}(\phi_0, t)$ and $\mathbf{A}(\phi_0, t)$] are computed once, whereas \mathbf{L} changes whenever the EOA is grown.

Once a query composition ϕ_q is received by the ISAT table, the binary search tree is initialized as a single leaf ($\phi_0 = \phi_q$) and the exact value of the reaction mapping is returned.

The subsequent steps are:

1. Given a query composition the tree is transversed until a leaf (ϕ_0) is found.
2. Equation (13) is used to determine if ϕ_q is inside EOA or not.

3. If ϕ_q is inside EOA, the reaction mapping is given by the linear approximation. This is the first of four outcomes, called *retrieve*.
4. If ϕ_q is outside EOA, direct integration is used to compute the reaction mapping, and the local error is measured by Eq.(12).
5. If the local error is smaller than tolerance, ε_{tol} , the EOA is grown according to the procedure presented in Pope (2008) and the reaction mapping is returned. This outcome is called *growth*.
6. If local error is greater than the tolerance ε_{tol} and the maximum number of entries in the binary search tree is not reached, a new record is stored in the binary search tree based on ϕ_q and the reaction mapping is returned. The original leaf is replaced by a node with the left leaf representing the old composition ϕ_0 and the right leaf the new one ϕ_q as shown in Figure 2. This outcome is an *addition*.
7. If the local error is greater than the tolerance ε_{tol} and the maximum number of entries in the binary search tree is reached, the reaction mapping is returned. This outcome is called *direct evaluation*.

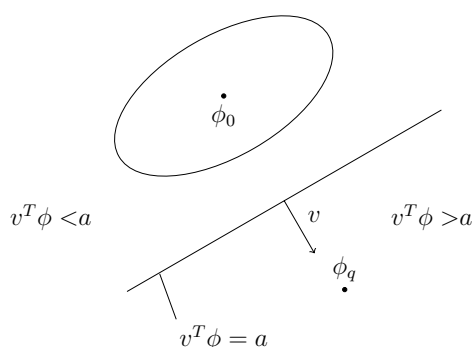


Figure 1. Cutting plane in relation to EOA position.

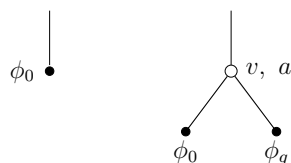


Figure 2. Binary search tree before and after the addition of a new node.

3. RESULTS AND DISCUSSION

In order to assess the accuracy and the performance of the ISAT technique implementation, this section presents benchmark tests which compare the calculation results obtained by the ISAT technique with those issued from the direct integration (DI) of the evolution equations in a PMSR.

3.1 Analysis of the ISAT Accuracy

The considered PMSR is initially filled with a fuel-lean (equivalence ratio = 0.7) mixture of CO/O_2 at 2948.5 K and 1 atm. The reaction of CO with O_2 involves 4 species and 3 reactions, Gardiner (2000). At every time step, a fuel-lean (equivalence ratio = 0.7) mixture of CO/O_2 enters the reactor at 300 K and 1 atm. The constant pressure and enthalpy equilibrium state associated to the inflow mixture is reached at 2948.5 K. Two time scales situations are studied for this PMSR, which are presented in Table 1. For the first one, which defines the first test case, $\tau_m/\tau_r = \tau_p/\tau_r = 1/2$, so that the pairwise/mixing time scales are of the same order of magnitude as the residence time, thus allowing to obtain partially stirred reactor (PaSR) conditions. For the second test case, which is defined by the second configuration of time scales presented in the Table 1, $\tau_m/\tau_r = \tau_p/\tau_r = 1/10$, so that the pairwise/mixing time scales are small when compared to the residence time. Thus, the reactor should behave almost as a perfect stirred reactor (PSR), where the processes of mixing and pairing occur instantaneously. This study uses a binary search tree with a maximum of 50,000 entries; time step of $\Delta t = 10 \mu s$; solver relative tolerance of $\varepsilon_{rel} = 10^{-6}$; solver absolute tolerance of $\varepsilon_{abs} = 10^{-9}$ and ISAT error tolerance of $\varepsilon_{tol} = 10^{-3}$.

Table 1. Parameters used in the simulation of a CO/O_2 mixture in a PMSR.

		Case 1	Case 2
number of particles	N	1024	1024
residence time (μs)	τ_r	200	1000
mixing time (μs)	τ_m	100	100
pairwise time (μs)	τ_p	100	100

Figure 3 shows the comparison between DI and ISAT computational results for the ensemble average of the reduced temperature $\langle T \rangle^*$ in both cases, where the ensemble average operator is defined as

$$\langle \psi \rangle \equiv \frac{1}{n_p} \sum_{j=1}^{n_p} \psi^{(j)}, \quad (16)$$

being ψ a generic property of the reactive system. For the result of case 1, which spans over a range of 500 residence times, one can observe good qualitative agreement. The ensemble average value rapidly increases from the initial value, then decreases to reach the statistically steady state regime around $\langle T \rangle^* = 0.35$. The analysis of this figure shows that the statistically steady state regime is reached after 10 residence times. In case 2, where a range of 250 residence times is computed, one can also observe a good qualitative agreement for the ensemble average of reduced temperature. Again, the overall history of the PMSR is the same for DI and ISAT. Similar results, not shown here, were obtained for the other thermochemical properties of the reactors.

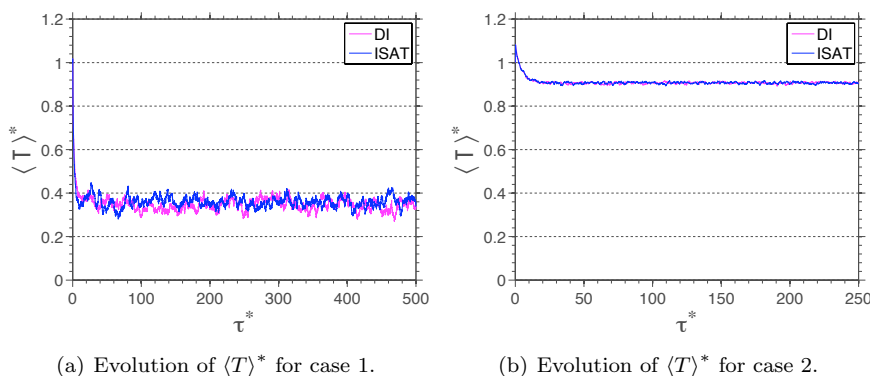


Figure 3. Comparison between DI and ISAT results of ensemble average reduced temperature.

Aiming to quantify the discrepancies between the values obtained via DI and ISAT, Figure 4 presents the evolution of the relative local error of the ensemble average reduced temperature, denoted by $\varepsilon_{r, \langle T \rangle^*}$. The relative local error is defined as the absolute value of the difference between DI and ISAT results over DI results. Concerning the errors in case 1 one can observe a large statistical variation due to stochastic nature of the PMSR model, with amplitudes reaching 40%. In case 2, relative errors of the order of 1% only can be observed.

The difference among cases is due to the behavior of each reactor at the statistically steady state regime. Indeed, the behavior of the reactor of case 2 is governed by a competition between the chemical and residence times only, therefore the thermodynamical properties steady state probability density function is spread over a smaller range than in case 1, where the mixing and pairing time scales are large. This behavior is illustrated in Figure 5, which presents the comparison between DI and ISAT computations of the mean PDF, averaged over the last 50 residence times, of the reduced temperature for cases 1 and 2. This figure underscores the influence of the controlling parameters of the PMSR, i.e., the time scales ratios, on the thermochemical conditions prevailing within each reactor. Indeed, the temperature within the reactor of case 2 is such that almost only burned gases are found. On the other hand, case 1 reactor is characterized by a bimodal temperature distribution with a large probability of finding $T^* = 0.1$ and a broader temperature distribution leaning to the burned gases.

In the early development of the ISAT technique Pope (1997) it was noted that the choice of the tolerance could affect the accuracy of the problem solution. In order to investigate the effect of the tolerance on the present results, Figure 6 presents the relative global error ε_g , as a function of the ISAT error tolerance for test

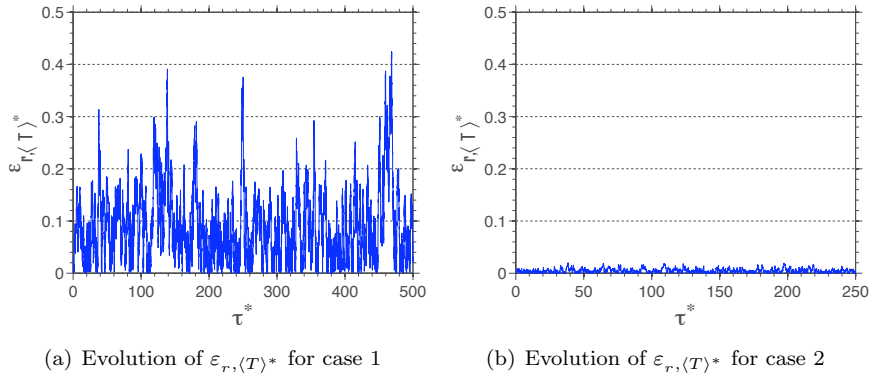


Figure 4. Evolution of relative local error of ensemble average reduced temperature.

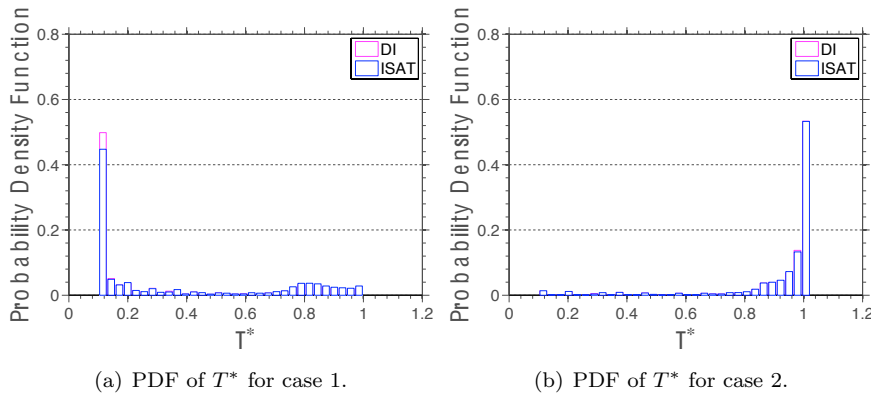


Figure 5. Comparison between DI and ISAT computations of the mean histograms of the reduced temperature.

cases 1 and 2. The relative global error is over a time interval $\Delta\tau$ is defined as

$$\varepsilon_g \equiv \frac{1}{\Delta\tau} \int_t^{t+\Delta\tau} \frac{\|\langle\phi\rangle(t')_{DI} - \langle\phi\rangle(t')_{ISAT}\|}{\|\langle\phi\rangle(t')_{DI}\|} dt', \quad (17)$$

where $\langle\phi\rangle$ denotes the ensemble average vector and the subscripts DI and $ISAT$ denote DI and ISAT calculations, respectively.

In both cases it is observed that the relative global error varies as the ISAT error tolerance is changed, reaching maximum and minimum values at $\varepsilon_{tol} = 10^{-3}$ and $\varepsilon_{tol} = 10^{-2}$ for case 1, and, $\varepsilon_{tol} = 10^{-2}$ and $\varepsilon_{tol} = 10^{-5}$ for case 2, respectively. From the analysis of the error metrics it is possible to characterize an ISAT table with 50k entries as one with a good qualitative reproduction of the results, accurate from a global point of view, but with low accuracy if the local properties are analyzed.

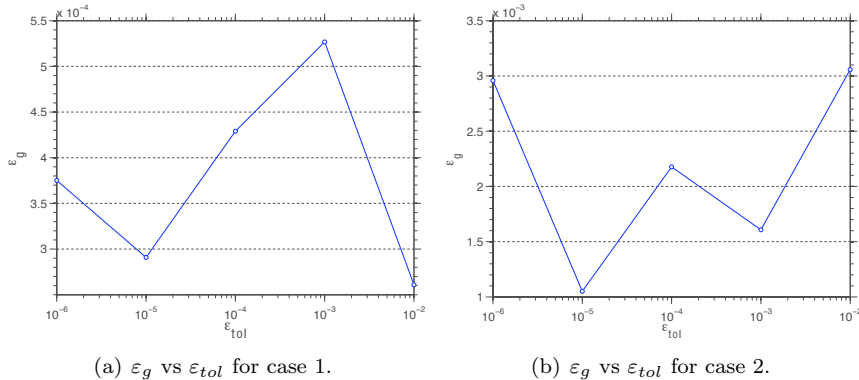


Figure 6. Relative global errors as function of the error tolerance, using a binary search tree with 50k entries.

3.2 Analysis of the ISAT Performance

The comparison of evolution of the ISAT algorithm outputs and of the height of ISAT binary search tree as well as the corresponding rates of change, for cases 1 and 2, which parameters are given in Table 1, is presented in Figures 7 and 8. A first important observation is that the number of additions in both cases reaches the maximum allowed value in the binary search tree of 50k. As a consequence of the saturation of binary search tree, the additions curve reaches a steady state after 5.4 and 1.2 residence times in the first and second cases respectively. Note that these residence times correspond to 108 and 123 PMSR events (see section 2.2), which indicates that the ISAT table was saturated earlier when mixing is slow.

Figures 7 and 8 also show the evolution of the height of binary tree, which reaches steady state after 36 PMSR events (1.8 time of residence) in the first case and 76 PMSR events (0.4 time of residence) in the second case. It is also noteworthy that, in both cases, the tree height is an order of magnitude smaller than the total number of entries in the tree ($\sim 17k$ in case 1 and $\sim 7k$ in case 2). This difference between height and total entries in the tree ensures the efficiency of the process of searching for a new query, which may be performed up to three and seven times faster in cases 1 and 2, respectively, than a vector search.

In the first case, Figures 7 and 8 show that the number of growths presents a sharp rate of change around 1 residence time whereas, in the second case, this occurs around 5 residence times. In both cases, growth steady state occurs after 10 residence times. During both simulations the number of growths is always smaller than the process of additions. This indicates that the desirable massive increase of the ellipsoids of accuracy to form a better estimate for the region of accuracy is not observed. This behavior might be circumstantial to the reaction mechanism of the carbon monoxide, since due to its simplicity (only 3 reactions) a small part of the realizable region should be assessed by the calculation.

Figures 7 shows that, after tree saturation occurs, the number of retrieves and direct evaluations exceed the number of additions in both cases. In case 1 there is a higher occurrence of the retrieve event, whereas in case 2 direct evaluation prevails. The number of retrieves exhibits a linear limit behavior in both cases. The ISAT behavior for the second case reflects the fact that the binary tree of this case is poor, i.e., contains too few compositions in the region accessed by the calculation. As a consequence, the number of direct evaluations vastly outnumbers the ISAT operations.

A sufficient condition for a calculation using the ISAT algorithm to be faster than the same calculation using DI is that the number of recoveries exceed the number of additions by a certain factor, which depends on the specific time of each output. From Figure 7 it is possible to estimate these factors as greater than or equal to 100 and 5 for cases 1 and 2, respectively. Further details may be found at Cunha Jr (2010).

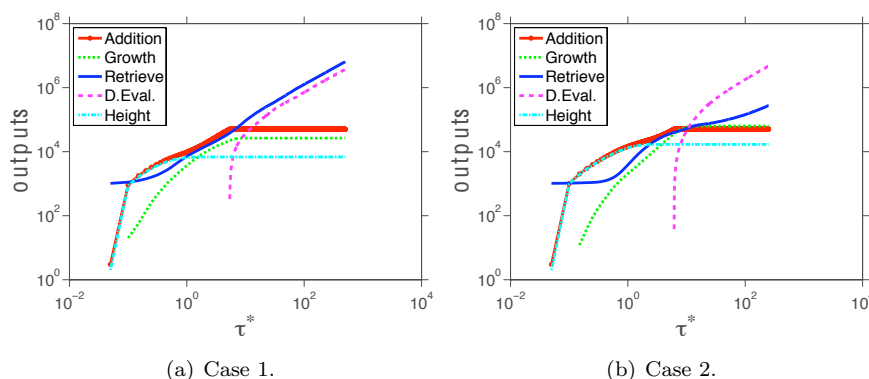


Figure 7. Evolution of ISAT algorithm outputs and of the height of ISAT binary search tree.

As can be seen in Table 2, where a comparison of computational time is shown, cases 1 and 2, for $\varepsilon_{tol} = 10^{-3}$ are computed using DI in 4.330 ks and 3.051 ks respectively whereas, with the use of ISAT, the same cases spent 2.348 ks and 2.113 ks, respectively. Speed-up factors of 2.3 (case 1) and 1.4 (case 2) are obtained, where the speed-up factor is defined as the ratio between the computational time spent by DI and the computational time spent by ISAT. This table also allows to compare the computational time spent by DI and ISAT for different values of error tolerance. An increase in processing time is obtained as ISAT error tolerance is reduced, which is to be expected, given the fact that lower values of ε_{tol} correspond to a smaller region of accuracy. Indeed, as ε_{tol} is decreased, it is less likely that ISAT returns a retrieve, which is the ISAT output with lower computational cost. Clearly, in all cases the ISAT algorithm offers an advantage in terms of processing time, when compared to the process of direct integration, reducing on average the processing time in 46% for case 1 and in 31% for case 2.

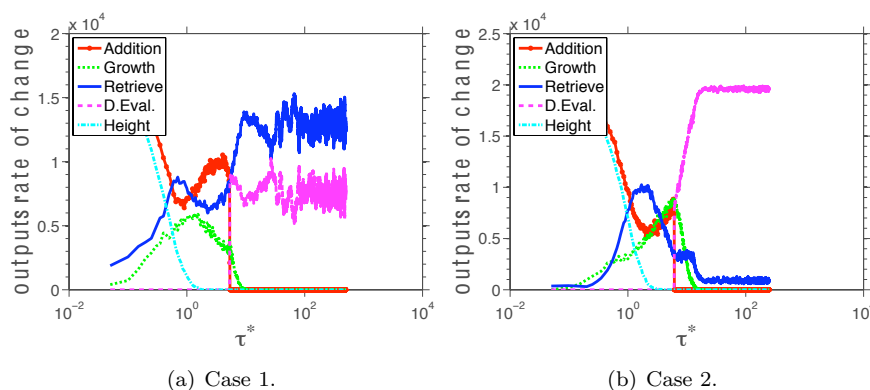


Figure 8. Evolution of the rates of change of each ISAT algorithm outputs and of the height of ISAT binary search tree.

Table 2. Comparison between the computational time spent by DI and ISAT in cases 1 and 2 and the corresponding speed-up factors.

ε_{tol}	Case 1		Case 2	
	time spent (ks)	speed-up	time spent (ks)	speed-up
DI	4.3		3.1	
10^{-2}	1.9	2.3	2.1	1.5
10^{-3}	2.3	1.9	2.1	1.5
10^{-4}	2.4	1.8	2.1	1.5
10^{-5}	2.5	1.7	2.2	1.4
10^{-6}	2.6	1.7	2.2	1.4

3.3 Analysis of ISAT Memory Usage

Cases 1 and 2 previously studied are both modeled by a reaction mechanism with 4 species and use a binary search tree with 50,000 entries for ISAT simulations. These parameters lead to a memory consumption by the ISAT algorithm of approximately 40 Mbytes, which is very small when compared to the available in the used computers. However, if the number of species in reaction mechanism increases, say 52 as in typical methane/air mechanisms, the memory storage cost grows, as shown in Cunha Jr (2010). Indeed, a simulation of PMSR filled with a methane/air mixture and using a binary search tree with 60,000 entries uses approximately 3.2 Gbytes. This huge expense of memory is perhaps the greatest weakness of the ISAT algorithm. Note that no attempt was made to optimize the code performance.

4. FINAL REMARKS

This work presented ISAT technique as an option to evaluate the system of governing equations in a computational model with detailed combustion thermochemistry. The technique is assessed for its accuracy, performance, and memory usage in the numerical simulation of PMSR filled with carbon monoxide/oxygen mixture.

The ISAT technique shows good accuracy from a global point of view, with the relative global error smaller than 0.35% for all the reactor configurations tested. Concerning the error from a local point of view, ISAT technique was characterized by values of the maximum error of the mean properties within the reactor of up to 41%, which could be unacceptable depending on the application.

In terms of performance, the ISAT algorithm allows to reduce the computational time of the simulations in all cases tested, achieving speed-up factors of 2.3 (case 1) and 1.4 (case 2).

Regarding the memory usage, the ISAT technique is very demanding. In the simulation of the methane/air mixture using a binary search tree with 60,000 entries, not shown here, the algorithm required 3.2 Gbytes. Thus, based on this test case, this work underscores the memory usage as the major drawback of the ISAT algorithm.

An extension of this work would be the coupling of a detailed thermochemistry mechanism, using the ISAT technique, with the hybrid LES/PDF model by Andrade (2009) and Andrade et al. (2009) for description of

turbulent combustion. This model currently uses a hybrid approach that combines large eddy simulation, for description of fluid dynamics, and the transport of the PDF with a single step global kinetic for modeling the combustion. The incorporation of a detailed thermochemistry mechanism would allow a better description of combustion, at the expense of a significant increase in computation time, which is not negligible in the case of a LES models. In this context, ISAT could be a viable option that may be able to decrease to an acceptable level the simulation time.

Finally, it is worth stressing that this study conducted verification tests of ISAT algorithm and PMSR reactor model only. No validation attempt was developed due to the difficulty of obtaining experimental data for such a homogeneous reactor configuration. This validation could be performed if carefully designed direct numerical simulations were available, or in more challenging flow problems, for instance.

5. ACKNOWLEDGMENTS

The authors acknowledge the support awarded to this research from Brazilian Council for Scientific and Technological Development (CNPq), Foundation for Research Support in Rio de Janeiro State (FAPERJ) and Brazilian Combustion Network. This work was performed while the second author was a Visiting Professor, funded by the Brazilian Petroleum Agency (ANP), on leave from Centre National de la Recherche Scientifique, France. The authors are indebted to Professor Guenther Carlos Krieger Filho from Universidade de São Paulo (USP), who provided the code that served as example to the code developed in this work, and for his hospitality during the authors visit to USP.

6. REFERENCES

- Andrade, F. O. (2009). *Contribution to the Large Eddy Simulation of a Turbulent Premixed Flame Stabilized in a High Speed Flow*. Doctoral Thesis, Pontifícia Universidade Católica do Rio de Janeiro, Rio de Janeiro. (in Portuguese).
- Andrade, F. O., Figueira da Silva, L. F., and Mura, A. (2009). A Hybrid LES/SGS-PDF Computational Model for Turbulent Premixed Combustion. In *Proceedings of COBEM 2009*.
- Correa, S. M. (1993). Turbulence-chemistry interactions in the intermediate regime of premixed combustion. *Combustion and Flame*, Vol. 93, No. 1-2, pp. 41–60. doi:10.1016/0010-2180(93)90083-F.
- Cunha Jr, A. B. (2010). Reduction of Complexity in Combustion Thermochemistry. M.Sc. Dissertation, Pontifícia Universidade Católica do Rio de Janeiro, Rio de Janeiro.
- Fox, R. O. (2003). *Computational Models for Turbulent Reacting Flows*. Cambridge University Press, Cambridge.
- Gardiner, W. C. (2000). *Gas Phase Combustion Chemistry*. Springer, New York.
- Golub, G. H. and Van Loan, C. F. (1996). *Matrix Computations*. John Hopkins University Press, Baltimore, 3rd edition.
- Knuth, D. E. (1998). *The Art of Computer Programming, Volume 3: Sorting and Searching*. Addison-Wesley Professional, Boston, 2nd edition.
- Pope, S. B. (1985). PDF methods for turbulent reactive flows. *Progress in Energy and Combustion Science*, Vol. 11, No. 2, pp. 119–192. doi:10.1016/0360-1285(85)90002-4.
- Pope, S. B. (1997). Computationally efficient implementation of combustion chemistry using *in situ* adaptive tabulation. *Combustion Theory and Modelling*, Vol. 1, No. 1, pp. 41–63. doi:10.1080/713665229.
- Pope, S. B. (2008). Algorithms for Ellipsoids. Technical Report FDA-08-01, Cornell University, Ithaca.
- Williams, F. A. (1985). *Combustion Theory: the fundamental theory of chemically reacting flow systems*. Wesley, Cambridge, 2nd edition.
- Yang, B. and Pope, S. B. (1998). An investigation of the accuracy of manifold methods and splitting schemes in the computational implementation of combustion chemistry. *Combustion and Flame*, Vol. 112, No. 1-2, pp. 16–32. doi:10.1016/S0010-2180(97)81754-3.